Radiation Protection Studies for Radiobiology

by

Roxana Rata

A thesis submitted to the University of Huddersfield in partial fulfilment of the requirements for the
degree of Doctor of Philosophy

in the

School of Computing and Engineering
International Institute for Accelerator Applications

June, 2018

"Imagination is more important than knowledge."

Albert Einstein

UNIVERSITY OF HUDDERSFIELD

Abstract

School of Computing and Engineering
International Institute for Accelerator Applications

Doctor of Philosophy

by Roxana Rata

Hadron therapy is a new treatment technique for cancer. Clinical studies [1] have demonstrated that hadron therapy is clinically more effective than conventional radiotherapy as it delivers the dose to the tumour, sparing the healthy tissue. Although this method reduces the additional dose delivered to the healthy tissues, due to the beam delivery systems the patients and the personnel are exposed to a secondary dose. Therefore, one of the main tasks for medical physicists is to make sure that the treatments are delivered according to the treatment plan.

This thesis is focused on the verification of the secondary dose received by the patient or the personnel during and after the irradiation sessions at three different facilities: the Clatterbridge Cancer Centre, the Christie Proton Therapy Centre and OpenMed at CERN. The ambient dose equivalent calculations were studied using the FLUKA Monte Carlo code. These calculations investigate whether the shielding methods meet the existing radiation protection requirements and if the dose delivered to the patients or staff is kept As Low As Reasonably Achievable (ALARA) [38].

Acknowledgements

Firstly, I would like to express my sincere gratitude to my advisor Prof. Roger Barlow who accepted me as his PhD student, for the continuous support and encouragement on daily basis from the start of my Ph.D study until today, for his patience, motivation, and advices. His guidance helped me in all the time of research and writing of this thesis. I could not have imagined having a better advisor and mentor for my Ph.D study. For all these, I sincerely thank him from the bottom of my heart and will be truly indebted to him throughout my life time.

Besides my advisor, I would like to thank to my co-supervisors: Dr. Andrzej Kacperek from the Clatterbridge Cancer Centre, Dr. Michael Taylor from the Christie Hospital and Dr. Ghislain Roy from CERN who provided me the opportunity to join their team and gave me access to the research facilities. I am grateful for their support, constructive criticism and counsel which led to the succesful completion of the research work.

My sincere thanks also goes to Dr. Cristian Bungau and Dr. Adriana Bungau for their valuable guidance, timely suggestions and stimulating disscussions.

I thank to my fellow David Lee for all his support and generous care and for all the fun we have had in the last four years.

I would like to express my special appreciation and gratitude to His Grace Bishop Ignatie. Your blessing and prayer for me was what sustained me thus far. Thank you for healing the wounds of my soul, for giving me hope when I was discouraged, for giving me peace when I was tired. Thank you for your care and thoughtfulness.

I am also grateful to David and Janice for spending their time to correct my English writing.

A special thanks to my family. Words cannot express how grateful I am to my mother for showing faith in me, for all the love, support and sacrifices that you did on my behalf. At the end I would like express appreciation to my beloved husband Emanuel for his love, support and understanding in my moments of weakness. Thank you for encouraging me throughout this experience and for being always around when I thought that it is impossible to continue.

My heart regards goes to my mother in law and my father in law for their love and support.

Last but not least, I thank God for giving me the strength to keep going, for helping me finish this Ph.D and for all the blessings.

Contents

List of Figures

List of Tables

Abbreviations

ICRU	**I**nternational **C**ommission of **R**adiation **U**nits
SOBP	**S**pread **O**ut **B**ragg **P**eak
MCS	**M**ultiple **C**oulomb **S**cattering
RBE	**R**elative **B**iological **E**ffectiveness
LHC	**L**arge **H**adron **C**ollider
SSB	**S**ingle **S**trand **B**reak
DSB	**D**ouble **S**trand **B**reak
DNA	**D**eoxyribo**N**ucleic **A**cid
LET	**L**inear **E**nergy **T**ransfer
Gy	**G**ra**y**
Sv	**S**ie**v**ert
SI	The **I**nternational **S**ystem of Units
FFAG	**F**ixed **F**ield **A**lternating **G**radient
TPS	**T**reatment **P**lanning **S**ystem
PET	**P**ositron **E**mission **T**omography
MC	**M**onte **C**arlo
FLAIR	**FL**uka **A**dvanced **I**nte**R**face
ICRP	**I**nternational **C**ommission on **R**adiation **P**rotection
IRR99	The **I**onising **R**adiation **R**egulations 1999

Dedicated to my husband Emanuel and my little angels Maria and Xenia

Chapter 1

Introduction

Nowadays cancer is becoming the leading cause of death world wide. Most cancer cases are treated with radiation therapy. Frequently, radiation therapy is combined with other therapies like surgery and chemotherapy [2].

The history of radiation therapy goes back to 1895 when Wilhelm Conrad Rontgen discovered the X-rays [3]. Ever since, ionizing radiation has been used for diagnosis and treatment for internal and external radiation therapy and implemented in cancer therapy programs worldwide. Ionizing radiation can be categorized into: low-LET like photons and electrons and high-LET like alpha-particles, accelerated ions and low energy-protons [3].

The principle of radiation therapy is that the radiation deposits the energy as an absorbed dose, causing damage to cancer cells which will lead eventually to cell death.

Therefore, the main purpose of radiation treatment is to eradicate the cancer while sparing the healthy tissue surrounding the tumour. Hadron therapy is a good method because it has the capability to deliver a higher dose to the tumour, while reducing the dose to the surrounding healthy structures [4]. The depth-dose curve for high-LET radiation is initially low and after that energy deposition increases rapidly and immediately it drops to zero. This feature is knows as the Bragg peak [5] The extent of the relative biological effectiveness increases with increasing LET. The relative biological effectiveness (RBE) is generally taken as 1.1 [32] but it is increasing with LET up to 100 keV/μm^{-1} and after is decreasing due to the overkill effect [33]. A detailed description of the RBE and LET relation is given in section 2.5.3. Figure 1.1 shows the dose rate in water as a function of depth for charged hadrons (protons and carbon ions), electrons, X-rays and ^{60}Co (γ rays).

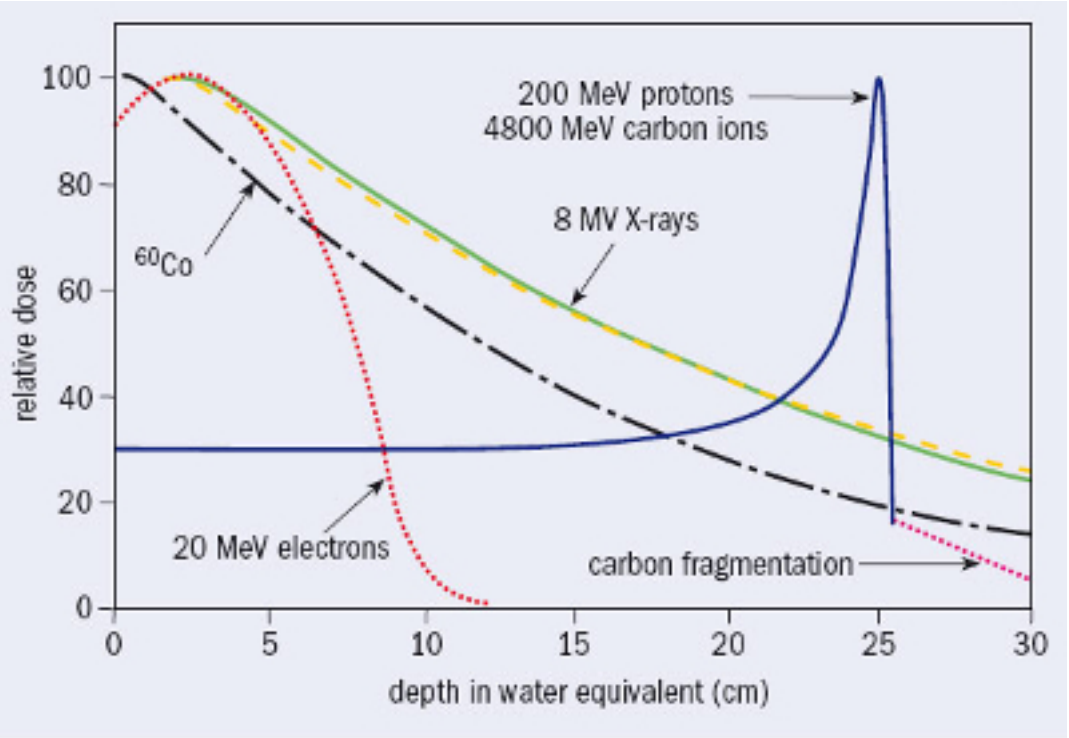

FIGURE 1.1: Dose rate in arbitrary units, as a function of depth for various particles as indicated. Taken from [6].

1.1 Research Objectives

Radiation is an important and disputed aspect of modern society. Even if people are exposed to natural radiation, people are also exposed to artificial sources when we refer to medical applications. Patients undergoing radiation therapy treatment and people working in these facilities are exposed to radiation. The radiation can be hazardous if it is not handled with care. Here is where the radiation protection is applied. The radiation protection is a field that has the role to protect humans and the environment from the harmful effects of radiation [7].

This thesis presents different aspects of radiation protection. These aspects are relevant as the results can affect the safety of personnel, patients and the general public.

This thesis covers only radiation protection for protons, helium ions, carbon ions and oxygen ions as these ions are used for cancer treatment or research at the facilities considered.

The objective of this thesis is to estimate the dose of the secondary particles, neutrons and photons, delivered to the patient or personnel during radiation therapy treatment. The calculations were made for three facilities: The Clatterbridge Cancer Centre [8], the Christie Proton Therapy Cancer Centre [9] and the OpenMed facility at CERN [10].

These results will be used to investigate if the proposed conditions of irradiation satisfy the radiation protection standards.

1.2 Methods

Monte Carlo simulations have a very important role in radiation therapy [11]. The simulations are mainly used to verify and to improve the quality of the radiation therapy treatment. For these studies, the FLUKA [12] Monte Carlo code was used to simulate the beam line components and the treatment conditions.

FLUKA is a general MC transport and interaction code based on Fortran, which was developed at CERN and it is mainly used in cosmic ray physics, neutrino physics, accelerator design, hadron therapy etc. The code has the capability to import CT scans and to correct the treatment planning systems but also to study the induced radioactivity and to simulate the transport of residual radiation. The code is mainly used at CERN for radiation protection calculations at the LHC but also for other facilities [12].

In the initial stage, an approach to data collection was taken for all three facilities. The second step was the geometry implementation and the analysis of the distribution of secondary particles produced. Then, ambient dose equivalent and the residual activity were calculated, in order to understand the influence on the total dose absorbed by the patient or personnel. Eventually, this study will lead to create efficient shielding for patient or staff safety.

The results showed that the production of the secondary neutrons during the irradiation is dependent on the material located in the proton beam path and also depends on the design of the beam line, so it is impossible to use a standard configuration. These results will later be verified by performing measurements during irradiation of various phantoms and using different types of detectors.

1.3 The Clatterbridge Cancer Centre

Chapter 4 gives an overview of the first (at present) and only proton therapy facility in UK. The facility is equipped with a cyclotron which provides a 60 MeV proton beam used to treat different types of ocular tumours [8]. The proton therapy treatment is delivered using the passive scattering method, therefore the patients will be exposed to a whole-body irradiation due to the secondary neutrons. As this dose is not added into the treatment plan, we considered that it is important to calculate the secondary dose to the patients, as, in time, this dose can lead to development of a secondary cancer.

This chapter discusses several aspects identified as central for radiation protection. The first aspect is the proton fluence and the proton dose along the beam line. This study is very important for the pre-therapeutic studies as it offers information about the quality of the proton beam distribution into the patient. The next aspect is the neutron fluence and the neutron dose along the beam line as this dose should be taken into consideration when the effective dose received by the patient is planned. The third aspect is the neutron dose equivalent as the radiation protection is based both on a principle of optimization and individual dose limits. The last aspect was the study of radioactivity induced in the collimator and in the treatment room as, even if people are benefiting from this practice, it can also give rise to exposure due to the radioactivity.

1.4 The Christie Proton Therapy Centre

Chapter 5 discusses the radiation protection calculations at the Christie Proton Therapy Centre. The Christie Proton Therapy Centre is a new facility under construction in Manchester, UK. The proton therapy facility is designed to have three treatment rooms and one research room and to deliver proton beams with energy up to 250 MeV [9].

The aim of the work presented in this thesis was to investigate the radiation exposure of the staff working in the research room and of the patients or public who have access to the surrounding facilities. The objective is to calculate the ambient dose equivalent for secondary particles like neutrons and photons and the radioactive nuclides produced by the irradiation of air and of surrounding structures, including the stainless steel floor. These studies will help us to calculate the external radiation exposure and also to verify if the doses are below the legal limits.

1.5 The OpenMed facility

Chapter 6 presents radiation protection aspects for the OpenMed/BioLeir project. This is a proposed facility at CERN which will provide different types of ion beams to be used for radiobiological studies, using an old synchrotron used to provide the heavy ions for the LHC. The LEIR facility is the only facility at CERN which is provided with a visitor platform. The initial radiation protection studies suggests that for the present situation, when only Pb ions are accelerated, the dose at the visitor platform level are below the the CERN regulations for supervised radiation area [10].

Under the new considerations, the FLUKA code was used to calculate the ambient dose equivalent for different ion beams and with three different beam losses. The aim is

to determine if LEIR provides appropriate shielding as the research laboratory will be placed near the accelerator room, and also to establish if the facility needs a roof on top of the machine.

Chapter 2

Proton Therapy

The idea of proton therapy started with the vision of a man. In 1946, Robert Wilson had the revolutionary idea that protons can be used clinically, because of the fact that the Bragg peak of proton beams can be used to place the maximum dose within the tumour, spearing the healthy tissue [13]. In 1954 the first patient was treated with protons at Berkeley Radiation Laboratory, but only in 1988 was this approved as radiation treatment for certain tumours like eye cancer, head and neck cancers, lung cancer, liver cancer, prostate cancer and spinal cancer.[14] By 2016, because of the increasing interest in proton therapy, there were 75 proton therapy centres worldwide and more than 154203 patients had been treated with protons [15].

2.1 Basic quantities used in proton therapy

Before describing the physical interactions, it is important to describe some basic quantities used in proton therapy.

2.1.1 Fluence

The fluence Φ is defined as the number of protons, during a given exposure, crossing the infinitesimal element of area dA normal to x axis. Fluence is a fundamental unit in dosimetry because it refers to radiation exposures [16].

$$\Phi = \frac{dN}{dA} \frac{\text{protons}}{\text{cm}^2} \tag{2.1}$$

2.1.2 Stopping power

The parameter used to describe the energy loss is the stopping power [16]. The stopping power is defined as the average ion energy loss per unit path length.

$$S = -\frac{dE}{dx}\frac{\text{MeV}}{\text{cm}} \tag{2.2}$$

The stopping power depends on the type and energy of the particle and on the type of material it passes through. Starting from this, we can describe the mass stopping power:

$$\frac{S}{\rho} = -\frac{1}{\rho}\frac{dE}{dx}\frac{\text{MeV}}{\text{g/cm}^2} \tag{2.3}$$

where $\rho(\text{g/cm}^2)$ is the local density of the stopping medium [16].

2.1.3 Physical absorbed dose

The physical absorbed dose is defined as the energy absorbed by matter per unit mass. The unit used in proton therapy is the Gray. Just to give an idea, a whole body dose of 4 Gy is lethal [16]! Another unit still used in U.S is 1 rad = 10^{-2} Gy [96].

$$D = \frac{E}{m}\frac{\text{J}}{\text{kg}} \tag{2.4}$$

1 Gy = 1 J/kg

The physical absorbed dose is not a good indicator for biological effects [7]. The radiation risk is described by the equivalent dose H_T. Equivalent dose is expressed in units of Sievert which implies that biological effects have been taken into account [17].

1 Sv = 1 J/kg as a biological effect [17]

2.1.4 The Ambient Dose Equivalent

The ambient dose equivalent is a quantity used to estimate the effective dose received by a person during the radiation treatment.

Ambient dose equivalent, $H*(d)$, was defined in ICRU Report 51 [124] as the dose equivalent that would be produced by an expanded and aligned radiation field at a depth d in the ICRU sphere. The reference depths are 10 mm for strongly penetrating

radiation and 0.07 mm for weakly penetrating radiation [18]. The unit used in radiation therapy is $\mu Sv/h$ [19, 20].

2.1.5 The fundamental equation in radiotherapy

The fundamental equation of radiotherapy is an expression of dose as function of fluence and stopping power.

If we consider that dN protons pass through an infinitesimal cylinder of area dA and thickness dx [16]:

$$D \equiv \frac{energy}{mass} = \frac{-\left(dE/dx\right) \times dx \times dN}{\rho \times dA \times dx} \tag{2.5}$$

equivalent to

$$D = \Phi \frac{S}{\rho} \tag{2.6}$$

.

Equation 2.6 is mainly used in beam line design or to estimate the dose rate in the patient [16].

2.2 Interactions of protons with matter

This section describes the interaction of protons with matter for a better understanding of the dose distribution in the patient. The protons interact with matter through three main processes: stopping, scattering and nuclear interactions [16].

2.2.1 Stopping

The most important aspect of proton therapy is the fact that beyond the stopping point, the proton dose is negligible. If the proton beam is monoenergetic, then all the protons will stop at approximately the same depth. This feature is called Bragg peak [16].

The theory of energy loss was proposed by Bethe in 1930 and Bloch in 1933 [16]. Referring just to protons and ignoring all the corrections (this is allowed in the radiotherapy energy range 3-300 MeV), the mass stopping power in a material with atomic number Z and atomic mass A is given by [3] :

$$\frac{S}{\rho} = -\frac{1}{\rho}\frac{dE}{dx} = 0.3072 \frac{Z}{A}\frac{1}{\beta^2}\left(ln\frac{W_m}{I} - \beta^2\right)\frac{\text{MeV}}{\text{g/cm}^2} \tag{2.7}$$

where $\beta = v/c$ is the velocity of the proton and

$$W_m = \frac{2m_e c^2 \beta^2}{1-\beta^2} \tag{2.8}$$

is the largest possible proton energy loss in a single collision with a free electron. $m_e c^2 = 0.511 MeV$ and is the electron rest energy.

I is the mean excitation energy of the target material. It cannot be calculated very precisely so it can be found by fitting measured range-energy values (where these are known) or by interpolation [21].

Knowing the stopping power, we can calculate the range of a proton entering the medium with kinetic energy E_0 until the energy reaches a very low value E_{final}

$$R(E_{initial}) = \int_{E_0}^{E_{\text{final}}} \left(\frac{1}{\rho}\frac{dE}{dx}\right)^{-1} dE \tag{2.9}$$

Another method to describe the range is via the expression

$$R = d_{80} \tag{2.10}$$

where d_{80} stands for the depth of water at the distal 80% point of the Bragg peak [21].

2.2.2 Multiple Coulomb scattering

A beam of protons travelling into a medium is slowing down and it also scatters, by interacting with atomic electrons. Due to the countless tiny deflections the process is called multiple Coulomb scattering (MCS). The MCS angular distribution is nearly Gaussian for small deflection angles, but not for large angles. In radiotherapy, only the Gaussian part is considered because it contains about 98% of the protons [22].

2.2.3 Nuclear Interactions

Even though the electromagnetic interactions are dominated, protons also experience nuclear interactions. Nuclear interactions are divided into two categories [16]:

1) Elastic- when a projectile is scattered off the target nucleus and the total kinetic energy is conserved;

2) Non-elastic- when the kinetic energy is not conserved (the projectile or the target nucleus may be excited into a higher quantum state, or a particle transfer reaction may occur).

The inelastic interactions are a special type of nonelastic reaction, where the ions are not conserving the kinetic energy, but they keep their identity before and after the collision, that means that the final nucleus is the same as the target.

Particles from inelastic and non-elastic nuclear interactions are called secondaries because the primary particles will be replaced by lighter fragments [16].

In the radiotherapy energy range, the secondaries produced from nonelastic reactions are protons, neutrons,γ rays, alphas and other secondaries. Most of the final energy will be found in protons, neutrons and photons as can be seen in figure 2.1:

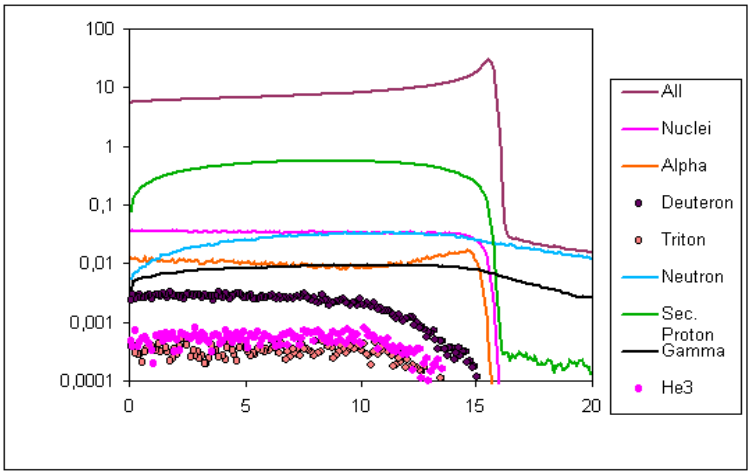

FIGURE 2.1: Contribution from secondary particles to the dose depth distribution from a 150 MeV proton beam in water. Taken from [23].

2.3 Accelerators and beam delivery techniques

In proton therapy the most important aspect is the dose distribution in depth, the energy has to be at the right value before entering the patient.

Therefore, even though some types of accelerator can produce the proton beam at the right energy and then deliver it to the patient, it is important to choose the appropriate technique to send the protons exactly to the tumour. The most common techniques used are passive scattering and active scanning [24].

The main accelerators used in proton therapy are cyclotrons and synchrotrons [24].

2.3.1 Cyclotrons

The cyclotrons used in proton therapy can accelerate a proton beam up to energies from 70 MeV (for superficial tumours) up to 250 MeV (for which the range in tissue is 32 cm) [24]. The cyclotron is a compact accelerator, providing a continuous beam of fixed energy. Even though the beam has a fixed energy, this can be adjusted very quickly and easily, using a degrader and an appropriate beam design. The most important components of a cyclotron are:

1) A radio frequency (RF) system - providing the strong electric field to accelerate the protons;

2) A proton source in the centre of the cyclotron, where the hydrogen gas is ionized and from which the protons are extracted;

3) A strong magnet to contain the proton beam during acceleration;

4) An extraction system to guide the particles to the gantry;

Cyclotrons used in radiotherapy require a high grade of reliability, low maintenance and should be easy to operate. The disadvantage of using a cyclotron in proton therapy is that it does not have the capability to change the energy of the extracted particles, therefore the energy has to be degraded by adding some material in the beam path and this will lead to secondary radiation production [24].

2.3.2 Synchrotrons

The synchrotron is a circular accelerator ring. It has the capacity to accelerate the proton beam until the desired energy is achieved and this allows the beam to be extracted at any energy. Due to this fact, a synchrotron is a good candidate for active beam delivery. Compared with a cyclotron, a synchrotron is much bigger, therefore the size reduction is of major interest.

Other accelerators being investigated for use in proton therapy are: Proton Linacs, FFAG accelerators, Dielectric Wall Accelerators and Laser-Driven Accelerators. These new accelerators are good candidates, but they still need to fulfil the safety requirements in order to prevent a wrong dose or a wrong location into the patient [24]. In conclusion, the cyclotron and the synchrotron remain the main accelerators used in proton therapy, and these machines are still improving.

2.3.3 Beam delivery using passive scattering

Passive scattering is a delivery technique which uses a scattering system to spread the proton beam and shaping devices to adjust the energy and lateral distribution [24]. A passive scattering delivery system is showed in figure 2.2.

There are some problems to be solved in order to achieve an appropriate dose deposition. First, the field aperture for the tumour treatment range (1cm up to 25cm) has to be covered with a homogeneous beam. For that, the beam has to be broadened using a single scattering foil (for small fields) or double scattering system (for large fields) [24].

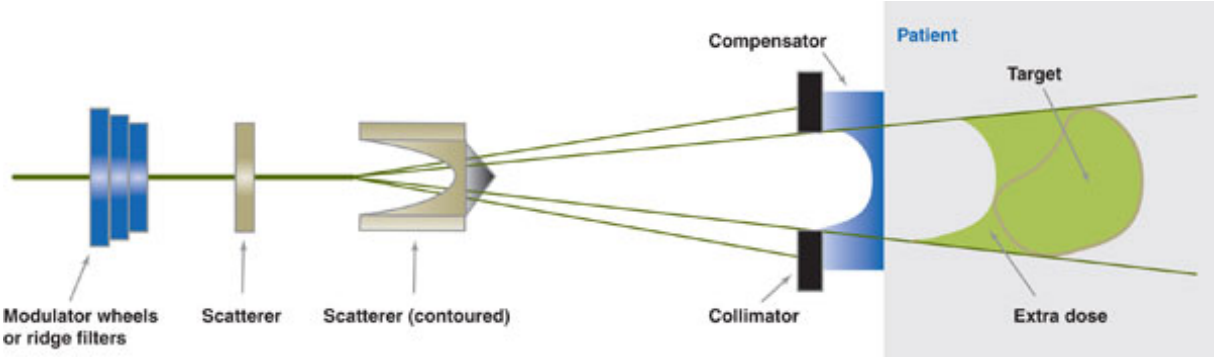

FIGURE 2.2: Schematic view of a passive scattering system. Taken from [25].

The second problem is covering the entire target. Obviously, the Bragg peak is too sharp to cover the entire volume so we need to combine proton beams with decreasing energy, transforming the Bragg peak into a uniform depth-dose region called the spread-out Bragg Peak (SOBP). This can be obtained using a range (wheel) modulator.

The modulator wheel was first proposed by Robert Wilson: "This can easily be accomplished by interposing a rotating wheel of variable thickness, corresponding to the tumour thickness, between the source and the patient" [26]. A range modulator wheel has various steps with different thickness, each step corresponding to a peak in the SOBP, so, by increasing the step thickness, a SOBP can be obtain. The modulator wheels are made of a low-material Z, like plexiglas or lexan, to limit the scattering.

A third problem is related to the conformation of the dose to the target. Usually, the treatment field is shaped using a collimator made of brass as shown in figure 2.3. The distal part of the dose is controlled using a range compensator, made of acrylic or wax, as shown in figure 2.4. The range compensator has the role of reducing the range of the protons and it is specific for every patient. The collimator and the compensator are mounted on the snout on the treatment head, as shown in figure 2.5 . This enables the air gap between the shaping devices and the patient to be reduced in order to minimize the effects of scattering in air and thus to reduce the beam penumbra [24].

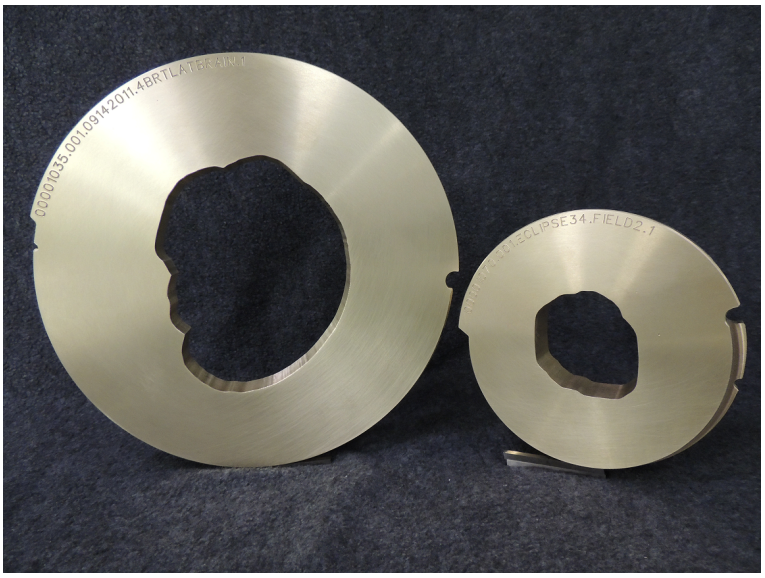

FIGURE 2.3: Collimators. Taken from [27].

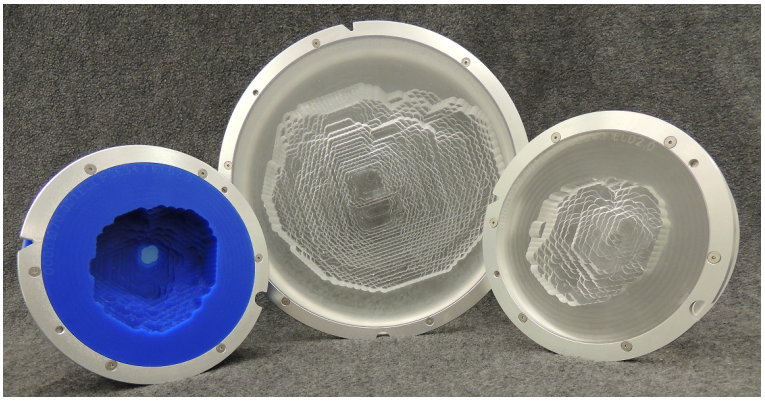

FIGURE 2.4: Range compensators. Taken from [27].

FIGURE 2.5: The brass aperture at the end of the snout.Taken from [28].

2.3.4 Beam delivery using active scanning

If the accelerator used for treatment has the capacity to extract the beam at different energies, the target volume can be scanned in a "slice by slice" manner as shown in figure 2.6 [24].

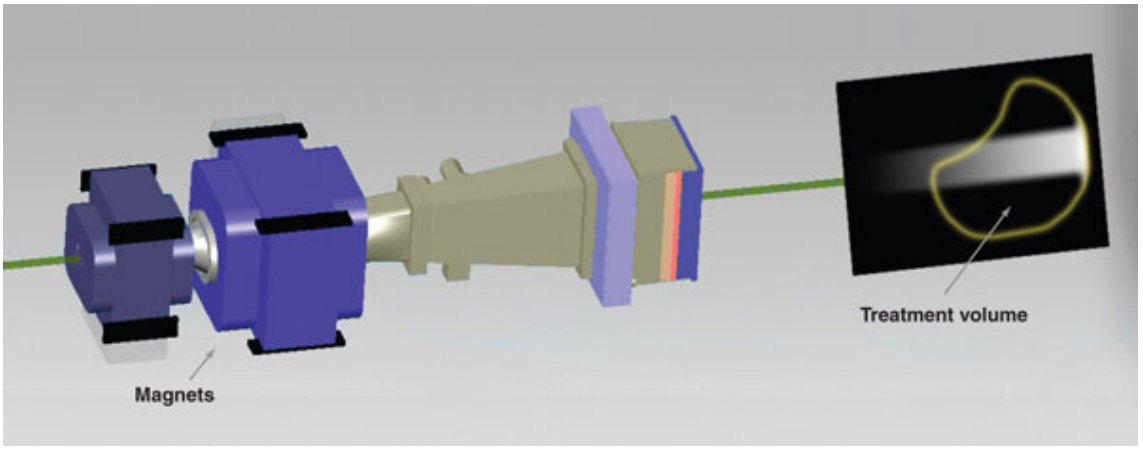

FIGURE 2.6: Schematical view of the active scanning system. Taken from [25].

The principle of the active scanning is that the scanning starts from the deepest layer (high energy) and does an x-y scan. After that, the energy is reduced and the next layer is scanned and so on until all the layers are scanned. There are three different techniques used in the active scanning method [24]:

1) Discrete spot scanning - A predetermined dose is delivered to a given spot at a given position, then the beam is switched off and the settings are changed for the next spot, so the dose will be delivered spot by spot. This method is implemented at PSI [24].

2) Raster scanning - Is similar with the discrete spot scanning, the only difference is that the beam is not switched off. This method is mainly used for heavy ions and was implemented at GSI [24].

3) Dynamic spot scanning - The target is continuously scanned [24].

The advantage of active scanning is that is no need for collimators or compensators and so the beam is interacting less with materials outside the patient, and as a result, the neutron production will be smaller. The disadvantage of this method is that it is very sensitive to organ motion [25].

In conclusion, the passive scattering method has several disadvantages compared with the active scanning method. The protons interact with the scattering material and this will create unwanted secondary particles. Another problem is that every patient needs to use a specific collimator and compensator which can be expensive. Despite these,

the majority of proton therapy centres are using this method to deliver the dose to the patients. The main reason is that the active scanning method requires a sophisticated beam control and feedback systems [25].

2.4 Clinical aspects of proton therapy

Clinical use of proton beams has many similarities with the use of conventional x-rays [16]. The objective of the treatment is to deliver the same amount of dose in every element of the target. For this, three volumes used as a guide for treatment planning as shown in figure 2.7:

1) Gross target volume (GTV)- refers to position and extent of the primary tumour;

2) Clinical target volume (CTV)- describes the microscopic extent of the tumour;

3) Planning target volume (PTV)- allows the uncertainties to be added into the planning and it includes the normal tissue structures in the vicinity of the tumour;

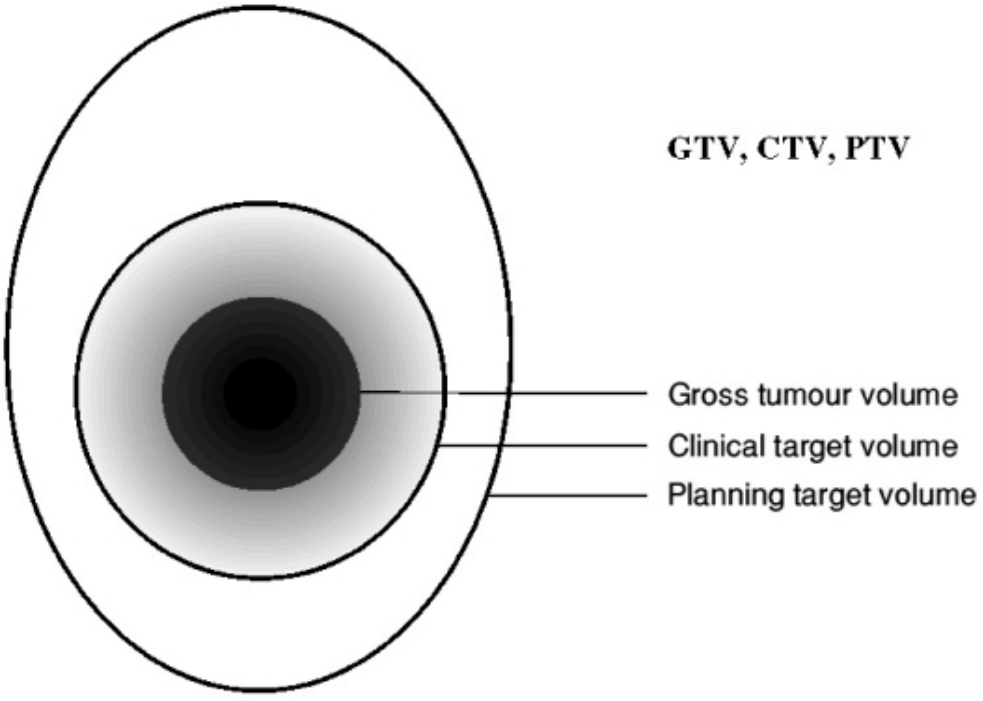

FIGURE 2.7: Schematical view of the radiotherapy planning volumes. Taken from [29].

As mentioned before, to obtain a homogeneous depth-dose distribution over the entire volume of the target, it is needed to interpose several Bragg peaks with different incident proton energies to obtain the spread-out Bragg peak (SOBP). The SOBP will increase the ability of the proton beam to spare the healthy tissue [24].

2.4.1 Treatment planning system

The treatment planning system (TPS) is based on clinical information like computed tomography (CT) and magnetic resonance imaging (MRI). The TPS also provides information about the treatment delivery system.

The TPS contains all the data to be used in the treatment such as the prescribed range, the modulation and the imaging information to be used for accurate patient positioning at the time of the treatment. It is important to take into account the limitations of the treatment planning system, especially when the dose calculation is involved [16].

2.4.2 Lateral penumbra

Proton therapy has another feature which makes it a good choice in treating cancer. The protons have a sharp lateral penumbra and this is essential for sparing the healthy tissue surrounding the tumour. The lateral penumbra depends on a series of factors like the beam delivery system and the uncertainties of the patient set-up.

For a passive scattering delivery system, the lateral penumbra depends on the position of the aperture, the range compensator, the air gap between the compensator and the patient and the penetration depth. In an active scanning system, the lateral penumbra is broadened by the air gap between the nozzle and the patient.[16]

2.4.3 Field size

In the majority of the cases, proton therapy is used to treat small tumours and this involves no major problems. Nowadays, proton therapy treatments are expanding for more diseases such as medulloblastoma (a type of brain tumour) and large sarcomas (a rare cancer affecting the muscle, bone, nerves, cartilage, tendons, blood vessels and fatty tissues) which involve much larger target volumes. Even if it is possible to expand the irradiation field to the largest field size possible, some practical considerations must be taken into account, for example: the size of the nozzle, the gantry size and the dose rate [16].

Scattering delivery systems can produce large fields, up to 25 cm in diameter, although the effective field size is approximately 22 cm. A small snout will allow lighter apertures and compensators and so the patient can be placed closer, which will make air gap smaller and therefore the lateral penumbra will be minimised. For the active scanning delivery system, larger fields will require stronger or longer scanning magnets [16].

2.4.4 Dose rate

An efficient beam produces a high dose rate, so that the treatment can be delivered in a short time. The treatment procedures, is that the patient is first set up by image guidance and after that, the treatment is delivered assuming that the patient has the same body configuration as in the last image procedures. This assumption is valid only for treatment which not take a long period of time, otherwise this aspect can affect the quality of the treatment, even if patient immobilization devices are used [16].

In proton therapy, there is no need to use a large number of fields, due to its capacity of sparing the healthy tissue around the target volume. Most of the treatments use two fields with different combinations, depending on the tumour position. For a regular treatment, the dose rate is about 1.8-4.0 Gy/min and depends on the target field size [16].

2.5 Proton biology

2.5.1 DNA Damage

The goal of proton therapy is to eradicate the tumour cells by damaging the DNA [30]. There are two types of lesions which can be induced: single strand break (SSB) and double strand break (DSB). In the case of SSB, only one strand of the double DNA helix is damaged, as a result, the DNA repair mechanism has the capacity to rebuild the damaged strand. In case of DSB, both strands of DNA helix are damaged, which makes the repair mechanism more difficult, if not impossible and this will cause cell death. In conclusion, for a better effect, the proton treatment must induce DSBs in the DNA [31].

In cancer therapy it is very important to understand cell survival as a function of dose. Cell survival curves represent the relationship between the number of cells that have lost the ability to proliferate and the absorbed dose as shown in figure 2.8. The linear-quadratic model is the accepted formula to express the survival curves. This model assumes that the cells can be killed in two ways [30]:

1. Single lethal event
2. Accumulation of sub-lethal events

$$S(D) = exp(-\alpha D - \beta D^2) \tag{2.11}$$

where S- is the fraction of cells surviving a dose

D- the dose

α and β are constants depending on the nature of the cells [30].

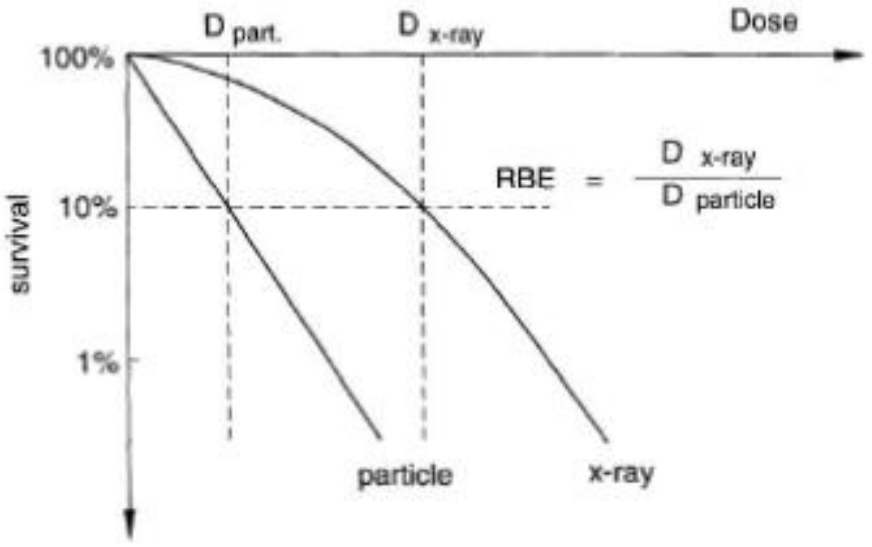

FIGURE 2.8: Cell survival curves. Taken from [31].

2.5.2 Relative biological effectiveness

Relative biological effectiveness (RBE) is a concept introduced to compare the effectiveness of the protons when compared with other types of radiation [32]. Thus, the RBE of protons is defined as the ratio between the photon dose and the proton dose used to achieve the same biological effect as shown in figure 2.8 [32]:

$$RBE = \frac{D_{x-ray}}{D_p} \tag{2.12}$$

where, D_{x-ray} is the photon reference dose and D_p is the proton dose.

Charged particles have different RBE. A high RBE is not an advantage because the same effect can be achieved with a higher photon dose. In proton therapy, the main advantage is that the RBE is increased over the Bragg peak area, and this will lead to increased damage in the tumour and not in the healthy tissue. In practice, the value used for RBE is 1.1 but this is mainly based on experiments performed at the beginning of proton therapy [32].

2.5.3 Linear Energy Transfer

Linear Energy Transfer (LET) is defined as the linear energy transferred to a medium per unit track length of the particle [32].

$$L = \frac{dE}{dx} \tag{2.13}$$

On a cellular level, the energy loss can only be approximated, because LET is a macroscopic parameter. The LET and the stopping power S described in equation 2.1.5 are closely associated but the difference is that LET refers to the local energy deposition and S is describing the total energy lost by the particle. For heavy charged particles, the LET and S are approximately equal [97]. Some examples of typical LET value are given in table 2.1 [32]:

Radiation	**Typical LET values**
1.2 MeV ^{60}Co gamma	0.3 keV/μm
250 kVp x rays	2 keV/μm
10 MeV protons	4.7 keV/μm
150 MeV protons	0.5 keV/μm
14 MeV neutrons	12 keV/ keV/μm
Heavy charged particles	100-200 keV/ keV/μm
2.5 MeV alpha particles	166 keV/ keV/μm
2 GeV Fe ions	1000 keV/μm

TABLE 2.1: Typical LET values [32].

The lethal effect of a charged particle depends on its LET and this affects the RBE [33]. As shown in figure 2.9, the RBE reaches a maximum value at an LET of around 100 keV/μm as a saturation effect. As the LET increases, the RBE increases slowly at the beginning and more rapidly as the LET increases beyond 10 keV/μm. After 100 keV/μ, the RBE is decreasing to lower values. This decrease in the high LET region represents a saturation effect due to "overkilling" [33, 35].

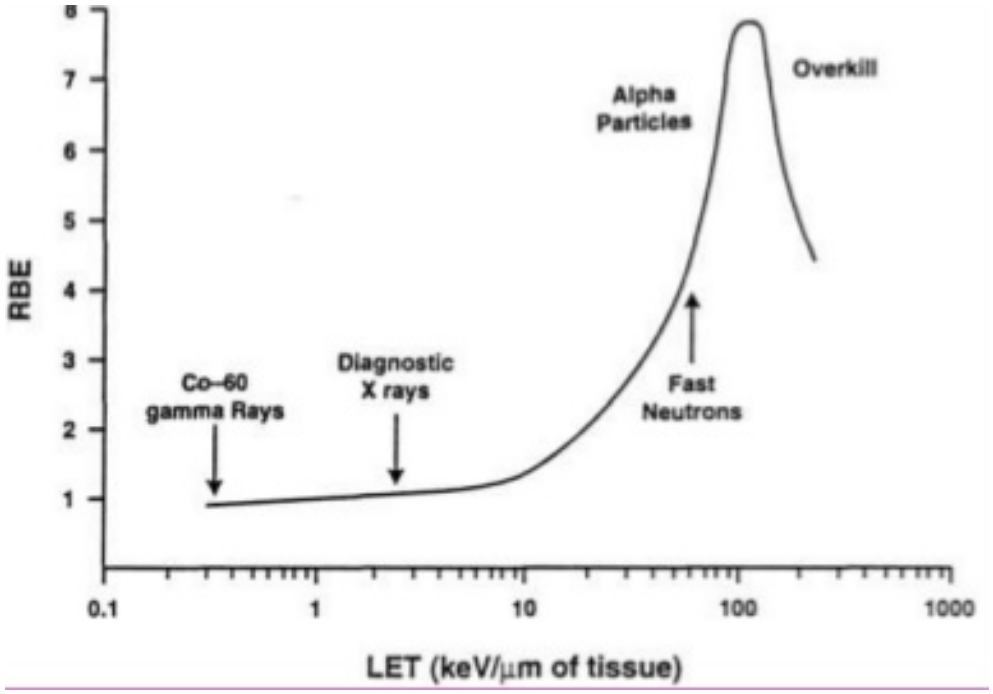

FIGURE 2.9: RBE as function of LET. Taken from [34].

2.6 Proton therapy's neutron problem

Secondary radiation production is a main concern in proton therapy, because the unwanted doses delivered by the secondary radiation can induce a secondary cancer into the patient. A disadvantage of proton therapy when compared with X-ray therapy is that the secondary dose received by the patients and staff is higher because of neutron production and activation [16].

Secondary radiation consists of prompt and residual radiation. Prompt radiation is produced while the accelerator is working, while residual radiation is produced by radioactive materials activated during machine operation. Secondary radiation is produced by the interaction of protons with the beam line components: energy degraders, beam shaping devices and the beam delivery system. Because of this, shielding is required. Secondary radiation is produced also in the patient, but these mechanisms are not well understood [16].

As mentioned earlier, the dose deposited by the secondary radiation in healthy tissue can have major consequences, affecting cognitive function, the functionality of organs or even leading to a secondary cancer. The malignancy risk remains even 30 to 40 years after the initial treatment. The risk also depends on the age of the patient and the type of tumour [16].

It has been proved that secondary cancers occur close to the primary cancer treatment field, where a high dose can induce a sarcoma and even a low dose is associated with a secondary tumour. This aspect has a huge importance, especially when treating children, because they are vulnerable to carcinogenic effects.[16]

2.6.1 Secondary neutron dose

When interacting with matter, the primary protons are generating secondary particles with different ranges: short-ranged ($<$ 1mm like α particles), medium-ranged (secondary protons) and long-ranged (secondary neutrons). The neutrons are produced when protons interact with the material in the beam path during the proton therapy treatment, but also with the patient tissue. Therefore, the patient is exposed to secondary radiation. The dose deposited by secondary particles must be considered, as even for a low dose, the neutrons can induce secondary cancers due to the fact that they have a high RBE [16]. The neutron production will depend on the material of the beam delivery system and on the design of the beam line.

The neutrons, according to [16], can be classified as following:

1. Thermal $E_n \leq 0.5$ eV;
2. Intermediate 0.5 eV $< E_n \leq 10$ keV;
3. Fast 10 keV $< E_n \leq 20$ MeV;
4. Relativistic $E_n > 20$ MeV;
5. High-energy neutrons $E_n > 100$ MeV;

In proton therapy, it is very important to know the neutron energy spectrum, because the biological effectiveness of the neutrons depends on their energy. The neutron energy deposition can be calculated using Monte Carlo simulations. In a typical proton therapy treatment, the dose is deposited by high energy neutrons (energy above 100 MeV) [16].

2.7 Radiation Protection

Radiation protection is a term used to describe concepts, requirements and operations applied to protect people against the harmful effects of ionizing radiation. Even though radiation is used in medical treatments for cancer, the exposure to radiation can lead to harmful effects such as radiation burns and secondary induced cancer. The major

purpose of radiation protection is to reduce the radiation risk as it can not be completely prevented [36]. According to the International Commission of Radiological Protection (ICRP) [37], the exposure of people to radiation and the radiological impact on environment should be kept as low as reasonable achievable (ALARA principle) and should be in accordance with the regulations of national professional bodies and with the recommendations of the international regulatory authorities. The ICRP stated in the Recommendation 60 [38] that three basic principles of radiation protection should be applied:

1. Justification: any exposure of persons to ionizing radiation has to be justified;
2. Limitation: personal doses have to be kept within the legal limits;
3. Optimization: personal and collective doses have to be kept as low as reasonably achievable (ALARA);

Radiation protection is provided as criteria and a guidance, according to the ICRP, which can be applied in cases such as nuclear power, radiation therapy and exposure to natural radiation. The guidance is established by the international organizations as the International Atomic Energy Agency (IAEA), the Commission of the European Communities (CEC) and the Nuclear Energy Agency (NEA). In every state, radiation protection concepts are implemented through national regulations issued by a regulatory authority. The regulatory authority has the power to license a source, to conduct inspections and to take enforcement actions. Therefore, the details for the rules of radiation protection differ throughout the world.[36] In UK, two sets of regulations are used for radiation protection against ionizing radiation and radiology [39]:

1. The Ionising Radiation Regulations 1999 (SI 1999 No. 3232) (IRR99) [40] addressed mainly to the safety of workers and general public but includes also the equipment aspects of patient protection;
2. The Ionising Radiation (Medical Exposure) Regulations 2000 (SI 2000 No. 1059) IR(ME)R 2000 [41] addressed to the safety of patients;

2.7.1 Radiation protection in clinical/research facilities

Radiotherapy with high energy hadrons is continuously developing and is already used in many countries as a treatment choice for several types of cancer. Although hadrons present several advantages over photons, there are several challenges in designing hadron therapy facilities that can treat a large number of patients efficiently and safely [26].

When designing a centre, several aspects have to be taken into account: shielding, activation, the safety system and monitoring. As high energy particles generate unwanted secondary particles, especially by neutrons, in order to maintain a safe environment two solutions are applied to avoid radiation hazards [42]:

1. Administrative controls to limit the exposure of the personnel;
2. Shielding to attenuate the radiation level to legal limits imposed by the national authority;

The evaluation of the radiation protection has to consider the parameters of the machine, like the beam rate and operation period, but, most importantly, the design that has to provide protection to patients and staff. This implies verification measurements of the shielding performance under various operation conditions, periodic reviews of the machine performance, and radiation measurements [61]. In order to establish the shielding needed for a hadron therapy facility, analytical techniques are used and verified with measurements and with Monte Carlo simulations. Recently, two studies [43, 44] from radiation protection conducted at the Northeast Proton Therapy Centre (NPTC) Boston, suggested that the Monte Carlo results are in better agreement with measurements than the analytical calculations. The Monte Carlo method has the advantage that complex geometries and shielding can be modelled in detail. As mentioned, several aspects have to be fulfilled to provide adequate protection from potential exposure to radiation. Periodic verifications have to be done to preserve safe working environment by ensuring that the personnel are not present in areas of high radiation fields. These safety verifications include also a variety of procedures and automated safety systems, including proton beam monitoring systems and area monitoring systems for neutrons, with acoustic and visual alarms if the legal limit is exceeded [42].

Although Monte Carlo methods are used to evaluate the effectiveness of neutron shielding, each hadron therapy facility will have different features that influence its shielding requirements, such as the accelerator type, beam delivery method and beam energy. In this section, the radiation protection for three different facilities will be discussed: the Advanced Proton Therapy Facility (APTRON) [45] under design in Shanghai, as the extracted beam energy will vary from 70 MeV to 250 MeV and the studies can be compared with the Clatterbridge Cancer Centre and the Christie Proton Therapy Centre cases evaluated in this thesis, the Italian National Centre for Oncological Hadrontherapy (CNAO) [46] in Italy as the facility have a cyclotron and a synchrotron and the results can be compared with both the Christie Proton Therapy Centre and OpenMed facility evaluated in this thesis, and CERN [47] as the OpenMed project will be based there.

2.7.1.1 The Advanced Proton Therapy Facility APTRON

The APTRON is a new facility planned to be built in Shanghai. The layout of the facility includes a 7 MeV Linac injector and a synchrotron capable of accelerating protons from 70 MeV up to 250 MeV. The dose equivalent limit is 2 mSv/year corresponding to 1 μSv/h for staff working full-time. The calculations were carried out for different energies assuming 100% beam loss and the radiation shielding evaluations were made with the FLUKA Monte Carlo code. The results showed that shielding wall thickness varies from 1.7 m to 3 m, as shown in fig 2.10, in order to obtain the values of the dose equivalent below the dose rate limit of 1 μSv/h outside the shielding wall [45].

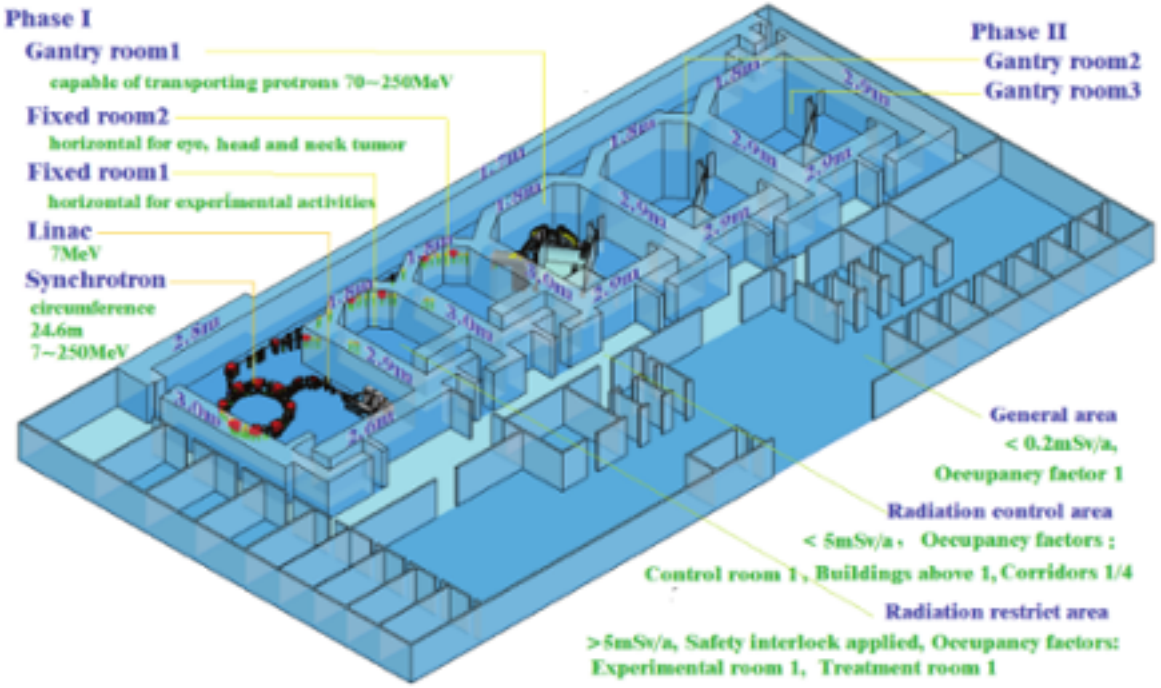

FIGURE 2.10: Schematic layout of the APTRON facility. Taken from [45].

2.7.1.2 The Italian National Centre for Oncological Hadrontherapy CNAO

The CNAO facility is equipped with both cyclotron and synchrotron machines. The cyclotron is designed to treat tumours with protons up to 250 MeV, while the synchrotron will accelerate carbon ions up to 400 MeV/u. At this facility, the recommendations of the ICRP Publication 60 were followed [25]. The dose objectives are 2-3 mSv/year for radiation workers and 0.25 mSv/year for non-exposed workers and the public. The limit for the activity of the air released into the environment is < 1 Bq/g. The radiation protection evaluation at this facility was done with the FLUKA Monte Carlo code. The effective dose (Sv/carbon ion) behind the shielding walls was evaluated. The dose was

calculated for a beam energy of 400 MeV/u and for wall thickness between 1 meter and 6 meters. The main contributors to the radioactivity released in air have an activation lower that 1 Bq/g for a 60 MeV beam being on for 24 hours continuously. Based on these calculations, the air activity concentration at CNAO is expected to be < 1 Bq/g [46].

2.7.1.3 CERN

CERN is an international research facility with many accelerator complexes able to accelerate particles up to 7 TeV. The radiation protection policy at CERN is based on ALARA principle and it complies with the regulations of the host states (Switzerland and France) and with the recommendations of competent international bodies [47]. All these recommendations are incorporated into CERN's radiation safety code [48]. According to this code, the areas inside CERN are classified by the effective dose received by a person during a stay in the area under normal working and operational conditions [48]:

1. Non-designated Areas;
2. Supervised Radiation Areas;
3. Controlled Radiation Areas;

The radiological classification and limits are shown in figure 2.11 taken from [49].

	Area	Dose limit [year]	Ambient dose equivalent rate		Sign
			Work place	Low occupancy	
	Non-designated	1 mSv	0.5 µSv/h	2.5 µSv/h	
Radiation Area	Supervised	6 mSv	3 µSv/h	15 µSv/h	
Radiation Area	Simple	20 mSv	10 µSv/h	50 µSv/h	
Radiation Area	Limited Stay	20 mSv		2 mSv/h	LIMITED STAY SEJOUR LIMITE
Radiation Area	High Radiation	20 mSv		100 mSv/h	HIGH RADIATION HAUTE RADIATION
Controlled Area	Prohibited	20 mSv		> 100 mSv/h	PROHIBITED AREA ZONE INTERDITE

FIGURE 2.11: Classification of Radiation Areas at CERN taken from[49].

The CERN dose limits comply with IRR99 dose limits as shown in figure 2.12 taken from [40]. As the majority of the workers at CERN are exposed to ionizing radiation, the dose received is monitored with personal dosimeters. For personnel working in Controlled Radiation Areas, where the dose rate is above 50 μSv/h, an additional operational dosimeter is mandatory [47]. Every facility at CERN has a combination of features that strongly influence the shielding requirements, therefore different methods are applied in order to keep the dose below legal limits. The Radiation Protection group uses the FLUKA Monte Carlo code to conduct studies for all facilities to evaluate the dose and the radioactivity induced in different elements like air, water and soil.

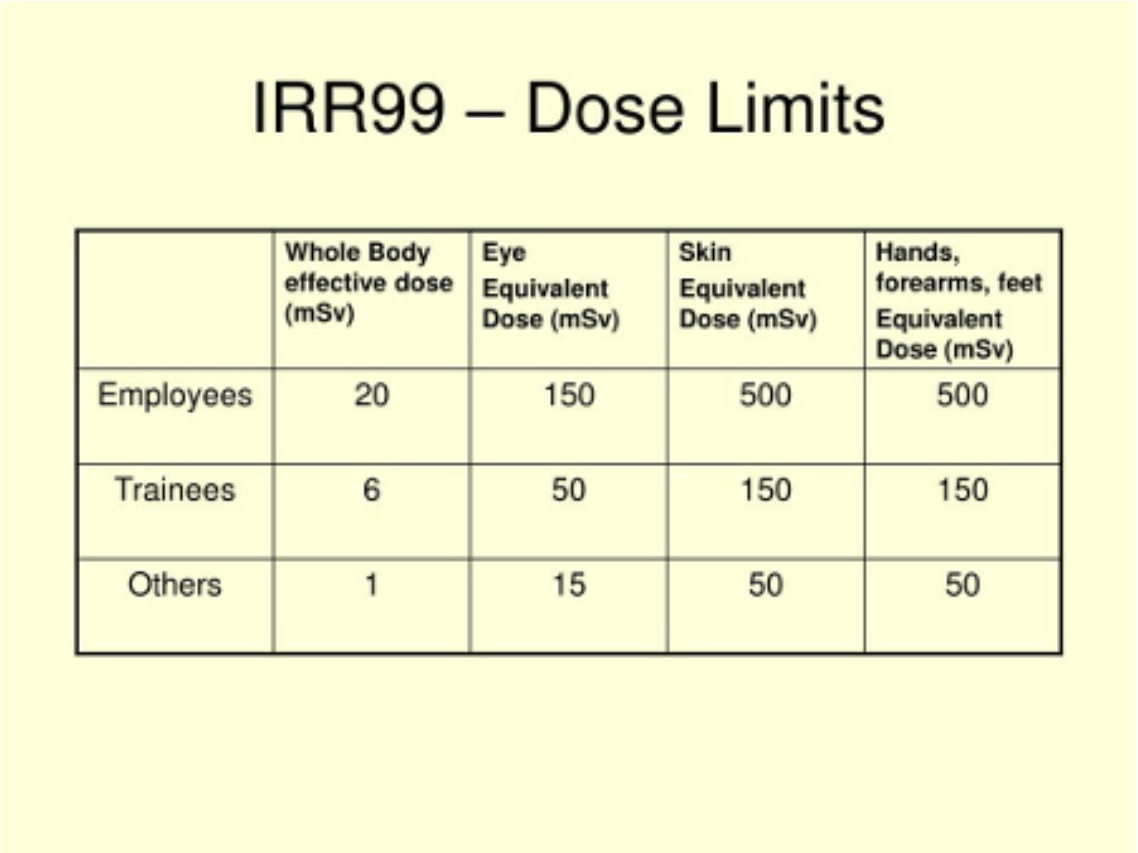

FIGURE 2.12: IRR99 dose limits taken from [40].

2.7.2 Monte Carlo codes used in radiation protection

Several studies [43, 44] have suggested that Monte Carlo calculations are in a good agreement with the relevant radiation measurements. Monte Carlo is a useful method to study new strategies in diagnosis and therapy, to evaluate new techniques and to plan the therapy treatment with accuracy [50]. The advantages of the Monte Carlo tools are that the complex geometries can be modelled in detail, a wide variety of physics processes can be implemented over an extended energy range, and the user has the possibility to

visualize the experimental set-up with a simple user interface. In the area of medical physics applications, several Monte Carlo codes are used, the most used are: GEANT4 [51], FLUKA [52] and MCNP [53]. A detailed overview of these codes is given in chapter 3.

2.7.2.1 GEANT4 Monte Carlo Code

GEANT4 [51] is a powerful tool which was originally developed for Particle Physics detectors and has been extended for use in diagnosis, radiotherapy and dosimetry. The GEANT4 simulation toolkit is a C++ library in which the user can write a program to define the problem. This code has the capability to model the experimental set-up in detail: beam line, radioactive sources and the patient anatomy [51].

The GEANT4 Electromagnetic Physics manages electrons, leptons, photons and muon interactions and provides implementations of ionization, Bremsstrahlung, multiple scattering, photoelectric absorption and Compton scattering. The GEANT4 Hadronic Physics offers both parametrization-driven models and theory-driven models and treatment of low energy neutron transport [51].

These features are relevant and offer advanced functionality for the GEANT4 simulation tool-kit which is used in various domains of medical physics: radiotherapy [54], brachytherapy [55, 56], hadron therapy [57], dosimetric studies at cellular level [58] and radiodiagnostic as PET and SPECT [59].

2.7.2.2 FLUKA Monte Carlo Code

FLUKA [52] is a general Monte Carlo radiation transport code that has the ability to track nearly all particles over an extended energy range. The FLUKA code was mainly developed for applications in detectors and accelerators, but new improvements have made FLUKA a standard tool to investigate beam-machine interactions, radiation damage and radiation protection issues. The FLUKA code is the principal tool used for radiation protection calculations for all accelerator complexes at CERN [52].

The FLUKA code is suitable for applications to hadron therapy as it provides reliable physical models for the description of the transport and the interaction of all components of the expected radiation field. Its physical database is based on laterally integrated depth-dose profiles, lateral dose distribution at different depths, secondary fragment yields and fragment energy spectra at different depths. Future developments of the FLUKA code will include the improvement of physical models for oxygen and helium ions as they are used in clinical studies for a possible use in hadron therapy [52].

2.7.2.3 MNCP

MCNP [53] is a general Monte Carlo particle transport code that can be used for single or coupled neutron/photon/electron transport. It has been widely used in nuclear power designs and it is clearly an old program as the documentation still refers to the input file as a "deck" of "cards" [79].

MCNP has been successfully used to calculate Bremsstrahlung spectra from medical linear accelerators, for modelling dose distribution, and to evaluate the dosimetric properties of a radioactive source. The code is used also to simulate radiation transport for neutron capture therapy treatment planning as the code has detailed physics models for neutron, photon and electron interactions. The MCNP code has the capability to record and to transport individual particles which is an advantage for treatment planning calculations [61, 62].

2.8 Activation processes in Accelerators

Activation induced in accelerator components represents one of the main radiation hazards of high-energy accelerators. Beam line components such as targets, collimators, magnets and beam dumps become highly radioactive as a result of direct interactions of the primary beam or indirect interactions of the secondary particles [68].

The hadronic secondary are produced along the beam line through spallation processes. The secondaries will activate the accelerator components as they pass through and the activity induced will be found even after the accelerator has shut down. Hence, high energy accelerators have a high radiological impact on the environment due to both prompt and residual radiation [63]. Neutrons and photons dominate the radiation field. The personnel will be exposed when handling, transporting, maintaining and storing the machine components. This exposure can exceed the permitted limits, therefore it is important to predict correctly the unstable radionuclides produced as they are unstable and will undergo radioactive decay [64].

The induced radioactivity will depend on the beam loss, the material composition and the production cross section of the isotope concerned. The radioactivity will depend also on the isotope half-life and the time that the accelerator was operational.[63, 64]

2.9 Radioactivity

Radioactivity or radioactive decay occurs when a high energy particle interacts with a nucleus which may emit secondary particles such as neutrons or protons or electromagnetic radiation as gamma radiation. That means that many nuclei are produced in excited states and de-excite by emitting neutrons, charged particles or fragments through a so called evaporation process. They may also de-excite by emitting gamma-rays. If the secondary particles have enough energy, they can cause further activation through spallation processes or they can be captured by nearby nuclei. The new nuclei produced have a high probability of being a radioactive isotope. Therefore, the radioactivity induced in an accelerator will strongly depend on the primary beam losses, on the primary beam energy, on the beam line material and on the secondaries produced. The derived SI unit for radioactivity is Becquerel (Bq) which is equal to one disintegration per second [63].

From the point of view of radiation protection, the most important radioactive isotopes are the long-lived ones as they can cause serious problems during maintenance and during decommissioning of an accelerator facility, and also because of the activation of the beam line components, concrete or air can induce radiation exposure to patients and workers [63, 64] The most common radioisotopes produced in an accelerator structure and their half life ($T_{1/2}$) are listed in table 2.2 [65–68].

As well as the machine components which are fixed, the air surrounding the accelerator and the cooling water will become activated also due to the secondary radiation. The radioactivity induced in air and water represents an additional hazard that needs to be studied in order to avoid a possible exposure of personnel and public if the radioactivity is released in the environment where the accepted levels may be low.

The most dangerous isotopes that are found in irradiated air and water are short-lived positron emitters that are produced in oxygen and nitrogen. The production of ^{7}Be and ^{3}He by spallation reactions in air and water and ^{41}Ar produced by thermal neutron capture in the natural argon in air, has to be evaluated in every radiation protection study for a high energy particle accelerator facility [69]. These isotopes are responsible for the dose received by humans.

Material	Radionuclide	$T_{1/2}$
Aluminium	^{3}H	12.33 y
	^{7}Be	53.22 d
	^{22}Na	2.6 y
Iron	as above plus	
	^{44m}Sc	2.44 d
	^{46}Sc	83.8 d
	^{47}Sc	3.35 d
	^{48}Sc	1.82 d
	^{48}V	15.97 d
	^{51}Cr	27.7 d
	^{52}Mn	5.59 d
	^{54}Mn	312.1 d
	^{55}Fe	2.74 y
	^{59}Sc	44.5 d
	^{56}Co	77.2 d
	^{57}Co	271.7 d
	^{58}Co	70.9 d
St. Steel	as above plus	
	^{59}Ni	75 y
	^{60}Co	5.27 y
Copper	as above plus	
	^{63}Ni	100 y
	^{65}Zn	243.7 d

TABLE 2.2: The most abundant radionuclides with half-life longer than 2 days present in accelerator structures after irradiation [65–68].

2.10 Hadron therapy

Nowadays, there are many facilities using protons, but there are some institutes who have developed therapy units for treatment of cancer with ^{12}C [70].

When compared with protons, there are some advantages and disadvantages to using ^{12}C ions. Due to the fact that ^{12}C is heavier, the ^{12}C ions are less scattered than ^{1}H in lateral direction, and the Bragg peak is narrower. Therefore, the ^{12}C ions can be used to irradiate tumours closer to organs, like the spinal cord or the optic nerve. These advantages make the ^{12}C suitable for deep seated tumours. Carbon ions have also a high RBE, which means that they are biologically more effective. Despite these, there are also some disadvantages. When the carbon ions interact with matter, they are fragmented due to collisions with the atomic nuclei. These interactions lead to an attenuation of the primary beam intensity and to production of secondary fragments (neutrons and lighter ions) which will have larger penetration ranges and will lead to a dose tail at the distal side of the Bragg peak. There is also a positive aspect, as the fragmentation process produces also lighter carbon isotopes which can be used for a positron emission

tomography (PET) analysis. Another disadvantage is that due to their larger charge, the energy loss is higher than that of protons, hence, the beam energy needs to achieve the same penetration depth is higher, which means that larger accelerators are needed. This is why synchrotrons are used in the existing facilities [71].

In the last decades, there has been larger interest to use ^{16}O ^{4}He and ^{20}Ne ions. While ^{4}He ions are similar to protons regarding their biological effectiveness, for ^{16}O the LET is high which makes it a good candidate for the irradiation of hypoxic tumours [70].

Chapter 3

Monte Carlo Simulations

3.1 Introduction

This chapter describes the Monte Carlo (MC) methods used to simulate interactions and transport of neutrons, protons and other particles in different media depending on their nature: photons undergo Compton scattering, photoelectric absorption and pair production, electrons undergo Bremsstrahlung, hadrons undergo elastic and inelastic scattering with atomic nuclei, charged particles suffer Coulomb scattering and energy loss [72]. This technique was developed in 1940 for the initial development of nuclear weapons and the name represents a reference to the famous casino in Monaco [73]. MC techniques are widely used in many areas of research as they can approximate solutions to quantitative problems through statistical sampling [74]. Monte Carlo simulations use random samples from a given distribution to evaluate or to approximate solutions for complex models or physical problems [72].

The difference between MC methods and analytical or numerical approaches is that the MC uses a random number generator and a set of probability distributions to sample parameter values for calculating a possible solution to the problem for a single "case" or "event". When multiple "cases" or "events" are simulated, average values can be obtained. Therefore the result is associated with a standard deviation that express the uncertainty. This type of uncertainty is not present when using analytical or numerical methods, but the analytical method can still present uncertainties due to the errors introduced in the model as it is difficult to analyse complex problems [75].

The MC method has the advantage that it can provide the solution of a problem, creating a virtual experiment based on an input. Provided with the correct information through the input (particles, energy, geometry, boundaries, material composition etc.),

the Monte Carlo method can simulate and track primary particles and also secondary particles created in the interactions.[72][74] This method is widely used in physics and more recently in applied fields such as medical physics to create different experimental conditions which are difficult to build experimentally [75].

The use of the MC method in modelling the particle transport through matter was described by Rogers and Bielajew [76]: "The Monte Carlo technique for the simulation of the transport of electrons and photons though bulk media consists of using knowledge of the probability distributions governing the individual interactions of electrons and photons in materials to simulate the random trajectories of individual particles. One keep of physical quantities of interest for a large number of histories to provide the required information about the average quantities." This description applies also for neutrons, protons and other types of particles.

In medical physics, the Monte Carlo method started to be used with the rise of the accelerators used for radiotherapy. Monte Carlo methods were developed for dose prediction and dosimetry. There are several reviews on the use of MC in medical physics [76–78]. These studies suggest that the MC results are in a better agreement with measurements than analytical methods as complex geometries can be implemented and the sources and the shielding can be modelled in detail. In radiotherapy, Monte Carlo is widely used to simulate the patient's, treatment conditions and also for dose calculation [77, 77]in order to ensure adherence to the safety regulations. Another advantage of using the Monte Carlo method in medical physics is that the user can manipulate the physics modelling through a number of transport parameters. The user can determine the cut-off energies or to choose which particles can be discarded. This will increase the efficiency of Monte Carlo calculations and the calculation speed will be increased [74].

For a dose calculation, the track of each individual ionizing particle through the volume is simulated. Along the path through matter, the particle will undergo different types of interactions: Compton scattering, Coulomb scattering or nuclear interaction. The MC method will use a random number generator and probability distribution for these interactions to sample the distance $\boldsymbol{l}$ to the next interaction for a particle at a given position and with a velocity $\boldsymbol{v}$ in a certain direction. The particle will be propagated with velocity $\boldsymbol{v}$ over the distance $\boldsymbol{l}$ to the interaction point and the MC code will choose a type of interaction that will occur. As the dose is defined as the amount of energy deposited per unit mass (J/Kg=Gy) [96], the code will calculate the energy loss: the energy of the projected particle minus the energy of the outgoing ones. If the dose is calculated in a specific volume, the code adds the contribution from all interactions occurring in this volume and divides this by the mass in the volume [75].

However, the results of any MC simulations could be affected by the physical models, by the accuracy of the information provided in the input or by the number of histories. Hence, the results should always be compared with experimental measurements where possible, if not, more that one simulation code should be used to compare (benchmark) the results [72].

There are three Monte Carlo codes that are widely used in radiotherapy : FLUKA [52], GEANT4 [51] and MCNP [53] [75].

For the work presented in this thesis, the FLUKA Monte Carlo Code was used. The reason of choosing FLUKA as the simulation code is that it is a free code, widely used in radiation protection evaluation and it provides an easy-to-use tool that helps the user to edit the geometry, to execute the code, and to visualize the results more easily. An additional reason for choosing this code is that several studies showed that the FLUKA results agree more with the experimental measurements than GEANT4 and MCNPX and it has a high simulation efficiency [42, 82]. During the research period various versions of the code were used, but all the results refer to FLUKA, 2011.2c-4 the latest version of the code [79, 80].

For the Clatterbridge Cancer Centre project, the results obtained with FLUKA were compared with MCNPX results obtained by Annelie Laidler. The MCNPX results were calculated using the same geometry for the beam line as in FLUKA.

For the Christie Hospital Centre project, the neutron dose equivalent values calculated with FLUKA were compared with MCNPX results obtained by Alex Flynn.

3.2 MCNPX

MCNPX [60] is a general-purpose Monte Carlo transport code that has the capability to track all particles at all energies. MCNPX is an extension of MCNP and it was developed at Los Alamos National Laboratory in 1994. The name MCNP stands for Monte Carlo N-Particle Transport Code. The Monte Carlo code is widely used for neutron studies, in the design of accelerator spallation targets, in investigations for accelerator isotope production and nuclear waste transmutation, medical physics, the design of shielding in accelerator facilities and research into accelerator-driven energy sources [61].

The MCNPX code can be used in several transport modes: neutron only, photon only, electron only, combined neutron/photon transport, neutron/photon/electron or electron/photon. The neutron energy regime is from 10^{-11} MeV to 20 MeV and the photon and electron energy regimes are from 1 keV to 1000 MeV [81].

One of the advantages when using MCNPX is that the code does not require any programming by the user. The user needs to provide an ASCII input file with the information about the geometry, the sources (energy and angular spectra), the tallies (energy deposition or track length) and the variance reduction techniques. The final results are provided as ASCII output files. A graphical user interface is available to generate input files and to visualize the output data. It has also the capability to allow the user to specify a wide range of source conditions without modifying the code. Independent probability distributions may be specified for the source variables of energy, time, position and direction and other parameters as starting cell or surface. The user can also request various tallies related to particle, current, particle flux and energy deposition. All tallies are normalized per starting particle [82].

MCNPX uses for nuclear data continuous-energy nuclear and atomic data libraries. The primary sources of nuclear data are taken from the Evaluated Nuclear Data File (ENDF), the Evaluated Nuclear Data Library (ENDL) and the Activation Library (ACTL). Nuclear data tables are available for neutron interactions, neutron-induced photons, photon interactions, neutron dosimetry or activation and thermal particle scattering [82].

For the energy range used in radiotherapy, the MCNPX code employs the tabulated data library for nucleon-induced reactions for projectile energies less than 150 MeV. The data file used for neutrons is LA150N and LA150H for protons. For this energy range, the MCNPX code uses the Bertini model as default, and Coulomb diffusion and elastic and inelastic scatterings are also considered. The cut-off energy is usually set to 100 keV for electrons, photons and protons and with no threshold for neutrons [82].

MCNPX code is a general-purpose, continuous-energy, generalized-geometry, time-dependent and with an energy deposition mesh-tally that makes it a good candidate for many applications in medical physics, including the dose calculations in partial body irradiation. There are several advantages in using the MCNPX code: the explicit modelling of complicated geometries, the extensive cross section library for low energy reactions (< 20 MeV), the capability to calculate the statistical uncertainties, the mesh tally that can provide spatial distributions independently of the problem model, the complete library of neutron cross section and the fact that the code is not requiring programming skills. The disadvantages are that the code is not a free source and the calculations can take time to obtain a suitable statistic for small regions. Another disadvantage is that the input format can be tricky to implement for a new user [81].

3.3 GEANT4

GEANT (GEometry ANd Tracking) [83] is a simulation toolkit that was originally developed for high-energy physics in the C++ language. Due to the latest development in particle, nuclear and radiation physics, new demands for accurate and comprehensive simulations had risen. As a response to these demands, the GEANT simulation code was developed. The code can be widely used in various studies, from basic phenomena to full-scale detector simulations for the LHC [83].

The GEANT4 code includes built-in steering routines and command interpreters which operate at the setup, run, event, particle transport, visualization and analysis levels. The software is based on a set of physics models that can handle particle interactions across a wide energy range. The software contains components like event generation, reconstruction and analysis that represent what are used for real data simulations. The code is very flexible and allows the user to customize and implement only the physics that is suitable for the study. The geometry of the experimental setup can be implemented through a large number of components with different shapes and materials [84].

The global structure of the simulation toolkit includes different categories that are capable of managing the runs, the events and the tracks. This allows the simulation of the event kinematics and the primary and secondary tracks. In GEANT4, the tracking does not depend on the particle type or the specific physics processes. The particle is moved step by step, which allows the optimization of the execution performance. The GEANT4 *Geometry* module allows the user to model the geometry structure and to propagate particles through it. GEANT4 *Electromagnetic Physics* can manage many particle interactions like: leptons, photons, muon, hadrons and ions. It also provides implementations regarding ionization, Bremsstrahlung, multiple scattering, photoelectric absorption, Compton scattering and synchrotron radiation. Low energy processes down to 250 eV for photons, electrons, hadrons and ions are also implemented. The GEANT4 *Hadronic Physics* offers various theory-driven models and also it treats low-energy neutron transport [84].

All these features make GEANT4 a powerful and versatile toolkit that can be used in medical applications, especially in the simulations of secondary particles in proton and ion therapy. GATE and TOPAS are two simulation platforms based on the GEANT4 toolkit that are used for radiation therapy and dosimetry applications The code can simulate a wide range of physics processes based on theory or experimental data. The GEANT4 toolkit is continuously improved and developed for many applications from medical physics to high-energy astrophysics or accelerator design [83]. Like any other Monte Carlo code, the GEANT4 simulation toolkit has advantages and disadvantages.

The mainly advantage is that the user can add extra features to extend the program to other areas that for which the code was originally intended. It is a free source code, very flexible and with the capability of implementing or modifying any physics processes without changing other parts of the software. Another important advantage is that the user can implement physics models according to the needs. But this advantage can be also a disadvantage as due to the variety of available hadronic models, the user has to combine them adequately to describe the initial interaction stage. Another disadvantage is the fact that the user needs to have C++ programming skills to be able to use the GEANT4 toolkit [85].

3.4 The FLUKA code

FLUKA is a general MC transport and interaction code developed for high-energy physics with fully integrated physical models which allows the users to add their own scoring and sources files [79, 86]. The code is written in Fortran and it is used for calculations of particle transport and interactions with matter. It can be applied in cosmic ray physics, neutrino physics, accelerator physics, particle physics, shielding design, dosimetry, space radiation, hadron therapy, neutronics etc. FLUKA was developed in 1962 by Johannes Ranft to be used for hadronic beams at CERN. Between 1970 and 1987, the code was used mainly for shielding calculations. The name of FLUKA was given later, when the code was used in calorimetry, and it stands for FLUktuierende Kaskade (Fluctuating Cascade). In 2003, a collaboration between CERN and INFN started with the aim of developing the code in areas of interest such as dosimetry, medical physics and radiobiology [86]. Presently, FLUKA has the capability to simulate with high accuracy the interaction and propagation in matter for more than 60 different particles with energies from 1 keV to TeV: neutrinos, muons with different energy, hadrons with energies up to 20 TeV and all the corresponding antiparticles, neutrons down to thermal energy and heavy ions. The program can also transport polarised and optical photons [87, 88].

This code has the capability to import CT scans and to correct the Treatment Planning System (TPS) and also to study induced radioactivity, decay and transport of residual radiation. Particle cascades produced by prompt radiation and residual radiation can be simulated in parallel in order to distinguish them. This allows the user to score the quantities independently. With FLUKA the user can calculate the prompt dose or the residual dose equivalent using a user-defined irradiation and cooling profile. All quantities can be presented in 1D, 2D or 3D plots [89]. FLUKA also has the capability to deal with low-energy neutron components of the cascade and this feature is very

important as the user can include electronics and other sensitive detector parts. In addition, radiation damage calculations and shielding design can be applied not only for proton accelerators but also for electron accelerators of any energy, photon factories or any type of radiation source, be it artificial or natural [90].

When compared with other MC codes, FLUKA has the highest simulation efficiency and is much faster. The simulation efficiencies studies showed that FLUKA is a factor of 4 faster than the MCNPX and a factor of 14 faster that the GEANT4 [42]. For a simulation with 10^6 primary histories (number of samples) there is no need for a supercomputer, as the running time is around 4 or 5 hours.

Despite of all these features, FLUKA has also disadvantages due to the code weaknesses: the physics is not exact (all codes are based on different physics models and some models are better than others), the code configuration cannot be modified, artefacts can occur due to the imperfect algorithms and data uncertainty. Problems may also be due to the user: material composition not always well known, geometries that may not be reproduced exactly and may be other area of user ignorance [79].

The FLUKA code is available without charge, together with the graphical interface FLAIR, that is available for output processing and plotting. As the role of the FLUKA code is to provide the best physics available, all the relevant physical models are implemented as packages. For particle therapy, FLUKA uses different physical models such as EMF (ElectroMagnetic FLUKA) which contains the electromagnetic physics which accounts for energy loss, straggling and multiple Coulomb scattering of charged particles. For ion projectile energies from 5 GeV/n down to 100 MeV/n, a relativistic Quantum Molecular Dynamics (rQMD) model is employed for nucleus-nucleus interactions [90, 91] For lower energies, a model based on the Boltzmann master equation (BME) theory is used to describe hadronic interactions. De-excitation of the excited fragments is processed by the FLUKA evaporation/fission/fragmentation module. The hadron-nucleus interactions are implemented in the PEANUT (Pre-Equilibrium Approach to Nuclear Thermalization) framework [90, 91]. For momenta below 3-5 GeV/c, the PEANUT package includes a very detailed Generalised Intra-Nuclear Cascade and a pre-equilibrium stage, while for high energies the multiple collision mechanism is included. Both modules are followed by equilibrium processes: evaporation, fission and gamma de-excitation. For neutrons with energy lower than 20 MeV, the FLUKA code uses its own neutron cross section library with more than 250 different materials used for simulations in physics, dosimetry and accelerator design [93]. All models described above have been benchmarked for both therapeutic proton and carbon ion beams [91, 92].

3.5 Physics settings for simulations

The results presented in the next chapters have been calculated using the latest version of the code. The physics settings were optimised to obtain accurate simulations. For all three inputs used for the Clatterbridge Cancer Centre, the Christie Proton Therapy Centre and the OpenMed facility, the configuration recommended for precision simulation was chosen. The default set of parameters was activated using the DEFAULTS card, with the PRECISIOn option, used for precision simulations. This option includes by default [37]:

Option
EMF model
Rayleigh scattering and inelstic form factor corrections to Compton profiles
Detailed photoelectric edge treatment and fluorescence energies
Low energy neutron transport down to termal energies
Fully analogue, the physical reality is simulated giving no importance to the geometry areas
Particle transport treshold set to 100 keV, except neutrons
Multiple scattering threshold at minimum allowed energy, for primary and secondary
Delta ray production with threshold of 100 keV
Heavy particle bremsstrahlung activated with explicit photon production above 300 keV
Muon photonuclear interactions activated with explicit generation of secondarie
Heavy fragment transport activated

TABLE 3.1: The default options includes in the FLUKA Monte Carlo simulations [37].

Additionally, the **Evaporation** and **Heavy fragments** options were activated for accurate description of the nuclear processes and to obtain the residual nuclei production [92, 93].

In order to calculate the fluence and the dose equivalent additional options were added to the PRECISIOn option:

- USRBIN - the USRBIN is used to score the distribution of different quantities (fluence, dose) independent of the geometry. Using this option, the user can select the structure of the mesh (spatial, cartesian or by region). Together with the fluence and the dose equivalent, USRBIN allows the user to score the activity or the energy deposited. In the inputs used for all simulations presented here, the USRBIN was selected to score the ambient dose equivalent.
- AUXSCORE - this option is always used together with URSBIN option as it allows the association of scoring detectors of certain estimator types with dose equivalent conversion factors, and filter particles or isotope ranges in accordance with the needs of the user. The reason of activating the AUXSCORE card is

that the user can provide the energy dependent coefficients for the conversion of fluence to ambient dose equivalent for neutrons, protons, charged pions, muons, photons and electrons. In the cases presented in the next chapter, the Ambient dose equivalent from ICRP74 [94] and Pelliccioni data (AMB74) [95] was chosen for proton, neutrons and photons [93].

For activation studies several other cards were activated:

- RESNUCLE - this option scores the residual nuclei produced on a region basis, for each object separately. The user can choose the type of products to be scored. For all three studies presented in this thesis, all residual nuclei were scored (spallation products and low-energy neutron) [93].
- RADDECAY was inserted for simulation of radioactive decays and sets the transport conditions like the cooling time. For the results presented here, five cooling times were used: after irradiation, 1 hour, 1 month, 3 months and 1 year. The RADDECAY option offers the possibility to perform on-line time evolution of decay radiation according to the user-defined irradiation profile and one or more decay times. The RADDECAY card requires the DCYSCORES card.
- DCYSCORES associates the detectors, the estimator type and the user decay time for radioactive product scoring. In the evaluations presented in this thesis, due to the fact that five cooling times were used, to each cooling time an index is assigned, following the order in which it has been added into the input. This index is then used in the DCYSCORE to assign that particular cooling time to the scoring detectors. DCYTIMES defines the decay times after irradiation for the radioactive product scoring. Multiple cards for this option can be added, up to a maximum of 20 decay times.
- IRRPROFI was used to define the irradiation profiles, such as the beam intensity and the irradiation time [93].

A complete list of the options used for simulations is given in the Appendix.

Together with FLUKA, the FLAIR software was used. FLAIR [93] stands for FLUKA Advanced InteR-face and is an advanced friendly interface for FLUKA to facilitate the editing of FLUKA input files, execution of the code, geometry debugging, checking of the output files and visualization of the final results. It is based on Python and Tkinter. It was developed by Vasilis Vlachoudis for FLUKA users to work on an intermediate level and to verify every option using the FLUKA manual. FLAIR provides also a geometry

editor which helps the user to visualize the geometry in 2D, to debug bodies and regions in a graphical way, to obtain a 3D rendering of the geometry and to display complex geometries [93].

In conclusion, all these capabilities make FLUKA a very powerful code which can be used in various domains according to the needs of the user.

Chapter 4

Neutron background studies at the Clatterbridge Cancer Centre

4.1 Introduction

The Clatterbridge Cancer Centre is the first and, at present, the only proton therapy facility in the UK. In 1984 a 62 MeV cyclotron was installed for treatments of radio-resistant tumours with fast neutrons [98]. The machine was called the Douglas Cyclotron after a benefactor who helped fund the equipment [99]. Because the 62 MeV proton beam is suitable for proton therapy, having a maximum clinical range of 31 mm in water, a room equipped with an ocular beam line was built. A schematic view of the ocular beam line can be seen in figure 4.1 [98]. The Clatterbridge cyclotron delivers the beam using the passive scattering method. The first patients were treated in 1989 and, since then, the facility has treated more that 2000 patients [98].

This studies were conducted at the request of Dr. Andrzej Kacperek to investigate neutron production during proton therapy treatment and to establish how this secondary dose influences the final dose received by the patient. The activation of the beam line components and the air activation in the treatment room were also considered, as these could lead to an additional exposure to radiation of the patient and the personnel. Finally, this study will help us to look for methods to reduce the neutron dosage and thus the risk of induced secondary cancers.

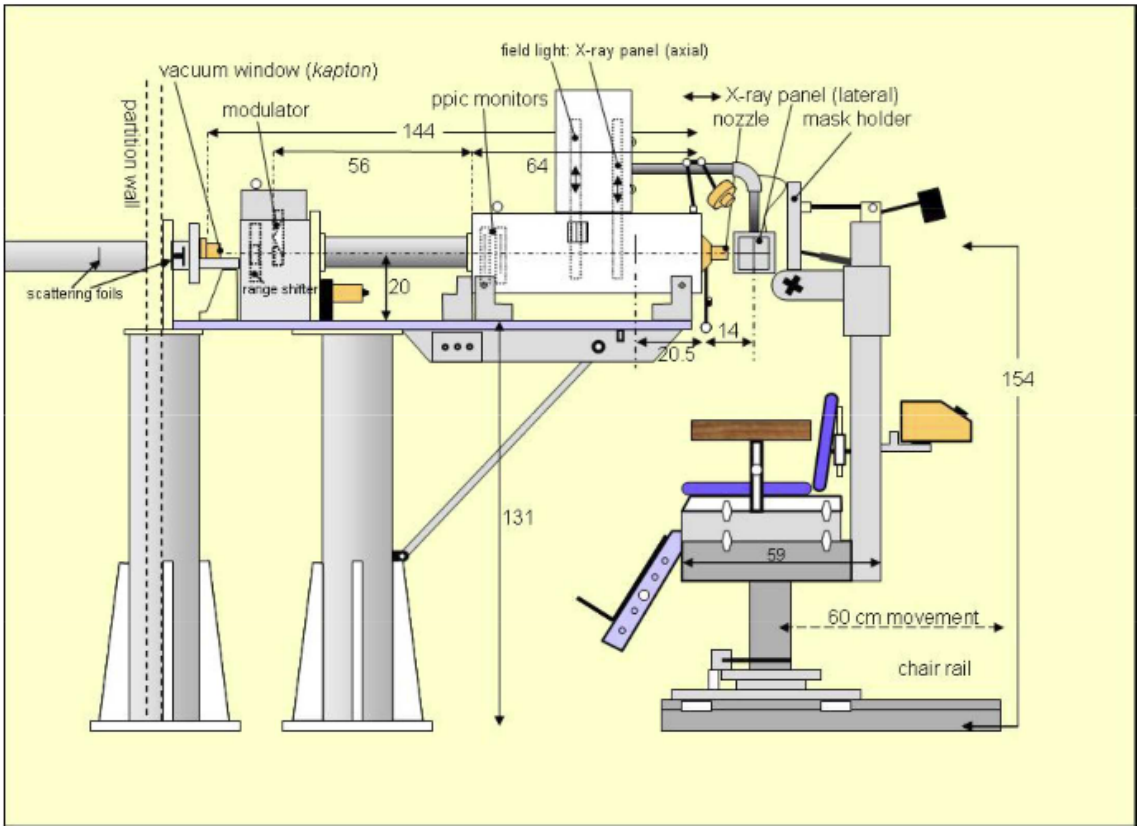

FIGURE 4.1: Schematic of the Clatterbridge beam line, courtesy of Dr Andrzej Kacperek.

4.2 The simulations

Monte Carlo simulations of the ocular beam-line were carried out using the FLUKA and MCNPX codes to compare the dosimetric accuracy for proton and neutron doses. The MCNPX simulations were done by Annelie Laidler and the results obtained are presented in [102]. For the activation studies and residual dose rates, only the FLUKA code was used.

For all simulations presented in this chapter, the latest version of the FLUKA Monte Carlo code was used: FLUKA 2011.2c.2. The pre-selected default PRECISIO was selected for all simulations. This options uses transport cuts of 100 keV for electrons, positrons and photons. The neutrons are transported down to thermal energies [93]. The electromagnetic physics was described by the EMF package, while the Boltzmann master equation (BME) theory was used to describe the hadronic interactions.[88] The hadron-nucleus nuclear interactions were treated by the PEANUT (PreEquilibrium-Approach-to-Nuclear-Thermalization) [88].

For activation studies, the IRRPROFI option was used to define the irradiation profile, while RESNUCLE and DCYSCORE options were used to estimate the activity of the

residual nuclei produced in the brass collimator and in air. The ambient dose equivalent rate was calculated using the USRBIN, DCYSCORE and AUXSCORE options. The results are given in μSv/s [93].

The results of the FLUKA simulations were calculated for proton beam energies between 55 MeV and 60 MeV. The maximum energy value was set at 60 MeV because this is the maximum energy provided by the Douglas Cyclotron.

For the MCNPX code, the proton transport physics of this code included energy straggling, multiple Coulomb scattering, elastic and inelastic scattering and nonelastic nuclear reactions. The neutrons were transported down to thermal energies. The results for the MCNPX code were calculated only for a proton beam with an energy of 60 MeV. More information about the MCNPX simulations can be found in [102].

For both codes, a simple geometry was used for simulations. A box ($8 \times 8 \times 15.9$ cm) was used as a water phantom (from 184.1 cm to 199 cm) in order to simulate the patient tissue. The water phantom was placed at 7 cm from the collimator which gave acceptable lateral beam spread.

The passive scattering components of the beam line were simulated, as shown in figure 4.2. The nozzle is 7 cm long and has a 34 mm internal diameter. A brass collimator was used to collimate the beam. The collimator aperture size was set at 1 cm. The total distance between the source and the patient is 180 cm. The simulations were performed using an un-modulated beam. The beam intensity is 3.12×10^{10} particles/s. Each simulation was made with a set of five runs, giving a total of 5×10^{6} protons which is enough for acceptable statistical error [89, 92].

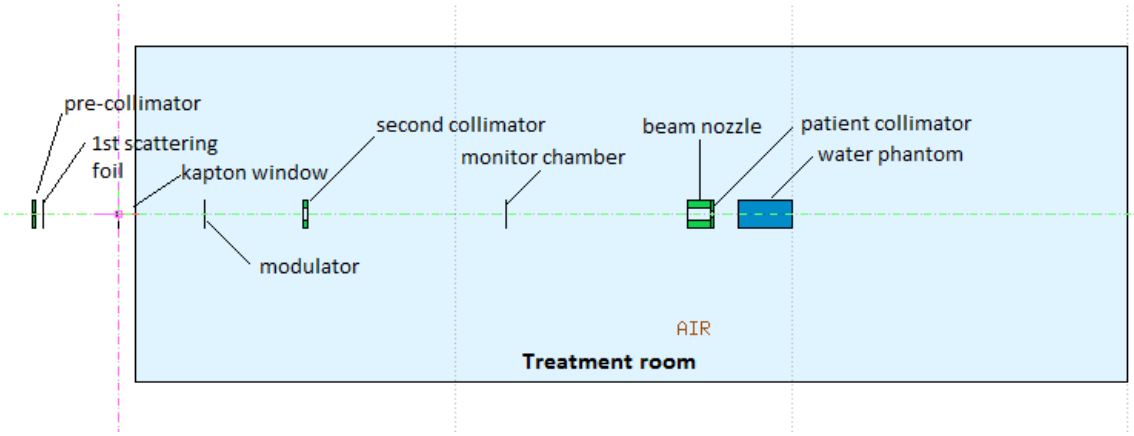

FIGURE 4.2: The Clatterbridge passive scattering system as simulated in FLUKA, showing the pre-collimator, 1st scattering foil, kapton window, modulator, 2nd collimator, monitor chamber, beam nozzle, patient collimator and water phantom (compare with figure 4.1).

4.3 Results

4.3.1 Bragg peak

For the first set of simulations, the Bragg peak was calculated in order to be compared with the experimental value. A 60 MeV proton beam was used to hit the water phantom. A pure mono-energetic proton beam was considered, as this represents the ideal case.

The FLUKA and the MCNPX codes were used for this Monte Carlo simulations and the results obtained were compared with the experimental values taken from [98]. The FLUKA simulation result showed that for a 60 MeV proton beam, the Bragg peak occurs at 3 cm depth in the water phantom as shown in figure 4.3. This is in agreement with the experimental results obtained in [98].

The FLUKA result was verified using the MCNPX code as presented in [102] and this is also shown in figure 4.3. The geometry used is the same as that used in FLUKA. The result shows clearly that the Bragg peak can be seen at approximately 3 cm depth. In conclusion, the peak location for 60 MeV protons showed no significantly differences between the FLUKA and the MCNPX codes when compared with the experimental measurements. This demonstrates that the FLUKA and the MCNPX Monte Carlo codes can reliable calculate the proton dose distribution.

The same simulations are conducted with the FLUKA code for proton beams with energies from 55 MeV up to 59 MeV, in order to study the depth-dose distribution as function of beam energy. The results showed that the depth-dose distribution increases in range when the proton beam energy is increased, as expected. The results are shown in figure 4.4.

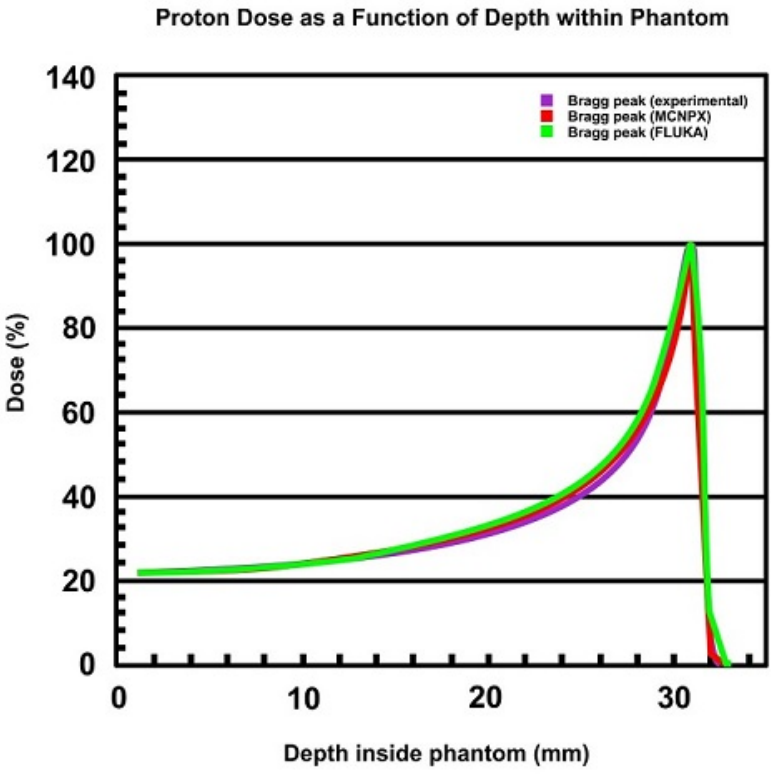

FIGURE 4.3: Depth-dose distribution in water phantom for a 60 MeV proton beam obtained with experimental results [98], FLUKA and MCNPX [102] along z axis.

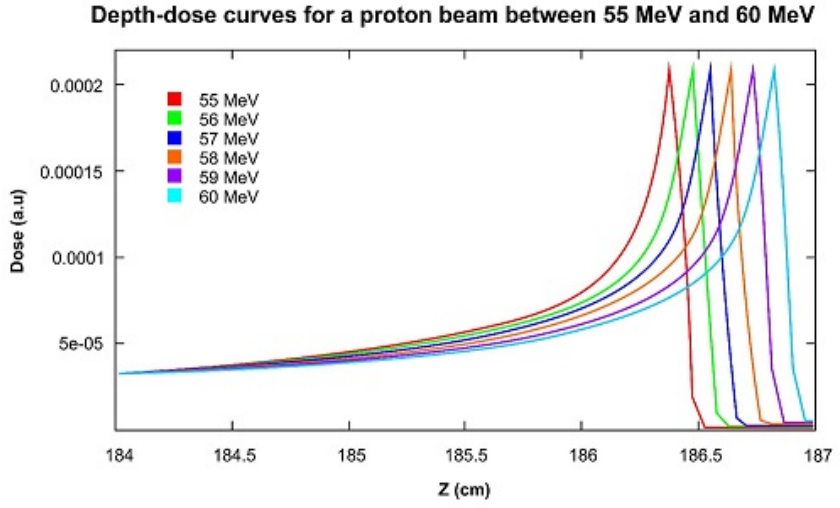

FIGURE 4.4: Depth-dose curves for a proton beam between 55 MeV and 60 MeV obtained in the water phantom (position between 184.1 cm and 199 cm in the FLUKA geometry) along the z axis.

4.3.2 Proton fluence and proton dose along the beam line

The next set of simulations was done to study the proton fluence distribution along the beam line.

The fluence is given in particles per cm^2 and it describes the density of particle tracks. The FLUKA results were normalized by the beam intensity which is 3.12×10^{10} particles/s so the fluences are presented for one second of operation.

This study is a very important aspect of pre-therapeutic studies as it offers information about the influence of the beam line components (scattering foils, range shifters, collimators) on the quality of the proton beam, which can be modified due to energy loss, multiple scattering and nuclear interactions. This can cause a non-uniform proton fluence distribution, hence a non-uniform dose distribution to the patient [100, 101].

The geometry used to study the proton fluence and dose is the same as used previously. The results are presented only for proton beams of 55 MeV and 60 MeV as these represent the extreme values used for treatment. The proton travels from left to right and at the furthest right it enters the phantom. For 60 MeV both FLUKA and MCNPX codes were used to determine the proton fluence.

Figure 4.5 shows the results for a proton beam with an energy of 55 MeV. The highest values was found in the modulating devices, 10^9 protons/cm^2, and in the brass collimator 10^6 protons/cm^2.

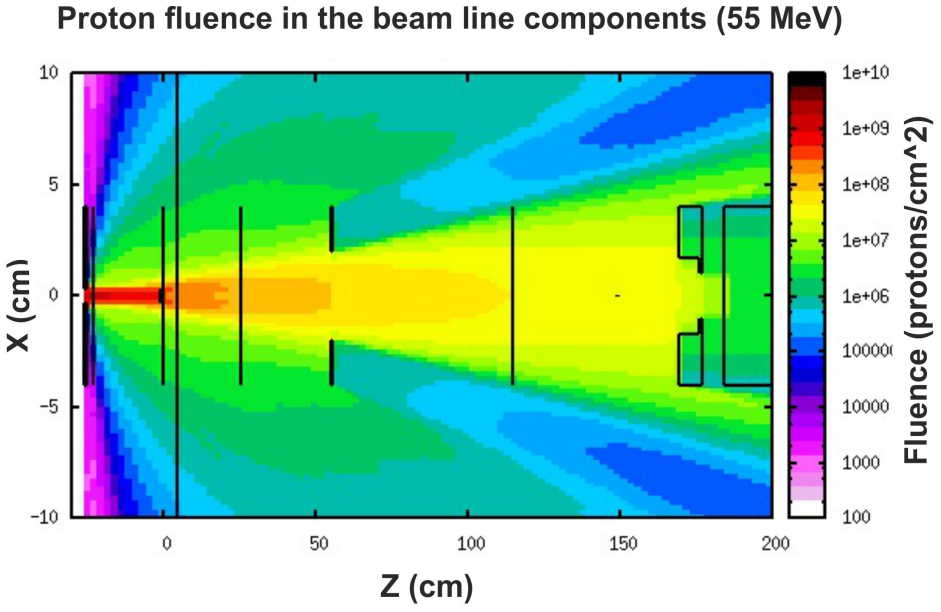

FIGURE 4.5: Proton fluence for 55 MeV along the beam line calculated in FLUKA.

Figure 4.6 shows the result obtained with FLUKA for a 60 MeV proton beam. The FLUKA result was compared with the MCNPX result showed in figure 4.7 for the same beam energy.

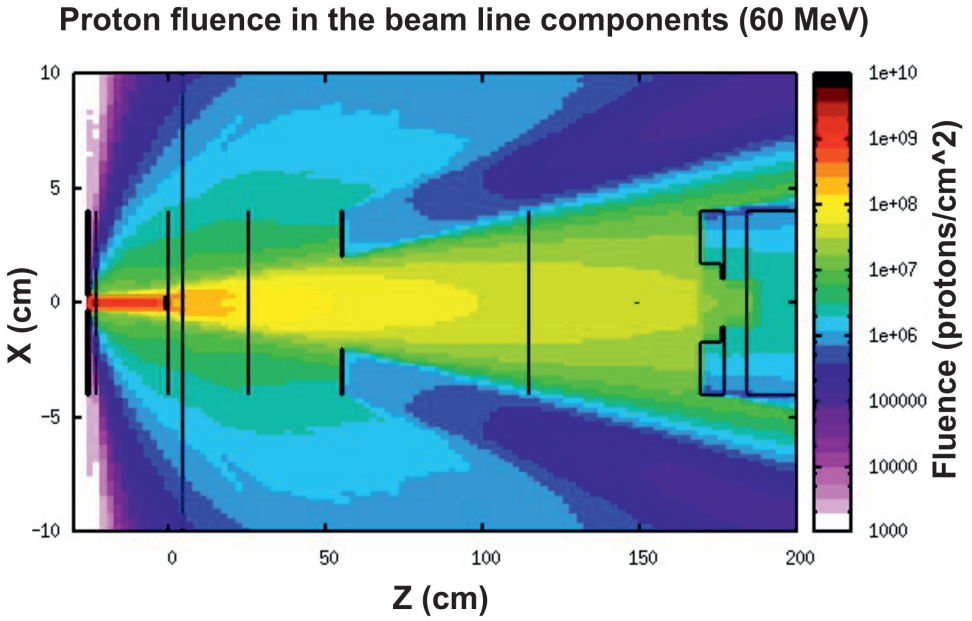

FIGURE 4.6: Proton fluence for 60 MeV along the beam line calculated in FLUKA.

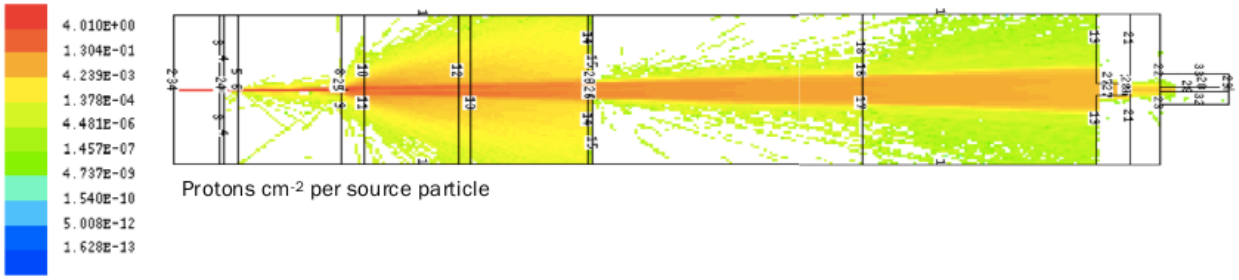

FIGURE 4.7: Proton fluence for 60 MeV along the beam line calculated in MCNPX. Taken from [102].

The results obtained with both Monte Carlo codes agreed very well. Most secondaries are obtained in the modulating devices and at the brass collimators. For a 60 MeV proton beam, the maximum fluence obtained is 10^9 protons/cm^2 into the modulating devices and 10^6 protons/cm^2 into the patient brass collimator. The MCNPX results are expressed in protons per cm^2 per source particle and need to be multiplied by the beam intensity 3.12×10^{10} particles/s, mentioned above, in making a comparison.

Next, the proton dose coming out from the beam line was calculated for a 55 MeV and a 60 MeV proton beam, using the same characteristics as previously. The results are

presented in figure 4.8 and figure 4.9. For this set of simulations, only the FLUKA Monte Carlo code was used.

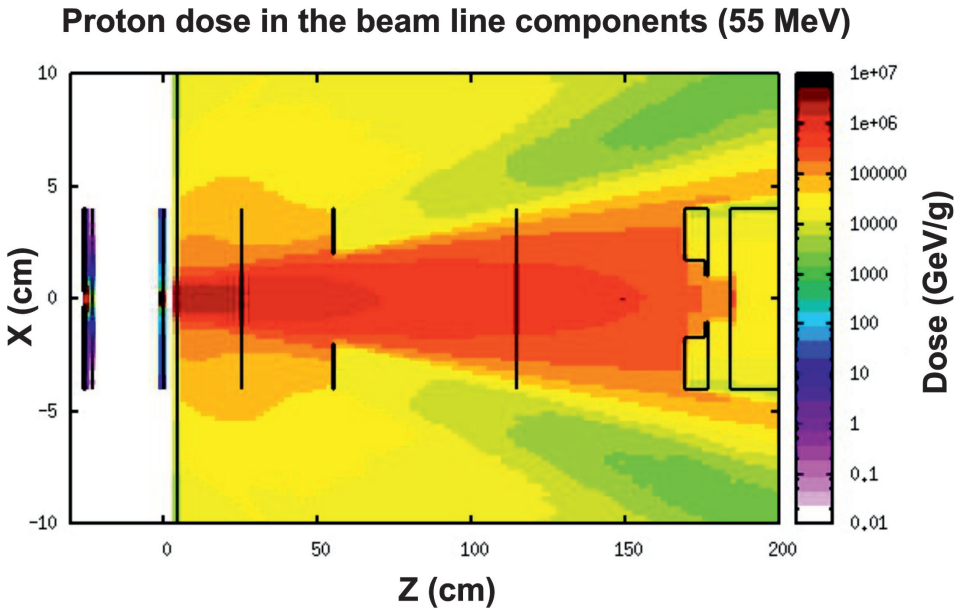

FIGURE 4.8: Proton dose for 55 MeV along the beam line calculated in FLUKA.

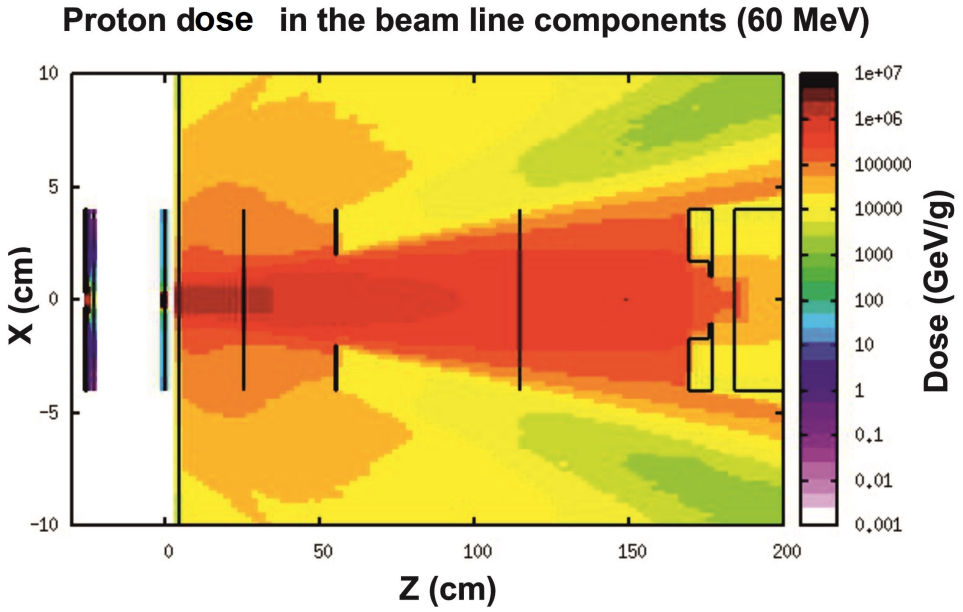

FIGURE 4.9: Proton dose for 60 MeV along the beam line calculated in FLUKA.

The results showed no important differences between a 55 MeV and a 60 MeV proton beam. The maximum proton dose coming out from the beam line is reasonably low 1×10^4 GeV/g. In conclusion, the beam line components does not alter the quality of the proton beam and most of the protons will reach the water phantom.

4.3.3 Neutron fluence and neutron secondary dose along the beam line

The dose delivered to the healthy tissue by the secondaries it is a possible way of concern. These calculations are important to see if the patient is exposed to a whole body irradiation.

The production of secondary neutrons will depend on the geometry and the materials of the proton beam delivery system. For this work the configuration used was the one described in figure 4.2. A brass collimator was used to conform the beam to the tumour volume [100].

For the simulation of the neutron fluence and neutron dose along the beam line, a 60 MeV proton beam was used. For neutron fluence along the beam line, the FLUKA results were compared with the MCNPX results.

The neutron fluence obtained with the FLUKA code is shown in figure 4.10. As for proton fluence, the neutron fluence was found to be higher in the modulating devices and the brass collimator, approximately 10^5 neutrons/cm^2.

The values obtained with the MCNPX code are showed in figure 4.11. The highest dose was obtained in the beam nozzle and in the brass collimator. The MCNPX results show a good agreement with the results obtained with the FLUKA code.

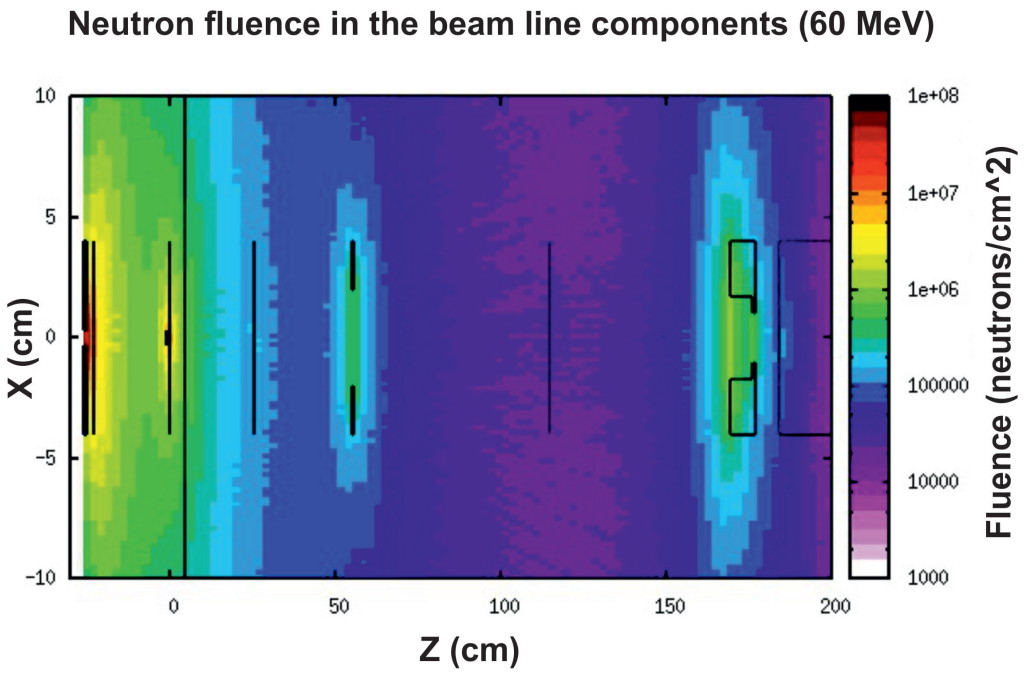

FIGURE 4.10: Neutron fluence for 60 MeV in the beam line calculated with FLUKA.

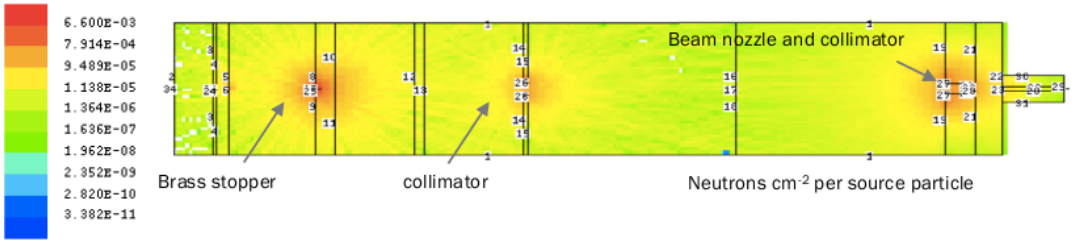

FIGURE 4.11: Neutron fluence for 60 MeV in the beam line calculated with MCNPX. Taken from [102].

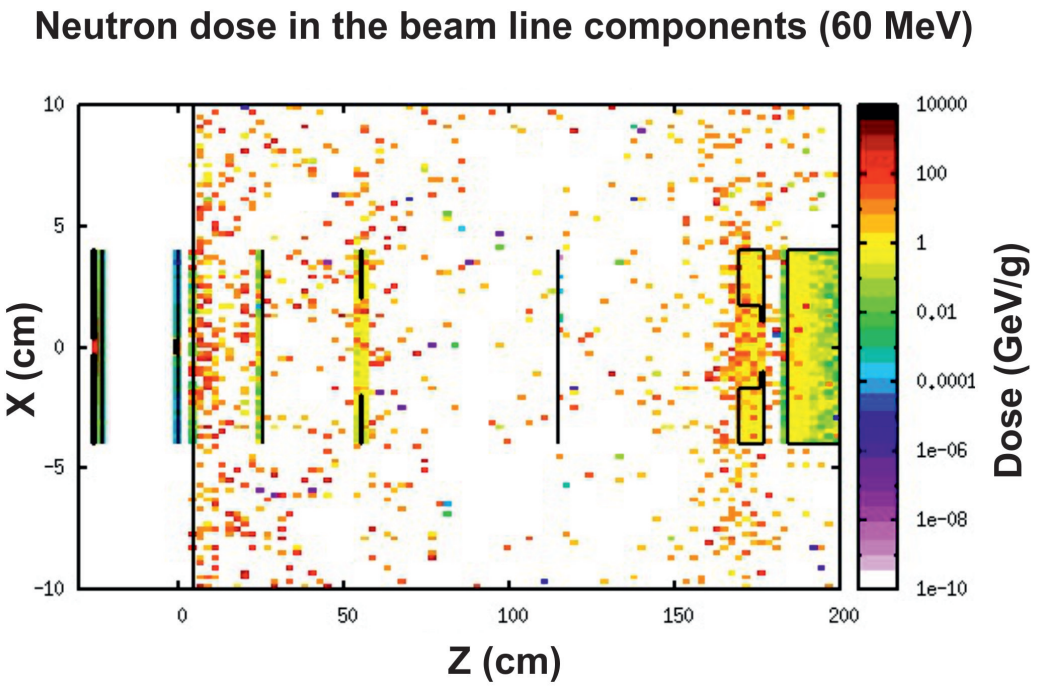

FIGURE 4.12: Neutron dose for 60 MeV in the beam line calculated with FLUKA.

The next task was to calculate the neutron dose. This was calculated with the FLUKA code using the same input and parameters as for proton dose.

The results showed that most of the neutrons dose is produced around the brass components of the beam line as shown in figure 4.12. The maximum neutron dose was found to be 1 GeV/g for each set of operation.

4.3.4 Neutron dose equivalent

The Clatterbridge Cancer Centre uses a passive scattering system to deliver the proton beam, therefore the patient will be exposed to a whole-body neutron dose.

The aim of this study is to estimate this potential exposure of the patient to secondary radiation. For this, the neutron ambient dose equivalent has been simulated. A model where the eye diameter was 24 mm and the tumour was in the centre of the eye where the Bragg peak occurs (approximately 3 cm depth) was considered [100].

In FLUKA, the dose equivalent is given in pSv/primary. As the maximum beam intensity delivered by the cyclotron is 3.12×10^{10} p/s, the normalization factor: $10^{-6}\times3.12\times10^{10}$ was used in order to obtain the results in μ Sv/s. This normalization factor is valid when the maximum beam intensity is used. If the proton treatments use a lower beam intensity, the normalization factor just scales. A proton beams of 55 MeV and 60 MeV were used for comparison. For radiation protection purposes, the AMB74 option (Ambient dose equivalent from ICRP74 [94] and Pelliccioni data [95]) was used. For 60 MeV, the result obtained with FLUKA was verified with MCNPX.

The neutron dose equivalent inside and outside the irradiation field was calculated. The FLUKA Monte Carlo results determined that the neutron dose equivalent goes to greater depths in the target as the proton energy is increased (energy range is 55 MeV-60 MeV).

For a 55 MeV proton beam, the neutron dose equivalent in the target volume was found to be 50 $\mu Sv/s$. Outside the target volume, the dose is between 10 $\mu Sv/s$ and 1 $\mu Sv/s$ and it goes up to 13 centimetres depth from in the water phantom as shown in figure 4.13.

When the energy was increased to 60 MeV, the neutron dose equivalent deposited in the target volume was found to be 70 μ Sv/s. After the target volume, the neutron dose equivalent is decreasing from 20 μ Sv/s to 1 μ Sv/s as shown in figure 4.14. This estimation is made for a neutron dose deposited in tissue not irradiated with primary particles. The MCNPX results showed a significant agreement with FLUKA results as shown in figure 4.15. The highest neutron dose was found around the Bragg peak, at 3 cm depth in the water phantom, around 4×10^{-6} μ Sv/h/primary and after, the neutron dose is decreasing down to 2.9×10^{-8} μ Sv/h/primary. This corresponds to 35 μ Sv/s and 25 μ Sv/s for a beam intensity of 3.12×10^{10} p/s.

These results are relevant only for eye treatment (low energy) and cannot be used to evaluate the radiation exposure of other tissues, as the ambient dose equivalent is sensitive to energy. These results do not take into account the neutron production in the

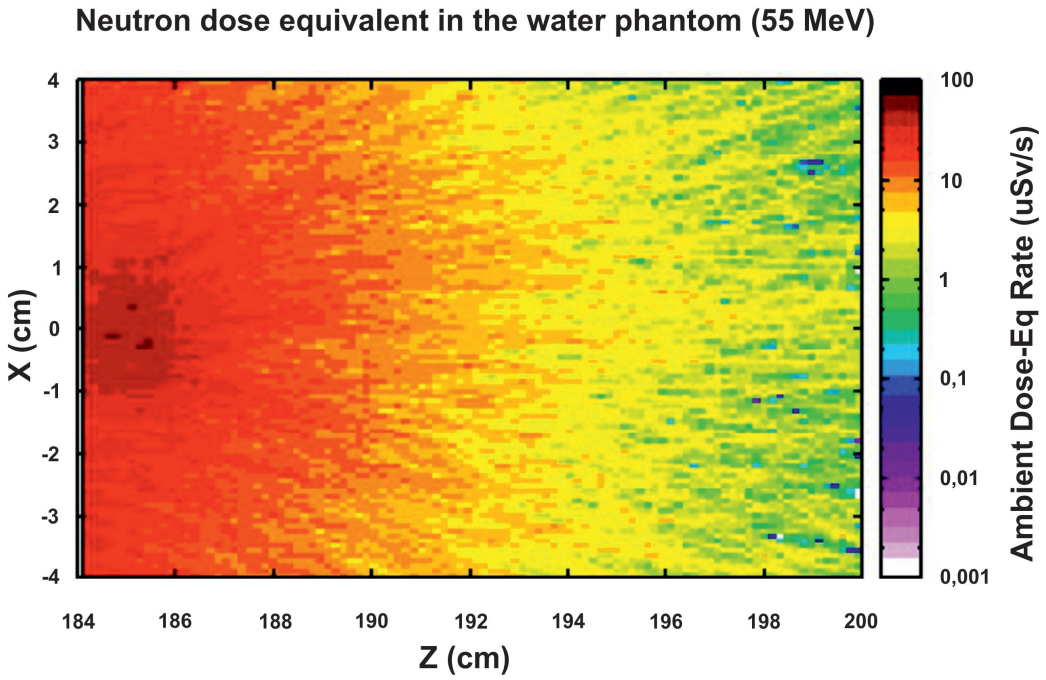

FIGURE 4.13: Neutron dose equivalent for 55 MeV in the water phantom calculated with FLUKA.

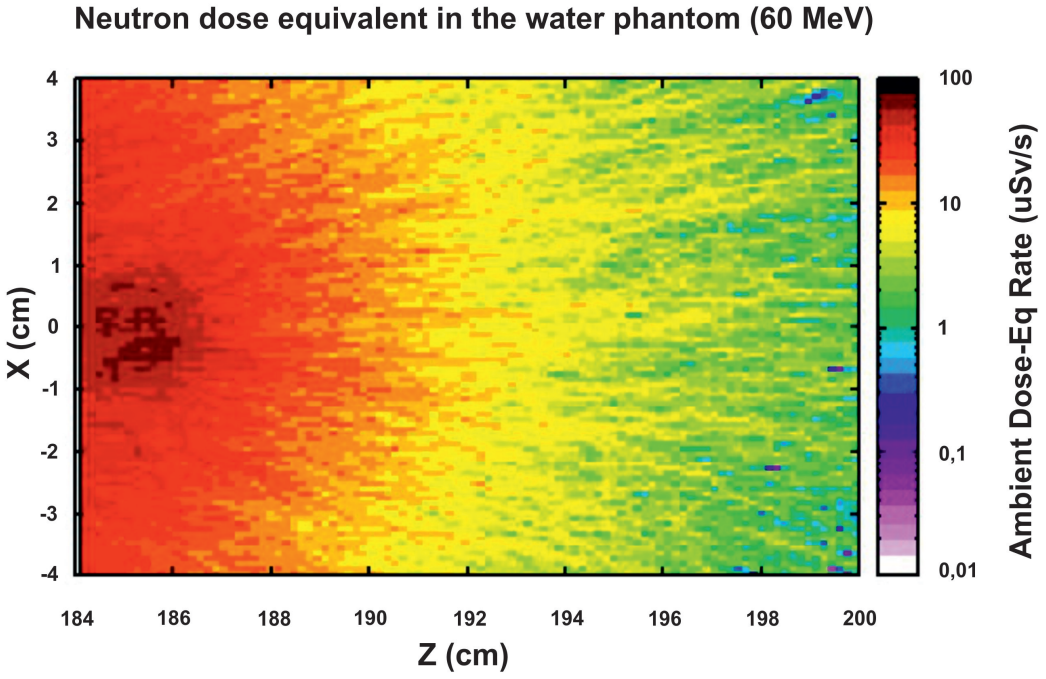

FIGURE 4.14: Neutron dose equivalent for 60 MeV in the water phantom calculated with FLUKA.

patient. Therefore, a full study will be needed to understand the mechanism of the secondary neutron generation inside the body and to estimate the complications induced by these internal neutrons [100].

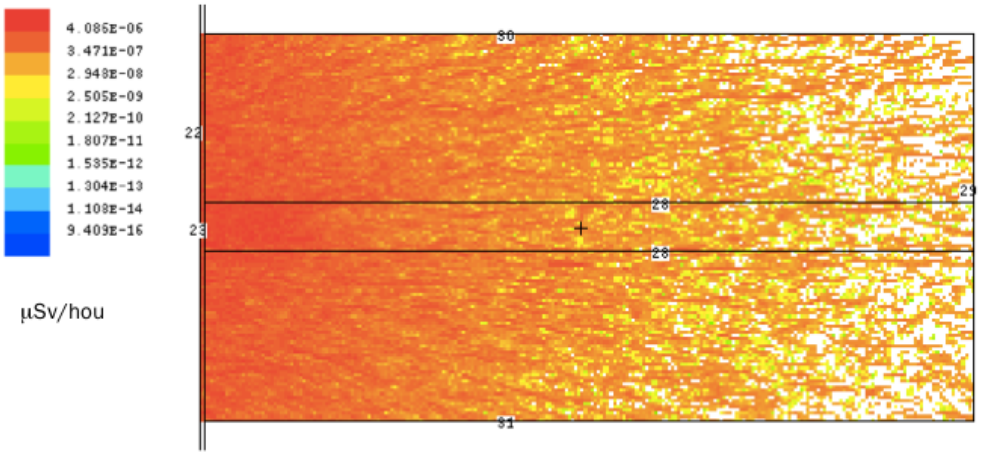

FIGURE 4.15: Neutron dose equivalent for 60 MeV in the water phantom calculated with MCNPX. Taken from [102].

In conclusion, for both Monte Carlo codes, the simulations showed that neutron dose equivalent is increasing, from 50 μ Sv/s to 70 μ Sv/s, as the incident beam energy is increased from 55 to 60 MeV and that the maximum value of the neutron equivalent dose is close to the position of the Bragg peak and, after this, it is decreasing gradually. These values indicate that the secondary neutron dose equivalent is small and not a problem for clinical treatments.

Unfortunately, the results obtained with the Monte Carlo methods can not be compared with any experimental measurements from Clatterbridge as no such type of measurements were conducted as this facility. Therefore, in order to benchmark the results presented in this section, the values of the neutron dose equivalent were compared with the experimental values measured at a similar facility, CCB IFJ PAN in Krakow [103]. The neutron dose equivalent was measured for a 60 MeV proton beam using a neutron rem meter in two locations: the patient chair and on the floor near the patient chair. The results obtained were 0.82 μ Sv/s at the patient chair and 0.25 μ Sv/s on the floor. These values are considered low and not hazardous for the patients as they are small compared with the limits set by The Ionising Radiation Regulations 1999 [40], where the maximum allowed dose for a person exposed to ionising radiations from the medical reasons is 5 mSv in any period of 5 consecutive calendar years [40].

4.3.5 Study of radioactivity induced in a patient-specific collimator and in the treatment room

Activity induced in beam line components by particle nuclear interactions is an important aspect of radiation protection. Elements such as collimators become radioactive as a result of induced activation. Induced radioactivity is produced due to direct nuclear

interactions of the incident beam or indirect interactions of secondary particles with the nuclei of the materials of the beam line components, in which unstable isotopes are produced. The activation causes ambient dose rates inside the facility room, and also in the accelerator components. Therefore, these components must be treated as radioactive waste [69]. This radiation induced in the accelerator components and air depends on several factors: particle type, energy, beam intensity and the materials irradiated.

The Clatterbridge Cancer Centre is delivering a beam using the passive scattering system. The passive scattering system requires several components in the beam line in order to provide uniform coverage of the target. The proton beam will interact with these components and will produce high-energy neutrons. The dominant source of the neutron dose is the final collimator located close to the patient [25].

The purpose of this study is to evaluate the radioactivity of a patient-specific brass collimator, calculating the residual dose rates and the activities of the radionuclides generated during the irradiation since this device is used consecutively during the treatment and this aspect is very important for patients' and therapists' safety[104–106]. The collimators are usually made of brass. Brass is an alloy of copper and zinc. The brass density can vary from 8.4 to 8.7 g/cm^3.

The collimator aperture has the shape of the target and has the role to shape the proton beam and to block the protons from the outer region of the tumour volume. This device is manufactured for every patient which means that the therapists have to change it after every treatment session and, therefore, the radioactivity studies are very important as these devices can become radioactive due to exposure to the proton beam [104–106].

The simulations were performed for a 60 MeV proton beam impinging a brass collimator, modelled as a brass block with a density of 8.52 g/cm^3 with a central aperture. The block dimensions are $8 \times 8 \times 2.5$ cm. The radius of the aperture is 1 cm. The irradiation profile was set for 1 minute irradiation time per day, for 3 days with one day off between the sessions. The beam intensity was set for 3.12×10^{10} protons per second as this is the intensity used for treatments. The radionuclides and the ambient dose equivalent rate were calculated for five decay times: at the end of irradiation, after 1 hour, 1 month, 3 months and 1 year.

The IRRPROFI option was used to define the irradiation profile, while RESNUCLE and DCYSCORE options were used to estimate the activity of the residual nuclei produced in the brass collimator. The ambient dose equivalent rate was calculated using the USRBIN, DCYSCORE and AUXSCORE options. The results are given in μSv/hour [93].

Radionuclide	$T_{1/2}$	**Activity (Bq)**	**Activity limit (Bq) [40]**
^{206}Bi	6 d	1.9×10^3	10^5
^{205}Bi	15.31 d	1.4×10^3	10^6
^{203}Pb	51 h	4.9×10^3	10^6
^{203}Bi	11.76 h	8.2×10^3	10^6
^{202}Bi	1.72 h	3.2×10^3	10^6
^{201}Tl	72.91 h	4.7×10^2	10^6
^{201}Pb	9.33 h	1.1×10^3	10^6
^{201}Bi	108 m	5.6×10^2	10^6
^{200}Tl	26 h	1.0×10^2	10^6
^{200}Pb	21 h	1.3×10^2	10^6
^{70}Ga	21.14 m	1.3×10^2	10^6
^{69}Zn	56.4 m	4.3×10^2	10^6
^{68}Ga	67.71 m	6.4×10^3	10^5
^{67}Cu	61.83 h	3.6×10^2	10^6
^{67}Ga	3.261 d	6.5×10^3	10^6
^{66}Ga	9.49 h	1.2×10^4	10^5
^{65}Ni	2.51 h	1.5×10^2	10^6
^{65}Zn	244.26 d	4.3×10^2	10^6
^{65}Ga	15.2 m	5.8×10^3	10^5
^{64}Cu	12.7 h	4.7×10^4	10^6
^{63}Zn	38.47 h	6.7×10^4	10^5
^{62}Zn	9.18 h	2.2×10^4	10^6
^{61}Co	1.65 h	7.5×10^2	10^6
^{61}Cu	3.33 h	7.4×10^4	10^6
^{60}Cu	23.7 m	1.1×10^4	10^5
^{58}Co	70.86 d	7.3×10^2	10^6
^{57}Co	271.7 d	1.5×10^2	10^6
^{57}Ni	35.6 h	5.2×10^2	10^6
^{56}Mn	2.57 h	93.7	10^5

TABLE 4.1: The most abundant radionuclides in the collimator after irradiation for a 60 MeV proton beam together with the limits allowed by IRR99 [40].

The activities of the most abundant radionuclides produced in the collimator immediately after irradiation, are listed in the table 4.1 together with the limits allowed by IRR99 [40].

After one hour of cooling time, the most abundant radionuclides can still be identified in the collimator as shown in table 4.2. After 1 month of cooling time, radionuclides with a longer half-lives are shown in table 4.3. The others fall essentially to 0. The radionuclides present after 1 month of decay are still present after 3 months of decay of cooling time, apart from ^{206}Bi, ^{67}Ga which have already disappeared as shown in table 4.4. The activity of radionuclides with half-lives longer than 1 year is insignificant, therefore the results will not be discussed.

Radionuclide	$T_{1/2}$	**Activity (Bq)**	**Activity limits (Bq) [40]**
^{206}Bi	6 d	1.9×10^3	10^5
^{205}Bi	15.31 d	1.4×10^3	10^6
^{203}Pb	51 h	4×10^2	10^6
^{203}Bi	11.76 h	7.7×10^3	10^6
^{202}Bi	1.72 h	2.1×10^3	10^6
^{201}Tl	72.91 h	4.6×10^2	10^6
^{201}Pb	9.33 h	1.1×10^3	10^6
^{201}Bi	108 m	3.9×10^2	10^6
^{200}Tl	26 h	1.0×10^2	10^6
^{200}Pb	21 h	1.2×10^2	10^6
^{70}Ga	21.14 m	8.0	10^6
^{69}Zn	56.4 m	3.1×10^2	10^6
^{68}Ga	67.71 m	3.5×10^3	10^5
^{67}Cu	61.83 h	3.6×10^2	10^6
^{67}Ga	3.261 d	6.4×10^3	10^6
^{66}Ga	9.49 h	1.1×10^4	10^5
^{65}Ni	2.51 h	1.1×10^2	10^6
^{65}Zn	244.26 d	4.3×10^2	10^6
^{65}Ga	15.2 m	3.8×10^2	10^5
^{64}Cu	12.7 h	4.4×10^4	10^6
^{63}Zn	38.47 h	2.2×10^4	10^5
^{62}Zn	9.18 h	2.1×10^4	10^6
^{61}Co	1.65 h	4.9×10^2	10^6
^{61}Cu	3.33 h	6.0×10^4	10^6
^{60}Cu	23.7 m	1.9×10^3	10^5
^{58}Co	70.86 d	7.2×10^2	10^6
^{57}Co	271.7 d	1.5×10^2	10^6
^{57}Ni	35.6 h	5.1×10^2	10^6
^{56}Mn	2.57 h	72	10^5

TABLE 4.2: The most abundant radionuclides in the collimator after 1 hour of cooling time for a 60 MeV proton beam together with the limits allowed by IRR99 [40].

Radionuclide	$T_{1/2}$	**Activity (Bq)**	**Activity limit (Bq) [40]**
^{206}Bi	6 d	70.3	10^5
^{205}Bi	15.31 d	3.6×10^2	10^6
^{65}Zn	244.26 d	3.9×10^2	10^6
^{58}Co	70.86 d	6.0×10^2	10^6
^{57}Co	271.7 d	1.4×10^2	10^6

TABLE 4.3: The most abundant radionuclides in the collimator after 1 month of cooling time for a 60 MeV proton beam together with the limits allowed by IRR99 [40].

Radionuclide	$T_{1/2}$	**Activity (Bq)**	**Activity limit (Bq) [40]**
^{205}Bi	15.31 d	23.9	10^5
^{65}Zn	244.26 d	3.3×10^2	10^6
^{58}Co	70.86 d	3.3×10^2	10^6
^{57}Co	271.7 d	1.2×10^2	10^6

TABLE 4.4: The most abundant radionuclides in the collimator after 3 months of cooling time for a 60 MeV proton beam.

The results obtained for this study, showed that the short-lived isotopes like ^{202}Bi ($T_{1/2}$= 1.72 h), ^{201}Bi ($T_{1/2}$= 108 m), ^{70}Ga ($T_{1/2}$=21.14 m), ^{69}Zn ($T_{1/2}$=56.4 m), ^{68}Ga ($T_{1/2}$=67.71 m) will not be accumulated in the collimator.

Other isotopes, with longer half-lives like ^{66}Ga, ^{64}Cu, ^{63}Zn, ^{62}Zn, ^{61}Cu and ^{58}Co will not decay completely and the activity will still be high after 1 hour of cooling time even though they are in the IRR99 limits by a factor of 10, the ALARA principle suggests that the exposure after one hour from irradiation should be minimized. Special attentions should be given to ^{64}Cu as the activity is high and this radioisotope is a gamma emitter causing radiation exposure and ^{58}Co is another dangerous radioisotope as it is considered carcinogenic [105, 106]. Direct contact should be avoided or tools should be used to handle the contaminated collimator. When compared with the activity limits recommended in IRR99 [40], the activity of certain isotopes like ^{68}Ga, ^{66}Ga, ^{64}Cu, ^{63}Zn, ^{62}Zn, ^{61}Cu and ^{60}Cu will have a significant activity but the values do not exceed the limits allowed by IRR99 [40] immediately after irradiation. Even after one hour of cooling, the activity of ^{66}Ga and ^{63}Zn is still only by a factor of 10 lower than the legal limits [40].

These findings strongly suggest that the patient collimator should be regarded as non-radioactive but the personnel should wait one hour before handling the brass collimator to minimize the external exposure.

In order to verify these results obtained with FLUKA Monte Carlo code, a collimator was measured using a Sodium Iodide counter. Unfortunately, no results were obtained as the collimator was older than a year. However this confirmed the absence of the long-lived isotopes as predicted.

After simulating the radioactivity induced in the patient collimator, another important aspect is to calculate the radioactivity induced in the air of the treatment room. The treatment room geometry was estimated from observation as no engineering plans were available. The dimensions considered were 6 x 4 x 3 m. The wall thickness is 3 m. These dimensions are general dimensions for a proton therapy treatment room [107]. During the proton treatment, the protons interact with matter, producing fast neutrons. The

fast neutrons will interact with the atoms from the air, producing short-lived radionuclides like ^{15}O, ^{13}N, ^{11}C [107]. After multiple collisions, the fast neutrons will slow down to thermal energies. The thermal neutrons will be captured by the ^{40}Ar from the air and radioactive ^{41}Ar will be produced. ^{41}Ar is a beta and gamma emitter and it represents the major contributor of the air activation [107, 108]. As these radioisotopes and ^{7}Be (produced by protons on nitrogen) are the principal ones responsible for the dose induced to public and staff [107], only the activity for these radioisotopes will be presented in the tables below.

Radionuclide	$T_{1/2}$	**Activity (Bq)**	**Activity limit (Bq) [40]**
^{41}Ar	109.61 m	6.1×10^{2}	10^{9}
^{15}O	122.24 s	5.4×10^{1}	10^{9}
^{13}N	9.96 min	4.7×10^{5}	10^{9}
^{11}C	20.33 min	5.4×10^{5}	10^{6}
^{7}Be	53.28 d	9.3×10^{3}	10^{7}

TABLE 4.5: The most abundant radionuclides in air after irradiation with a 60 MeV proton beam.

After irradiation, the simulations showed that ^{15}O, ^{13}N, ^{11}C and ^{7}Be are the primary activation products of air as shown in table 4.5. For ^{11}C, the activity was found to be 10 times lower than the limit suggested in IRR99 [40]. For ^{41}Ar, ^{15}O and ^{13}N the activity in air is significantly lower than the IRR99 limit [40], while ^{7}Be has the lowest activity. These findings suggest that immediately after irradiation, the induced activity in air is lower than the legal limits and the treatment room can be freely accessed as the personnel will not be exposed to a radiological risk.

After 1 hour from the irradiation, the ^{15}O has entirely disappeared as shown in table 4.6, while the activity of ^{41}Ar, ^{13}N, ^{11}C and ^{7}Be will be 10 times lower.

Radionuclide	$T_{1/2}$	**Activity (Bq)**	**Activity limit (Bq) [40]**
^{41}Ar	109.61 m	4.1×10^{2}	10^{9}
^{13}N	9.96 min	7.2×10^{3}	10^{9}
^{11}C	20.33 min	7.0×10^{4}	10^{6}
^{7}Be	53.28 d	9.3×10^{3}	10^{7}

TABLE 4.6: The most abundant radionuclides in the air after 1 hour of cooling time with a 60 MeV proton beam.

The medium half-live radiosotope ^{7}Be will still be present in the air after 1 month, 3 months and 1 year of cooling time, but the activity will be significantly lower.

The results demonstrate that immediately after irradiation, the activity induced in air is lower than the IRR99 limits [40], therefore, the radioactivity induced in air does not represent a radiological risk to the personnel. Nevertheless, for these results the air was

considered stationary. If the ventilation system is operational during treatment sessions this could release radioactivity into the environment. This will require expanded study.

In order to calculate the induced residual dose rate produced by the interactions of protons with the beam line components, air and concrete in the treatment room, further simulations were made using the same irradiation profile as above: 1 minute irradiation time per day, for 3 days with one day off between the irradiation sessions. The dose rate was calculated for 4 cooling times (after irradiation, 1 hour, 1 month and 3 months). As mentioned before, treatment room dimensions were just assumed as no engineering plans were available. The ambient dose equivalent was calculated along the central axis X-Z of the collimator. The results are given in μSv/hour.

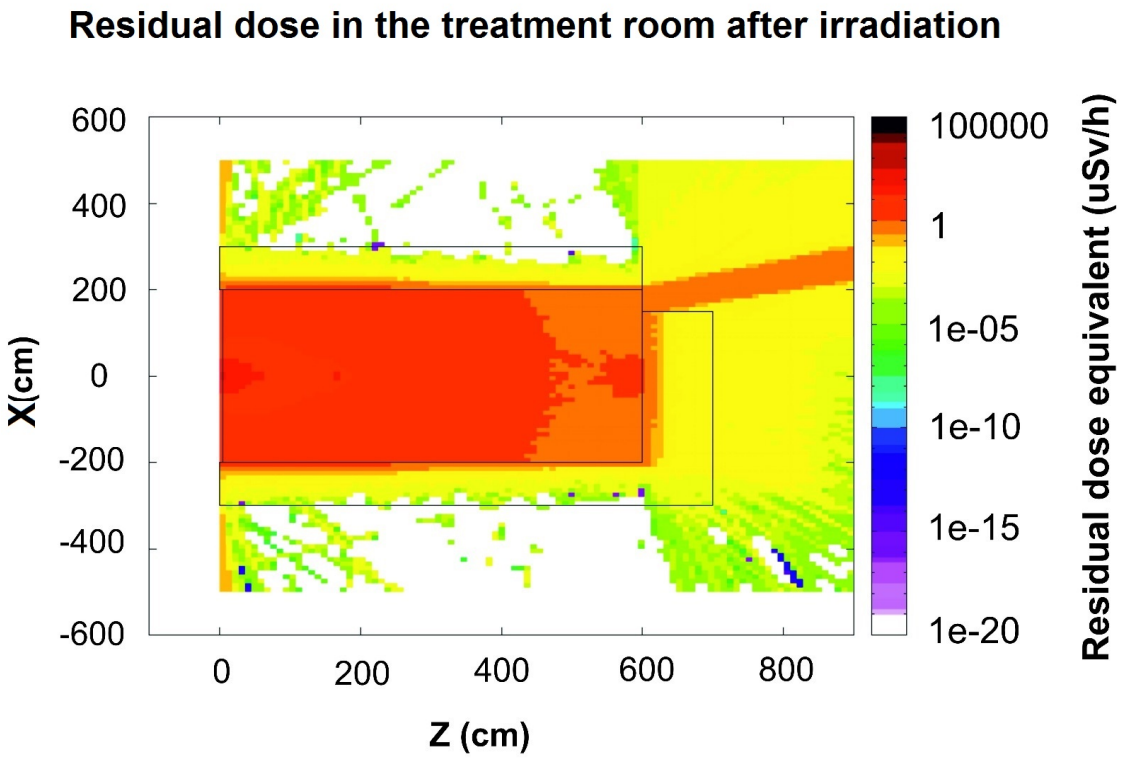

FIGURE 4.16: Residual dose in beam line, concrete and air after irradiation for a 60 MeV proton beam.

The results showed that the residual dose in the treatment room, immediately after irradiation is of the order of several μ Sv/h, especially near the beam line and it decreases gradually, to 1 μ Sv/h near the exit, as shown in figure 4.16. Due to the fact that no door was added in the simulations, the dose outside the treatment room is around 1 μ Sv/h in the doorway and it decreases behind the shielding wall. After 1 hour the dose near the beam line is still of order of 5 μ Sv/h, but near the exit, the value is lower than 1 μ Sv/h, as shown in figure 4.17. Behind the shielding wall, the dose decreases down to 10^{-5} μ Sv/h. After 1 month, the value of the dose is 0.5 μ Sv/h in the beam line

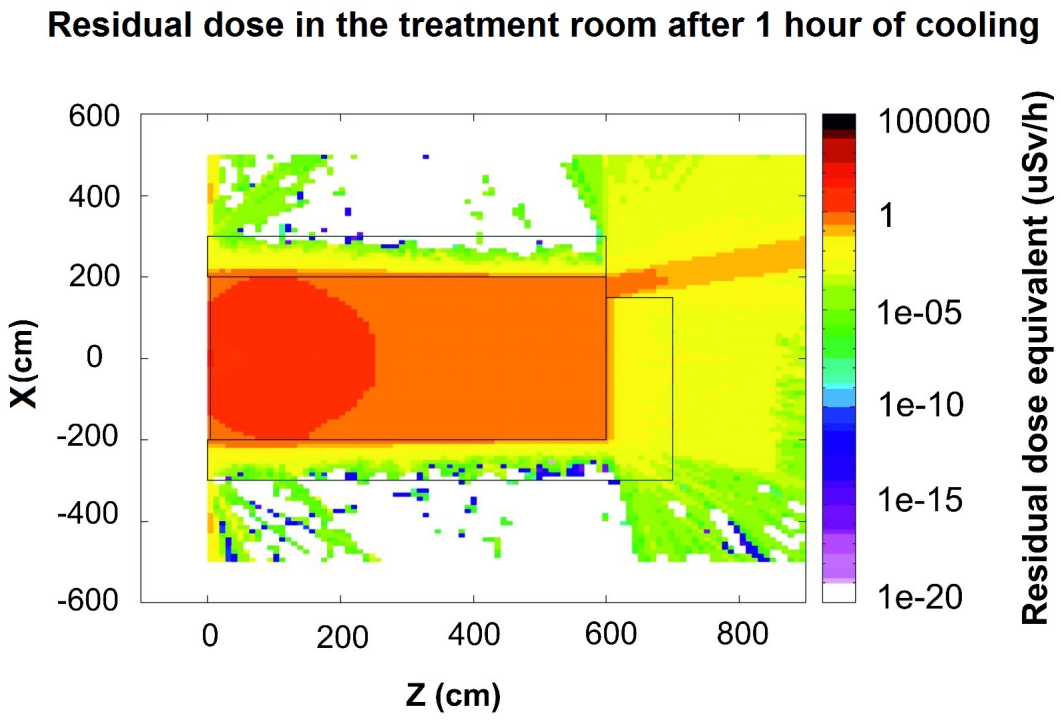

FIGURE 4.17: Residual dose in beam line, concrete and air after 1 hour of cooling time for a 60 MeV proton beam.

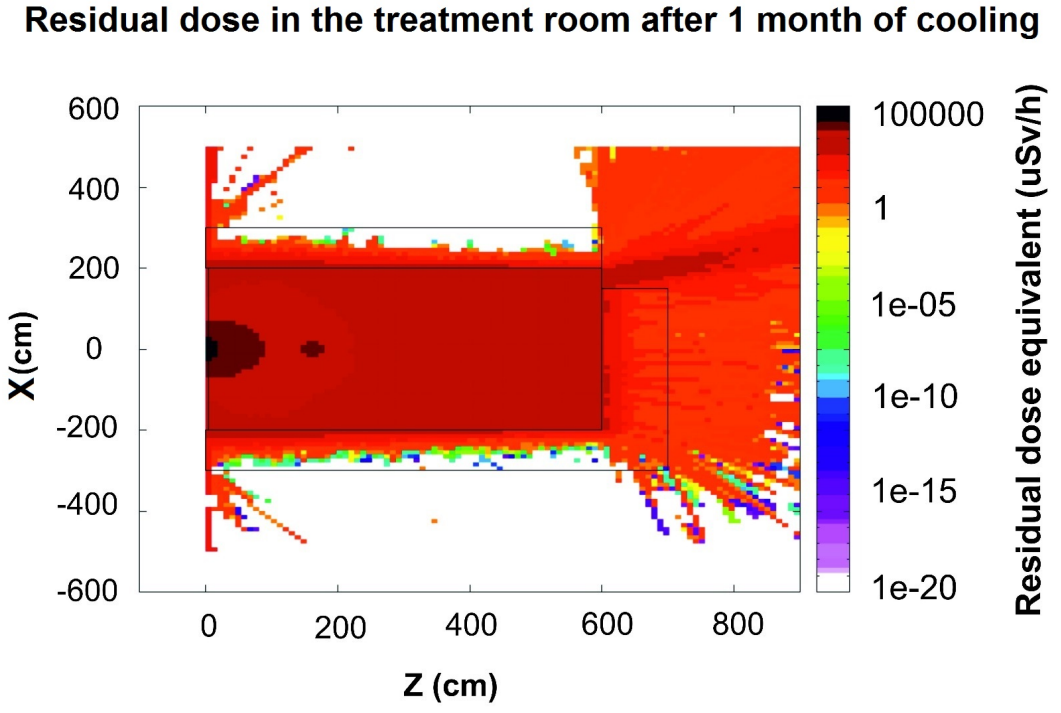

FIGURE 4.18: Residual dose in beam line, concrete and air after 1 month of cooling time for a 60 MeV proton beam.

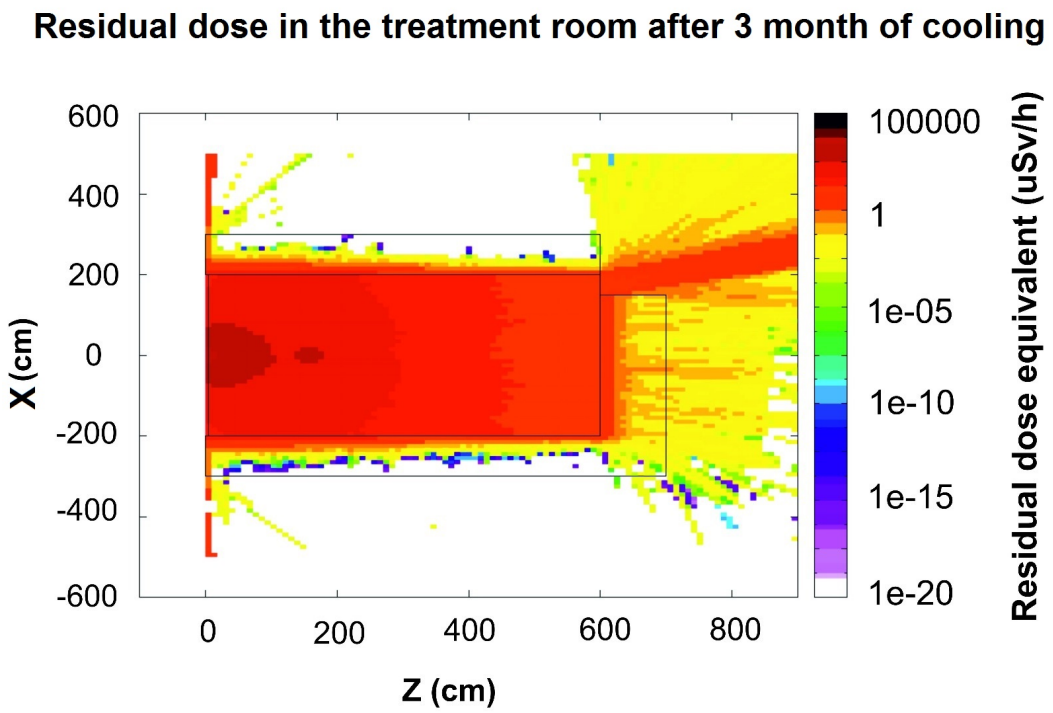

FIGURE 4.19: Residual dose in beam line, concrete and air after 3 month of cooling time for a 60 MeV proton beam.

area and around 10^{-5} μ Sv/h outside the treatment room as shown in figure 4.18. After 3 months from irradiation, the residual dose equivalent decreases down to 0.05 μ Sv/h near the beam line and it decreases down to 10^{-6} μ Sv/h at the exit point as shown in figure 4.19.

The aim of these calculations was to provide residual dose values for radiation safety purposes for patients and personnel. They should help to ensure compliance with the UK regulations and to reduce the potential harmful of external radiation exposure. As the UK regulations are [40]: 20 mSv in a calendar year for employees aged 18 years or over, including members of the public and 1 mSv in a calendar year for any other person, including members of the public and employees under 18 who cannot be classed as trainees and pregnant employees, the results obtained show that the ambient dose equivalent values are well within these limitations.

4.4 Conclusion

Proton therapy is a complicated technique and the accuracy of the treatment depends on several factors arising from the physical and biological properties of the processes involved and practical constraints of the treatment itself.

An important aspect in proton therapy is the secondary radiation produced during the treatment. The secondary particles, like neutrons, can induce an unplanned dose in the healthy tissue and that could lead to a secondary cancer.

For this work, Monte Carlo simulations were performed, using beam line parameters of the Clatterbridge Cancer Centre, to calculate the proton depth-dose distribution, the proton and neutron fluence in the beam line, the neutron dose equivalent in the water phantom, the radioactivity of beam line components and the activation of air.

The proton depth-dose distribution was calculated for a proton beam with an energy between 55 MeV and 60 MeV. For 55 MeV, the Bragg peak was found to be at approximately 2.2 cm depth in the water phantom and the depth-dose distribution is increasing with energy. At 60 MeV, the Bragg peak occurs at 3 cm depth. The experimental calculations were verified with the FLUKA and the MCNPX Monte Carlo codes. The results showed a good agreement between the codes and the measurements and give confidence in the simulations.

The proton fluence and the proton dose were calculated in order to establish if the quality of the proton beam is altered along the beam line. The result showed that most of the particles are produced in the modulating devices and in the brass collimator, but even in these components, the proton fluence was found to be low. The proton dose was found to be 10^5 GeV/g which is very small. The proton dose was calculated with both FLUKA and MCNPX codes and the results show a good agreement. These findings suggest that the beam line components will not influence the quality of the proton beam delivered to the patient.

The neutron fluence and the neutron dose were also calculated. The results showed that the highest fluence of 10^5 neutrons/cm^2 is found in the brass collimator. The neutron dose was found to be low, even around the brass components it was found to be 1 GeV/g. The contribution of the neutrons to the dose was also determined. For a 60 MeV proton beam, the maximum neutron dose equivalent ranged between 50 μ Sv/s and 70 μ Sv/s in the target volume and between 20 μ Sv/s and 1 μ Sv/s outside the target. These findings indicate that for the Clatterbridge Cancer Centre, the secondary neutron dose equivalent induced to the patient is low below the UK limitations [40].

Certain FLUKA simulations have been verified with MCNPX code and the results showed a substantial agreement, but it will be important to validate the simulations with experimental data. As no experimental measurement of the neutron dose equivalent are available for the Clatterbridge Cancer Centre facility, the results obtained were compared with the experimental measurements conducted at a similar facility at CCB IFJ PAN in Krakow [103]. The measurements at this facility were done for a 60 MeV

proton beam using a neutron rem meter. The results obtained were 2.89 mSv/h at the patient chair and 0.9 mSv/h on the floor. These findings suggest that the secondary dose received by the patient do not exceed the legal limits suggested in the IRR99 [40].

The activity induced in the patient collimator and in the air inside the treatment room was investigated. The activation results indicate that the short-lived isotopes like ^{202}Bi, ^{201}Pb, ^{70}Ga and ^{69}Zn will not be accumulated in the patient specific collimator but other isotopes like ^{66}Ga, ^{64}Cu, ^{63}Zn, ^{61}Cu, ^{58}Co will produce radioactivity even after an hour of cooling time. The activity of these isotopes does not exceed the limits recommended in the IRR90 [40] but even after one hour of cooling time, the activity of ^{66}Ga and ^{63}Zn will be only by a factor of 10 lower that the legal limits [40]. These results suggest that the collimator is non-radioactive but the personnel should treat it with care to minimize the radiological risk. Nevertheless, the total activity and the dose rate will strongly dependent on the irradiation profile: beam intensity, duration of each irradiation session and the time between the irradiation sessions.

The activation of the air inside the treatment room was also calculated for the same irradiation profile. The results showed that the medium and long-lived isotopes like ^{15}O, ^{13}N, ^{11}C and ^{7}Be are the primary activation products of air. The activity of ^{11}C was found to be 10 times lower than the limits set by the IRR99 [40]. These results suggest that immediately after irradiation, the induced activity in air is within the legal limits and the access in the treatment room should not be limited. In practice, the induced activity will depend on the duration of each run and of the number of air changes in the treatment room.

The residual dose equivalent was also calculated in the treatment room for four cooling times. The results showed that even after immediately irradiation the residual dose equivalent was found to be only 10 μSv/h. This value suggest that the residual dose equivalent is low and it complies with the UK regulations [40].

Chapter 5

Radiation protection studies for the Christie Proton Therapy Centre

5.1 Introduction

The Christie Proton Therapy Centre is a new facility under construction with the aim of treating the first patient in 2018. The proton therapy centre is designed to deliver proton beams with energy up to 250 MeV. The facility is planned to have 3 treatment rooms and 1 research room. The treatment rooms will be fitted with a Varian ProBeam System which will provide pencil beam scanning and a 360° rotating gantry. The research room is planned to have 2 fixed beam lines, one for radiobiological studies and one for technical investigations. All four rooms are attached to a cyclotron, as shown in figure 5.1, that has an intensity of 10 nA [9, 109, 113].

Due to the fact that the rooms will be irradiated with high energy protons, radiation protection studies need to be done in order to ensure that the safety limitations comply with the law, and that the radiation dose is kept as low as reasonably practicable.

The aim of this project is to conduct radiation protection studies for the research room. In order to do that, the ambient dose equivalent for secondary particles (neutrons and photons) and the residual dose rates have been calculated at some of the points of interest, such as the isocentre, the maze, the corridor, the facility room and the adjacent treatment room. The ambient dose equivalents for neutrons and photons were calculated for proton beams with several energies 70 MeV, 100 MeV, 150 MeV, 200 MeV and 250

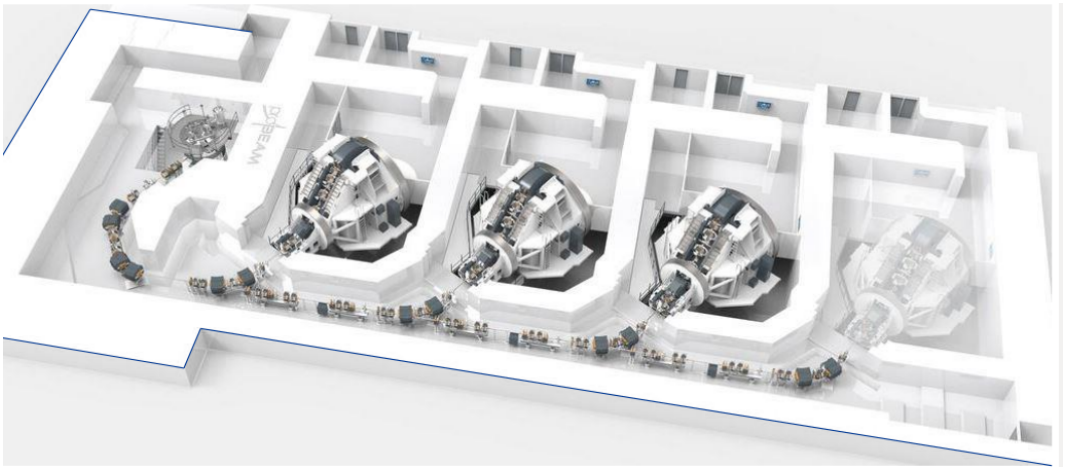

FIGURE 5.1: Christie Proton Therapy Centre design. Taken from [109].

MeV. In addition to secondary dose rates, the generation of radioactive nuclides within the air and in the steel floor is also described in this chapter.

5.2 The simulations

For all the studies presented in this chapter, the FLUKA Monte Carlo code was used. The default PRECISIO was used for all simulations. This option uses transport cuts of 100 keV for electrons, positrons and photons. The neutrons are transported down to thermal energies [93]. The electromagnetic physics was described by the EMF package, while the Boltzmann master equation (BME) theory was used to describe the hadronic interactions. The hadron-nucleus nuclear interactions were treated by the PEANUT (PreEquilibrium-Approach-to-Nuclear-Thermalization) nuclear interaction model [88]. All these FLUKA options are explained in chapter 3.

The simulations were made with a set of five runs, every run with 10^6 primary protons, giving a total of 5×10^6 primary protons. This number was used to obtain good statistics [89, 92] with a reasonable running time: 4 hours up to 48 hours, depending on the ion species, energy and scoring type [93]. For radiation protection purposes, the AMB74 option was used. The AMB74 is a set of coefficients for ambient dose equivalent implemented for photons and electrons by ICRP74 and M. Pellicioni [94, 95]. The results of neutron ambient dose equivalent were compared with MCNPX results taken from [113]. For air and floor activation and also for residual dose equivalent, the IRRPROFI option was used to define the irradiation profile, while RESNUCLE and DCYSCORE options were used to estimate the activity of the residual nuclei produced in the stainless steel floor and in air. The neutron and photon ambient dose equivalent rates were calculated using the USRBIN, DCYSCORE and AUXSCORE options. The

results of the ambient dose equivalent are given in μSv/hour [93]. The input file used for the evaluation of the ambient dose equivalent is presented in appendix.

In order to be able to compare shielding requirements needed in the proton treatment range, a proton beam with an energy of 70, 100, 150, 200 and 250 MeV was simulated. The beam is considered to be mono-energetic. The intensity is presumed to be 0.44 nA. This corresponds to 2.75×10^9 protons per second [109].

The beam line is assumed to be 150 cm above the floor level and to be perfectly horizontal [109]. It enters the research room under a 60 degrees angle. These information was provided as primary details for the simulations but later designs changed the height of the beam line to 125 cm above the floor with the beam entering perpendicular to the wall. This will not greatly affect the results.

Figure 5.2 represents the research room model as built with the FLAIR interface for FLUKA as described in chapter 3. Figure 5.3 represents the elevation view at the maximum height of Y = 5 metres and the maximum length of Z = 30 metres, including the maze corridor. The FLUKA model was designed according to the last civil engineering plans that were used at the building of the facility [110]. Small differences regarding the walls' angles and maze dimensions may exist due to the fact that is not possible to model the exact physical geometry in terms of fixed shapes and regions as required in a Monte Carlo code. No ceiling was added in the model for clarity.

The materials used in the FLUKA simulations are shown in the table 5.1.

Structure	**Material**	**Density (g/cm^3)**
Walls	Concrete	2.34
Beam tube	Aluminum	2.70
Target	Graphite	2.26
Room	Air	0.00120484
Floor	Stainless Steel	8.0

TABLE 5.1: Materials used in the FLUKA geometry.

The beam line is modelled as a 10 m long Aluminium pipe, with an outer radius of 5 cm and a thickness of 2 mm. These dimensions were assumed as it is not yet known the exact dimensions that will be used. They are typical for a fixed proton beam line used for research purposes. Inside the beam pipe, it is assumed to be vacuum. The quadrupole magnets that would normally be present to focus the proton beam are omitted, as they introduce unnecessary complexity in the geometry, with a negligible effect on the external radiation fields.

After passing the beam tube, the beam impinges a graphite phantom ($10 \times 10 \times 45$ cm) with the longest dimension in the beam direction. The graphite phantom length

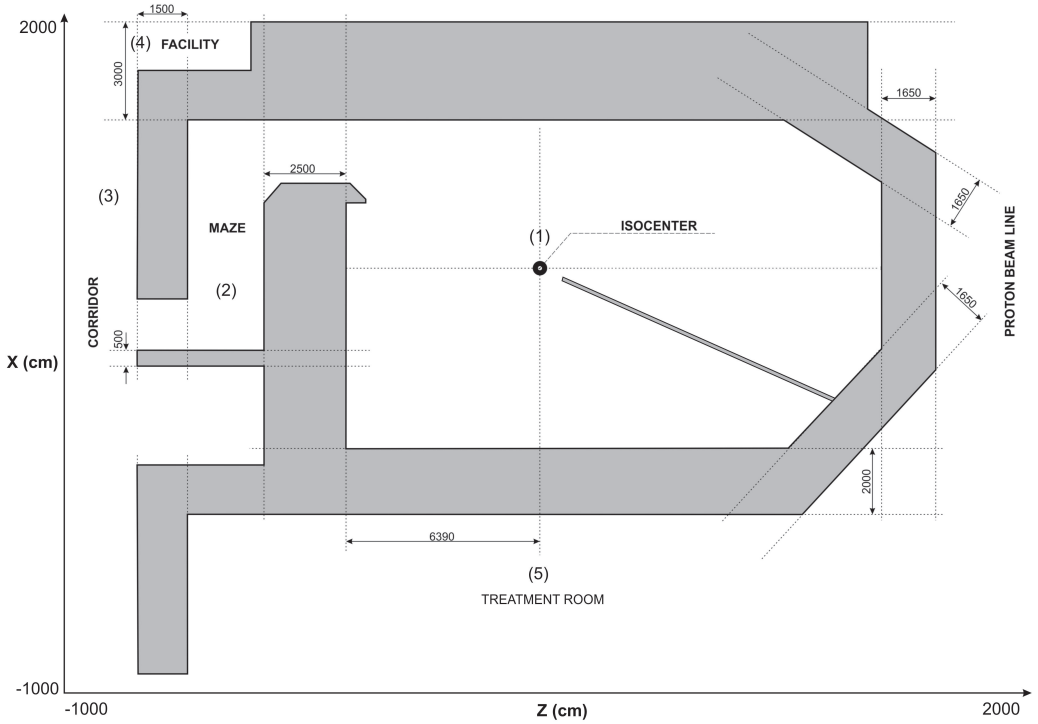

FIGURE 5.2: The layout of the research room as modelled in FLUKA. The positions of the detectors: (1), (2), (3), (4) and (5) are shown.

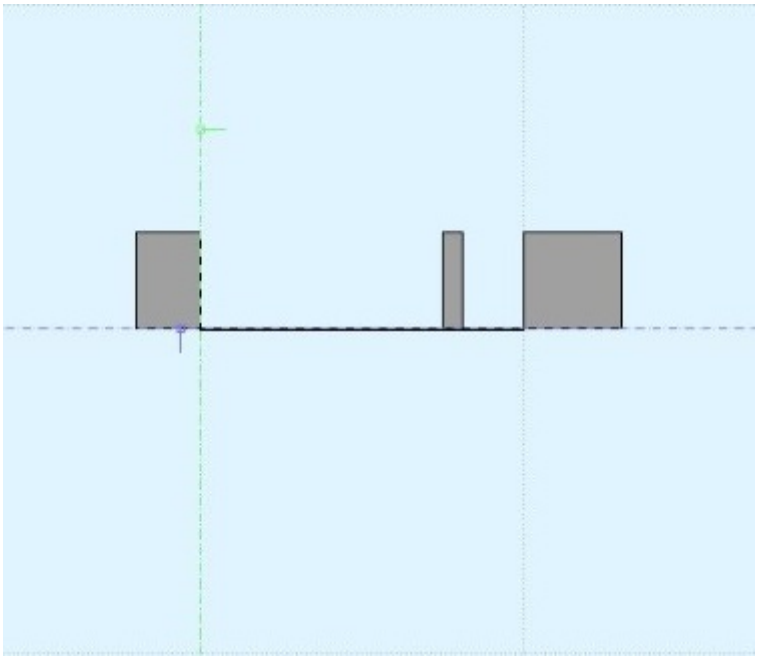

FIGURE 5.3: The elevation view of the research room as modelled in FLUKA with the maximum height of Y = 5 m and the maximum length of Z = 30 m.

is appropriate for a proton beam with an energy of 250 MeV in order to stop all the protons from the proton beam as the maximum range for a proton beam with an energy of 250 MeV is approximately 40 cm [125]. The phantom is made of graphite as this is

typically used for calibration of a proton beam. A false floor was also included and it has the role to sustain the weight of the beam line components. This is 2.5 cm thick and is made of stainless steel. The floor is extended up to the maze corridor.

The ambient dose equivalent was calculated in several points of interest: the phantom (at the isocentre) (1), the maze (2), the corridor (3), the facility room (4) and the adjacent treatment room (5). The isocentre was chosen in order to be able to compare the results with the calculations performed for the NHS treatment rooms. All these points of interest where the dose was calculated are marked in figure 5.2. The floor is also included in the FLUKA model. Next to the research room the facility rooms and one of the treatment room will be placed.

5.3 Results

5.3.1 Neutron and photon dose equivalent

In radiation protection, the secondary particles that are of most interest are neutrons and high energy photons (0.1-10 MeV) [111, 112]. The neutrons represent the main concern as they are relatively abundant and highly penetrating [24]. It is very important to calculate the neutron and photon dose equivalent in the research room, as the facility room and one of the treatment rooms are adjacent.

The position of the detectors can be seen in figure 5.2. The particle transport threshold is set at 100 keV. The simulation geometry as built in FLUKA is also shown in figure 5.2. The proton beam enters the research room and passes through the aluminium pipe before impinging the graphite phantom.

Figure 5.4 shows the predicted neutron dose from a 70 MeV proton beam. The neutron dose equivalent around the beam line and at the isocentre is around 50 μSv/h and at the maze level it decreases to 1 μ Sv/h. Outside the shielding walls, at the points of interest like the facility room, the corridor and the treatment room, the neutron dose equivalent is less than 1 μ Sv/h. The photon dose equivalent follows the same pattern. The photon ambient dose equivalent is high around the aluminium beam line and the graphite phantom, approximately 10 μ Sv/h, and decreases to 0.1 μ Sv/h at the maze and the facility room and 0.05 μ Sv/h on the corridor and the treatment room as shown in figure 5.5. These values indicate that for a 70 MeV proton beam, in the areas of interest, the neutron and photon ambient dose equivalent is low and can be regarded as safe for employees or member of public as the dose rate is lower than the limits

recommended by the IRR99 [40] for uniform irradiation of the whole body: 6-20 mSv/y for radiation workers and 1 mSv/y for other personnel.

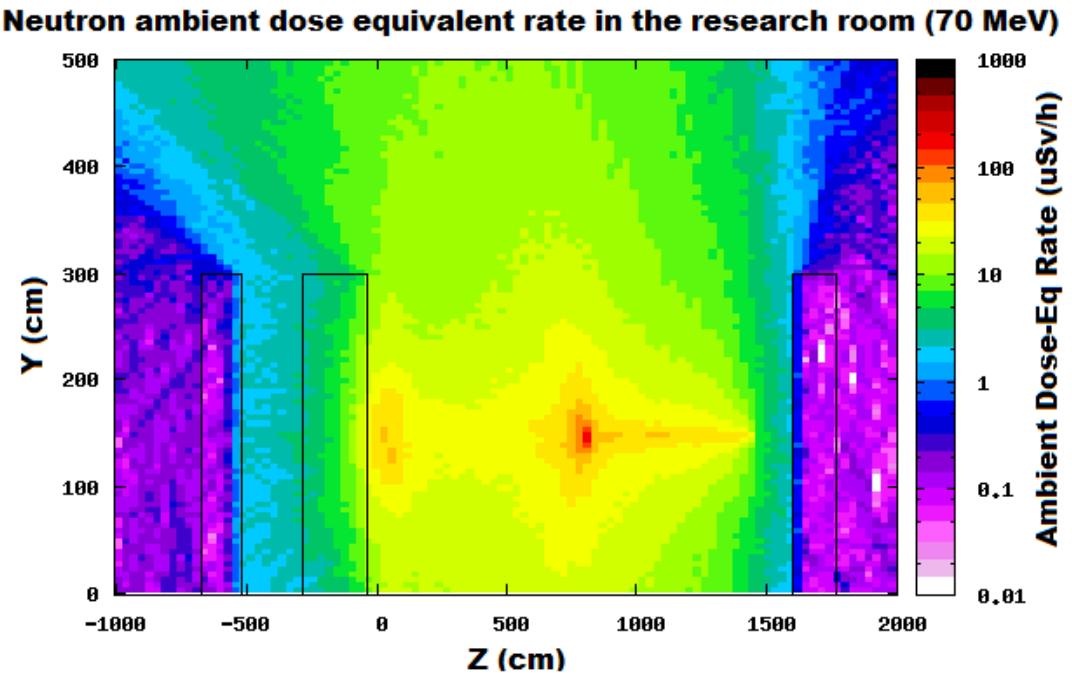

FIGURE 5.4: Neutron dose equivalent for a 70 MeV proton beam in the research room.

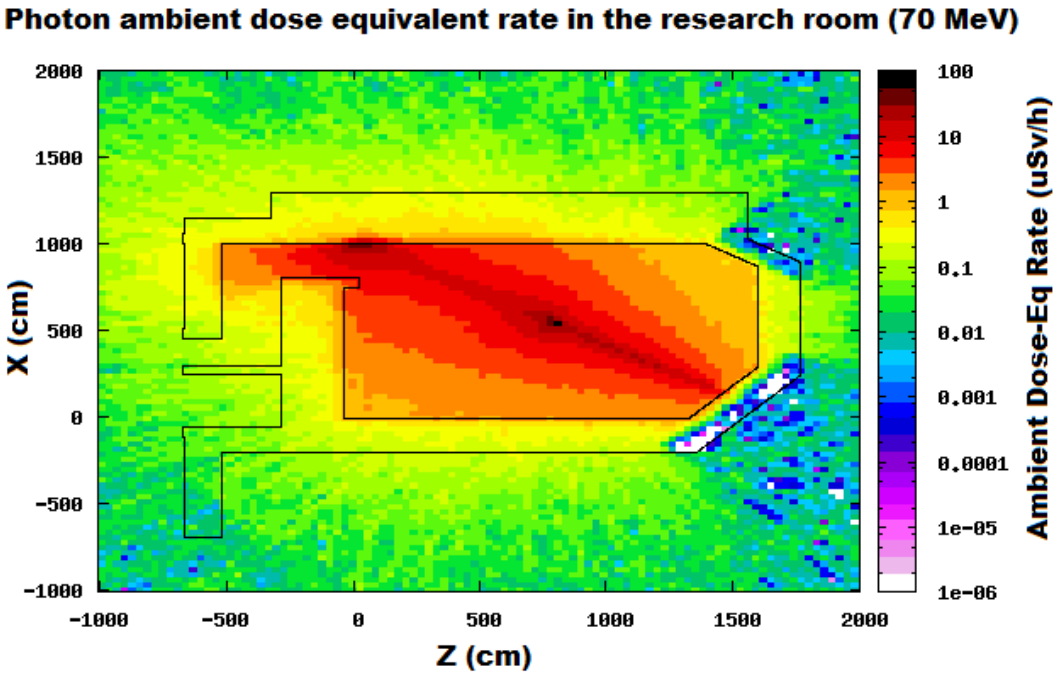

FIGURE 5.5: Photon dose equivalent for a 70 MeV proton beam in the research room.

The results of the neutron dose equivalent are shown in an elevation view and the photon dose equivalent in a plan view. This is merely for reasons of presentation and consistency, and wishing to show both views without adding a large number of plots shown. For each beam energy the shapes of neutron and photon dose distributions are broadly the same, differing only in overall intensity.

For 100 MeV, as shown in figure 5.6, the neutron dose equivalent increases to 200 μ Sv/h at the isocentre, while at the maze, the dose is 10 μ Sv/h. Outside the research room, the dose decreases to 1 μ Sv/h in the corridor and in the treatment room. In the facility room, the dose reaches 5 μ Sv/h. For photons, as shown in figure 5.7, the dose is lower. At the isocentre it is 50 μ Sv/h and in the maze it is 0.5 μ Sv/h. In the corridor, the dose is around 0.5 μ Sv/h, the same as in the treatment room, while in the facility room, the dose is higher, around 1 μ Sv/h. As the particles are hitting the Aluminium beam pipe and due to the fact that the beam pipe is shown in such a small scale, the photon dose is shown as a line.

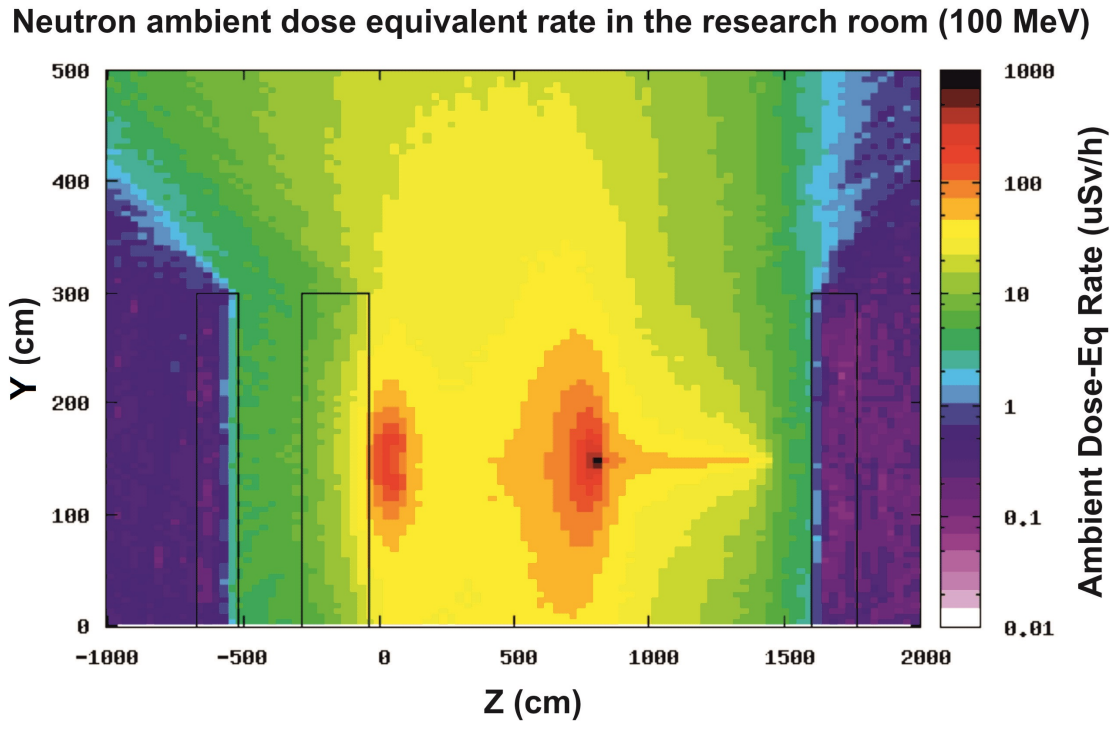

FIGURE 5.6: Neutron dose equivalent for a 100 MeV proton beam in the research room.

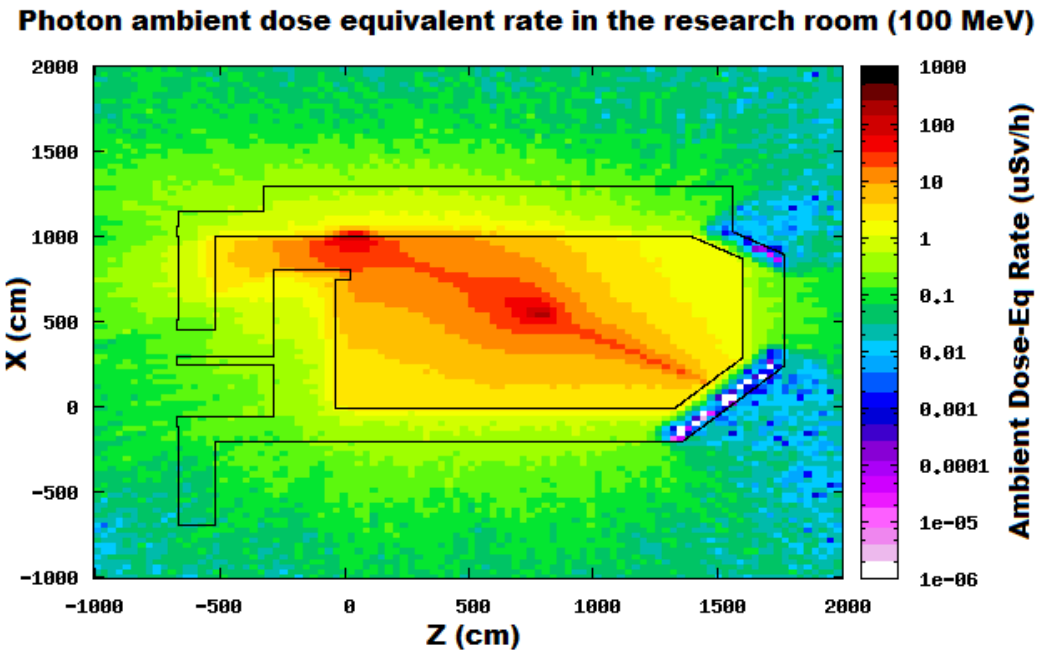

FIGURE 5.7: Photon dose equivalent for a 100 MeV proton beam in the research room.

Increasing the proton beam energy to 150 MeV, the neutron ambient dose equivalent at the isocentre increases up to 10^3 μ Sv/h, while in the maze area, the dose is around 10 μ Sv/h as shown in figure 5.8. In the corridor and in the treatment room, the neutron dose is around 1 μ Sv/h, while in the facility room, it was found to be 8 μ Sv/h. Comparing figure 5.6 and figure 5.8, it should be noticed that the colour scale is changed, as the maximum value changes from 1000 μ Sv/h to 10000 μ Sv/h. This is a feature of the FLUKA code.

The photon ambient dose equivalent is increased as well to 5×10^4 μ Sv/h at the isocentre and decreases to 7 μ Sv/h in the maze, 1 μ Sv/h on the corridor and in the treatment room and approximately 10 μ Sv/h in the facility room as shown in figure 5.9. The dose of the high energy photons is 50 times higher than that of the neutrons at the beam line level, although the overall influence of the photon dose at the periphery of the research room is not large. The same effect can be observed at 200 MeV and 250 MeV as shown in figures 5.11 and 5.13.

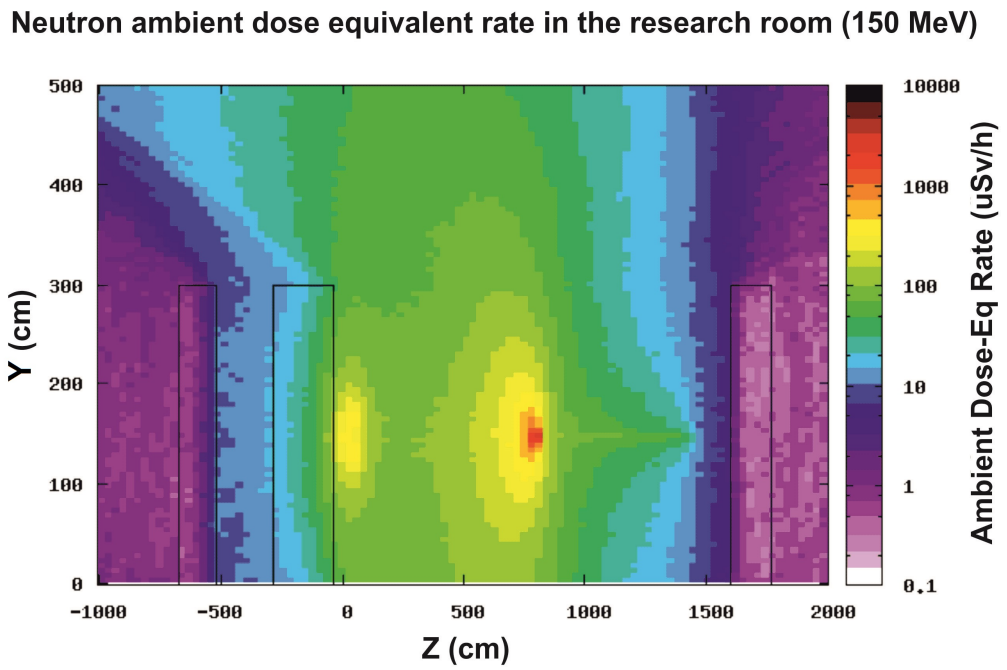

FIGURE 5.8: Neutron dose equivalent for a 150 MeV proton beam in the research room.

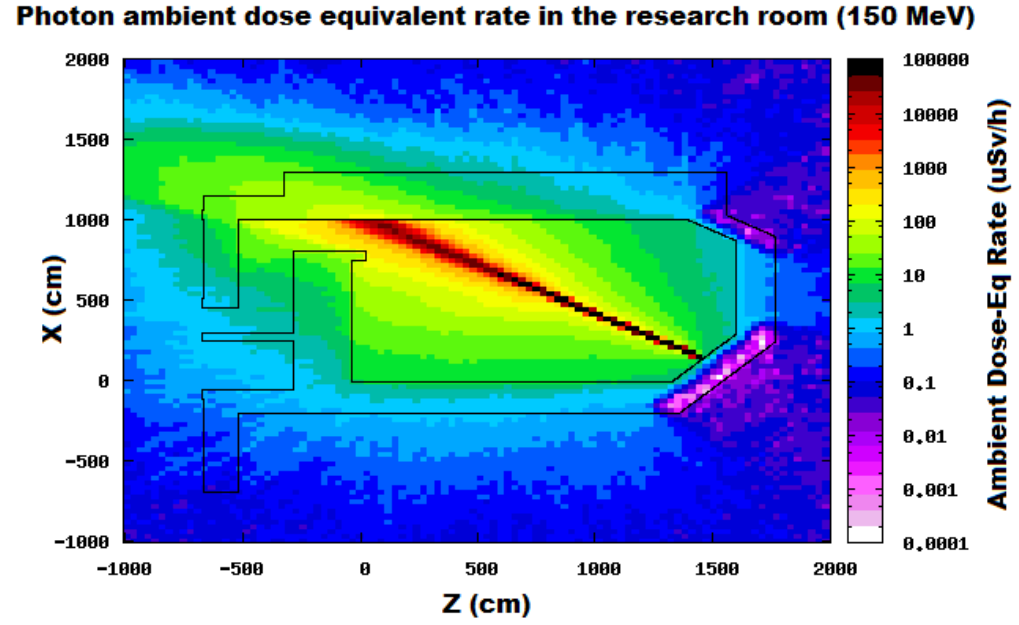

FIGURE 5.9: Photon dose equivalent for a 150 MeV proton beam in the research room.

At 200 MeV, the neutron dose equivalent is around 2 $\times 10^3$ μ Sv/h around the isocentre and approximately 10 μSv/h in the maze. Outside the shielding walls, the dose is 5 μ Sv/h in the corridor and in the treatment room and around 8 μSv/h in the facility room as shown in figure 5.10. The photon ambient dose equivalent was found to be

$7{\times}10^4$ μSv/h at the isocentre, 10 μSv/h in the maze, 5 μSv/h on the corridor and in the treatment room and 50 μSv/h in the facility room as shown in figure 5.11.

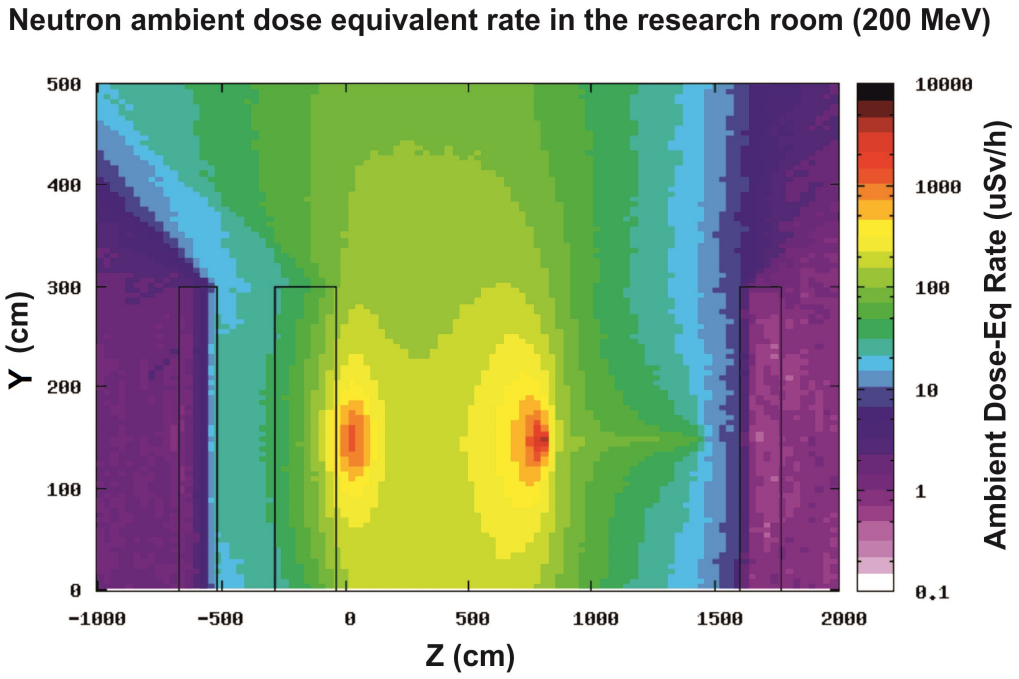

FIGURE 5.10: Neutron dose equivalent for a 200 MeV proton beam in the research room.

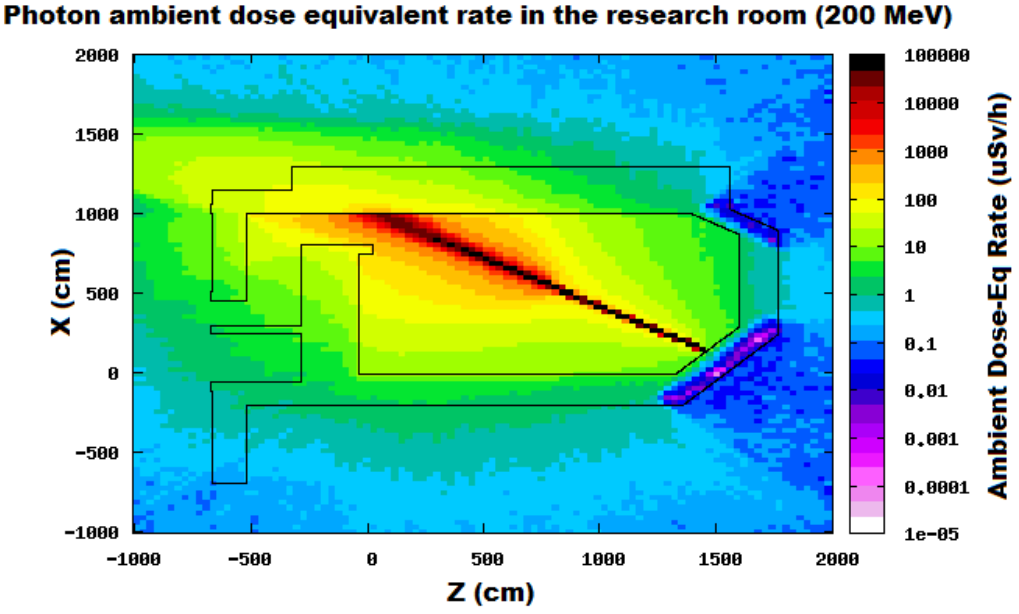

FIGURE 5.11: Photon dose equivalent for a 200 MeV proton beam in the research room.

At the maximum energy (250 MeV), the neutron dose equivalent is approximately 6 $\times 10^3$ μSv/h at the isocentre, 80 μSv/h in the maze and 8 μSv/h in the corridor and in the treatment room, while in the facility room, the dose is 10 μSv/h as shown in figure 5.12. The photon dose equivalent is 8 $\times 10^4$ μSv/h at the isocentre, 50 μSv/h in the maze and approximately 10 μSv/h in the accessible areas around the research room. If we consider that the irradiation time is approximately 520 hours per year, the neutron dose received by a worker in one year is approximately 41 mSv/year if the person is present all 520 hours in the maze while the accelerator is operating, which is an unrealistic scenario. Therefore, even at the maximum energy the neutron dose values can be regarded as sufficiently low as the local regulations for controlled and public areas limits introduced by IRR99 are: 20 mSv in a calendar year for employees aged 18 years or over and 1 mSv in a calendar year for members of the public. However, it will be useful to assess the radiation exposure using radiation monitors.

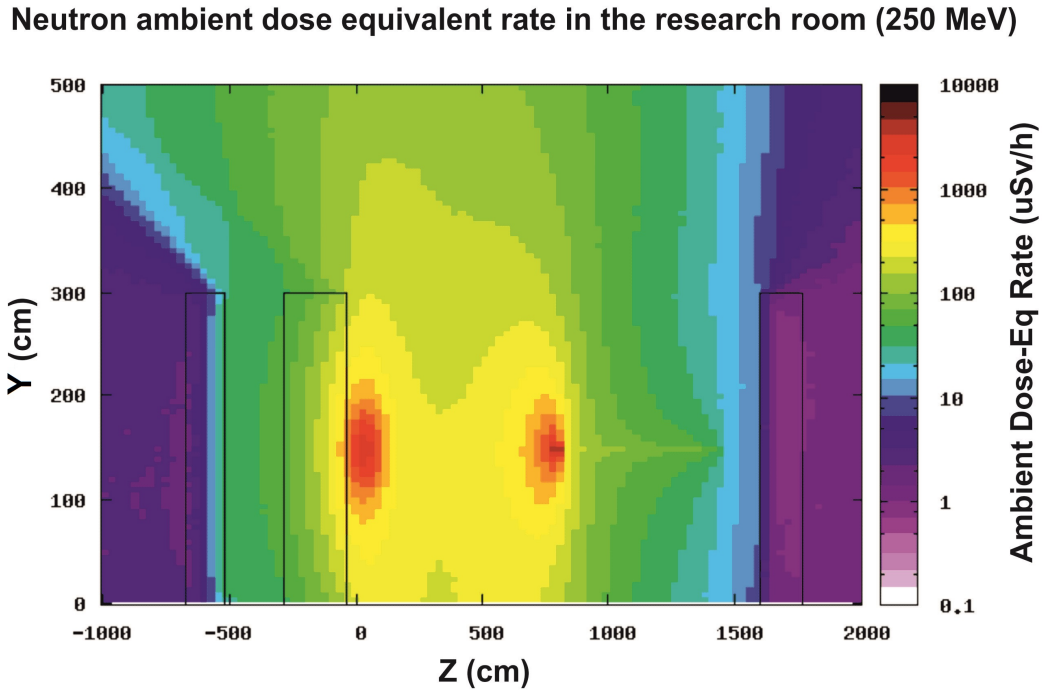

FIGURE 5.12: Neutron dose equivalent for a 250 MeV proton beam in the research room.

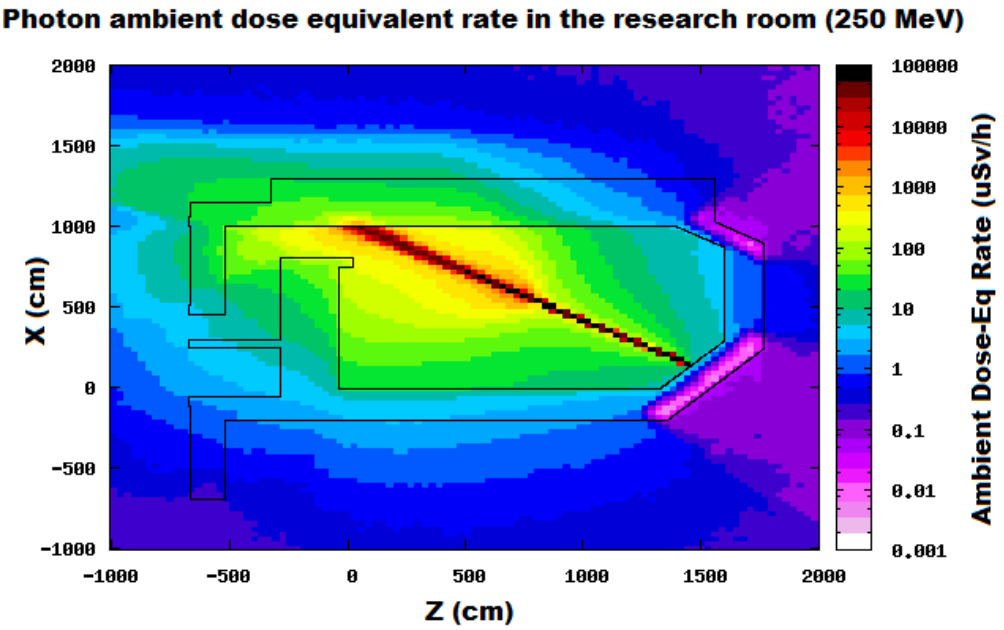

FIGURE 5.13: Photon dose equivalent for a 250 MeV proton beam in the research room.

The FLUKA results were compared with MCNPX results obtained by Alex Flynn, an MSc student from Manchester University as part of his dissertation. The results obtained are presented in Ref.[113]. The MCNPX results are presented in mSv/year. In the model considered in [113], the annual irradiation time is 520 hours. The results obtained with the Monte Carlo codes are presented in table 5.2.

Structure	**Dose in FLUKA (mSv/year)**	**Dose in MCNPX (mSv/year)**
Maze	2.5	1.36
Corridor	2.0	1.44
Facility	5.0	3.54
Treatment room	1.5	0.01

TABLE 5.2: Annual effective dose rates obtained with FLUKA and MCNPX at 250 MeV beam energy.

The comparison between the FLUKA and the MCNPX showed that the values calculated with FLUKA are higher than the values calculated with MCNPX. In the maze, the dose equivalent calculated with FLUKA is 1 mSv higher than the dose equivalent calculated with MCNPX, while on the corridor, the dose equivalent has approximately the same value for both codes. The dose in the treatment room was found to be 100 times higher with FLUKA. This is a big difference and the explanation is not clear: it could be due to a significant difference between the materials and/or geometry used in the two simulations. The FLUKA dose in the treatment room is lower than the other

points recorded, but not by very much, whereas in MCNPX the dose in this location is a factor of one hundred smaller than the others: something very different is being described. Nevertheless, these are results based on an early and simplified geometry and an additional set of simulations should be done with a more detailed geometry.

5.3.2 Study of radioactivity induced in the research room

As a result of nuclear interactions, radioactive nuclei will be produced due to the proton interactions with the surrounding materials. The decay of these radionuclides produces a source of radiation, therefore, the study of radioactivity induced in the treatment/research room is very important aspect as this represents a potential radiation hazard to personnel or patients [111]. Calculations have been carried out to determine the residual dose rate in the research room as a function of time after irradiation. Using the FLUKA code, the beam was simulated to pass through an Aluminium beam pipe before hitting the graphite phantom with three different energies (70 MeV, 150 MeV, 250 MeV) and for four different cooling times: after irradiation, 1 hour, 1 month, 1 year. The electromagnetic cascade was turned on (EMF-ON) together with the RADDECAY card in order to allow the calculation of the residual dose rates based on the production of radioactive isotopes. The EVAPORATION and COALESCENCE models were also activated using the PHYSICS card for accurate description of the nuclear processes and to obtain the residual nuclei production [92, 93]. These FLUKA options were described in chapter 3. For all studies, the irradiation profile chosen for this set of simulation was 1.4 hours per day (approximately 10 hours per week) [113] of irradiation at maximum intensity.

We have to consider separately the activation of air and the activation of the concrete, beam pipe and other materials. The difference is that the air may move through the ventilation system, while all other components will stay fixed. The air activation will be considered first.

As mentioned in 4.3.5 when protons interact with matter, they will produce fast neutrons which will interact with the atoms from air, producing short-lived radionuclides. Table 5.3 lists the isotopes found most abundantly in the atmosphere [126]. After multiple collisions, the fast neutrons will slow down to thermal energies producing ^{15}O, ^{13}N, ^{11}C and ^{7}Be from collisions with the oxygen, nitrogen and carbon atoms from air [107].

The thermal neutrons will also be captured by ^{40}Ar from the air and radioactive ^{41}Ar will be produced. ^{41}Ar is a beta and gamma emitter and is well-known to be the major contributor to the air activation [107, 108]. The clinical staff are likely to receive more dose equivalent from radionuclides with half lives of the order of 15-20 min than

Isotope	**Percentage by volume in the atmoshere**
^{14}N	78.1
^{16}O	21.2
^{40}Ar	0.46
^{15}N	0.28
^{18}O	0.04
^{12}C	0.015
^{17}O	0.008
^{36}Ar	0.0016

TABLE 5.3: The most abundant isotopes found in the atmosphere.

Isotope	$T_{1/2}$	**A (Bq)**	**A (Bq)**	**A (Bq)**	**Limit from IRR99 (Bq)**
		70 MeV	**150 MeV**	**250 MeV**	
^{41}Ar	109.61 m	5.9×10^{2}	3.4×10^{3}	8.9×10^{3}	10^{9}
^{15}O	122.2 s	2.5×10^{5}	4.8×10^{5}	8×10^{5}	10^{9}
^{13}N	9.96 m	4.7×10^{5}	5.8×10^{5}	9.5×10^{5}	10^{9}
^{11}C	20.33 m	7.2×10^{5}	9.6×10^{5}	1.3×10^{6}	10^{6}
^{7}Be	53.28 d	1.1×10^{4}	1.5×10^{4}	2.3×10^{4}	10^{7}

TABLE 5.4: The most abundant radionuclides present in air after irradiation for 70 MeV, 150 MeV and 250 MeV proton beams with he limits allowed by IRR99 [40].

from shorter- or longer-lived radionuclides, according to Knowles, Orthel and Hill [111]. Therefore, the resulting activity of the most important isotopes and the ones considered harmful are shown in table 5.4.

a) Immediately (after irradiation)

Immediately after irradiation at 70 MeV the most abundant isotopes are ^{15}O, ^{13}N and ^{11}C, while at 150 MeV it was found that the activity of ^{41}Ar increased, simultaneously with the activity of ^{15}O, ^{13}N and ^{11}C. For most radioisotopes at most energies, the activity induced in the research room air is below the limits given in IRR99 [40]. However, if the accelerator is operated at maximum energy, ^{11}C will exceed the limit as shown in table 5.4. Under these circumstances personnel should not have access to the research room until a cooling-off period, commensurate with the 20 minute half-life, has elapsed. Apart from that, these results demonstrate that the research room has a low risk of contamination and the personnel will not be exposed as the activity of the most important radioisotopes is below the legal limits suggested in the IRR99 [40].

b) 1 hour (after irradiation)

After 1 hour of cooling time, the activities of the most radioactive radioisotopes like: ^{13}N, ^{11}C will decrease by several factors of 2, while the ^{41}Ar falls off more slowly as shown in table 5.5.

Isotope	$T_{1/2}$	**A (Bq)**	**A (Bq)**	**A (Bq)**	**Limit from IRR99 (Bq)**
		70 MeV	**150 MeV**	**250 MeV**	
^{41}Ar	109.61 m	4.1×10^{2}	2.3×10^{3}	6.1×10^{3}	10^{9}
^{15}O	122.2 s	3.5×10^{-4}	6.6×10^{-4}	1.09×10^{-3}	10^{9}
^{13}N	9.96 m	7.3×10^{3}	9×10^{3}	1.4×10^{4}	10^{9}
^{11}C	20.33 m	9.3×10^{4}	1.2×10^{5}	1.7×10^{5}	10^{6}
^{7}Be	53.28 d	1.1×10^{4}	1.5×10^{4}	2.3×10^{4}	10^{7}

TABLE 5.5: The most abundant radionuclides present in air after 1 hour of cooling for 70 MeV, 150 MeV and 250 MeV proton beams with the limits allowed by IRR99 [40].

After 1 month, the activity of the medium half-live radionuclides as ^{41}Ar will considerably decrease down to 10^{-9} Bq. Therefore, the activity of the isotopes, after 1 month and 1 year of cooling time, are not presented as the activity is negligible.

Overall, these results demonstrate that, immediately after irradiation, the personnel working in the research room will not be exposed to radiation exposure as the radioactivity is below the legal limits presented in IRR99.[40] Therefore, no additional mitigation is considered necessary for irradiation of the air in the research room. However, the activity must of course be monitored. Nevertheless, these results are based on early information and simplified geometry and for effective dose assessment more information is required like: calculations for the entire machine, volume of the air and ventilation parameters.

The next task was to calculate the residual dose equivalent rate in the research room due to the activation of the beam pipe, graphite phantom, concrete and air (the air is also included in the simulations). For aluminium beam pipe, the main contributors to the dose rate are: ^{18}Fe, ^{24}Na and ^{22}Na. For concrete, the main contributor to the dose rate is ^{24}Na. The calculations have been performed using the same irradiation profile as before: 1.4 hours per day (approximately 10 hours per week) [113] of irradiation at maximum intensity, for a proton beam with different energies and for six periods of cooling time: after irradiation, 1 hour, 1 day, 1 month, 3 months and 1 year. The dose rate is normalized in terms of μSv/h. For a 70 MeV proton beam, the residual dose equivalent in the research room immediately after irradiation is shown in figure 5.14.

The plots suggest that the residual dose is higher in the beam line direction and decreases with distance. Immediately after irradiation, the residual dose in the direction of the

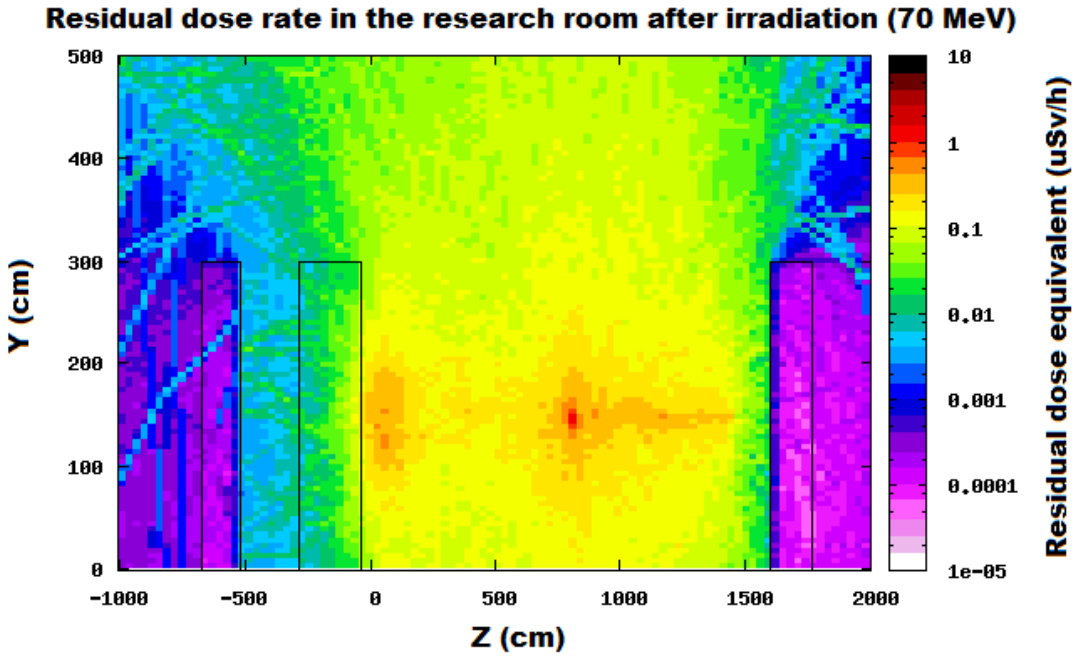

FIGURE 5.14: Residual dose equivalent in beam pipe, graphite phantom, concrete and air after irradiation with a 70 MeV proton beam.

beam line is approximately 20 μSv/h, around 10 μSv/h in the maze and 1 μSv/h around the shielding walls, even in the adjacent treatment room. In the corridor, the residual dose is around 10^{-4} μSv/h which is negligible.

After 1 hour of cooling time, the residual dose has a value of 1 μSv/h around the isocentre and 0.1 μSv/h in the maze. The dose falls to 0.5 μSv/h after the shielding walls in the adjacent rooms as shown in figure 5.15. These values indicate that for a 70 MeV proton beam, the residual dose is low, even immediately after irradiation. Therefore, it is safe for workers to access the research room immediately after the irradiation sessions and also for members of public who are in the adjacent areas.

The residual dose equivalent was calculated also after 1 day and 1 month of cooling time. The results shows that after 1 day the residual dose around the isocentre decreases down to 10^{-2} μSv/h and at the shielding wall and on the corridor the dose goes down to 10^{-5} μSv/h as shown in figure 5.16. After 1 month, the results showed that the dose decreased significantly. In the research room, the residual dose is 10^{-4} μSv/h and outside the room, it is approximately 10^{-6} μSv/h as shown in figure 5.17. These results suggest that after 1 day and 1 month of cooling time, the residual dose decreases significantly and the staff working outside the shielding walls will not be exposed to radiation.

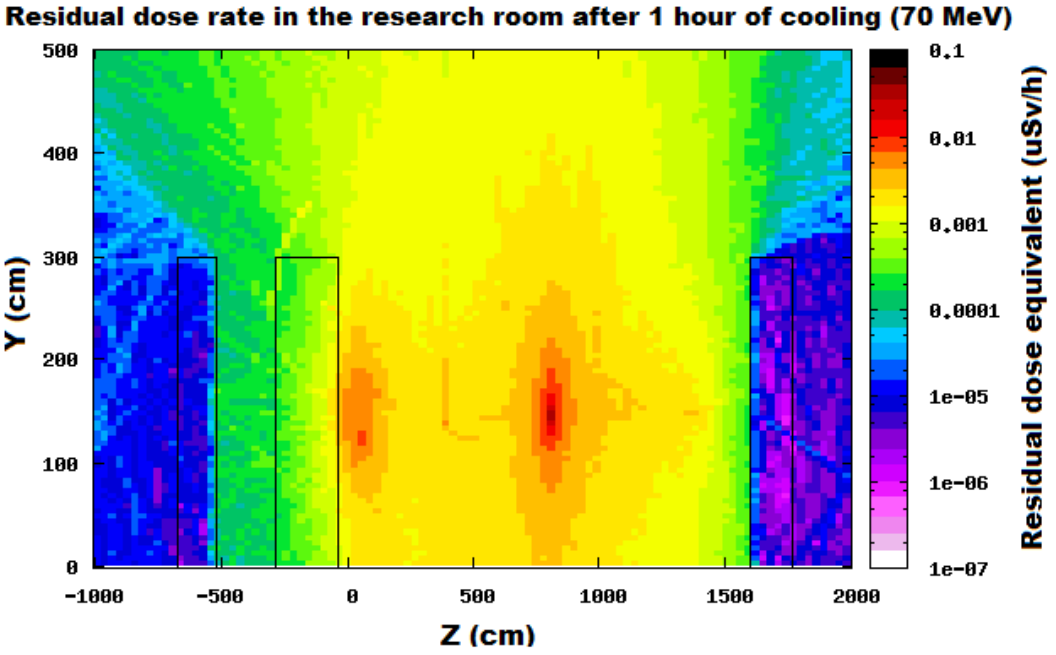

FIGURE 5.15: Residual dose equivalent in beam pipe, graphite phantom, concrete and air after 1 hour of cooling for a 70 MeV proton beam.

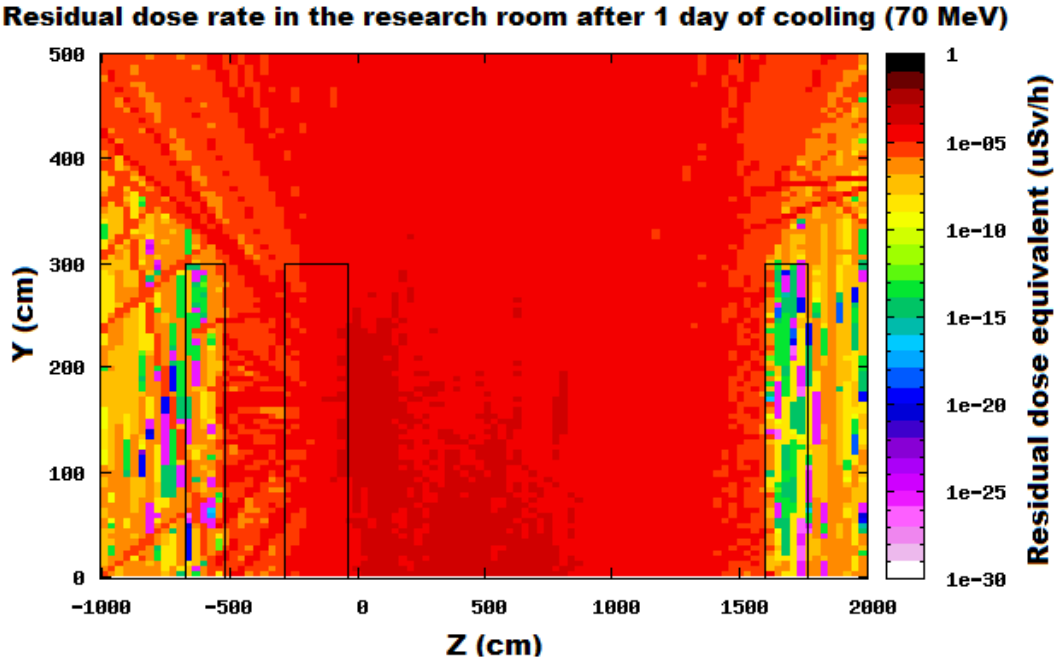

FIGURE 5.16: Residual dose equivalent in air after 1 day of cooling at 70 MeV proton beam.

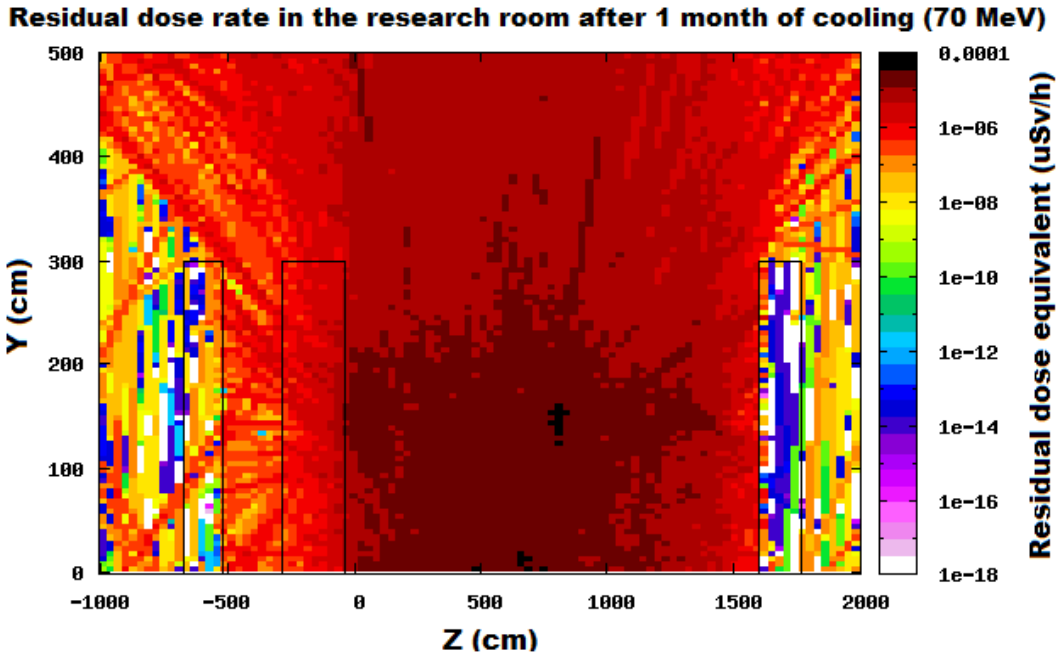

FIGURE 5.17: Residual dose equivalent in beam pipe, graphite phantom, concrete and air after 1 month of cooling at 70 MeV proton beam.

The residual dose was also calculated at 3 months and 1 year after irradiation to consider the cumulative effect of many experiments over a period of time and also because it is an important aspect for decommissioning. As expected, the doses around the beam line are 10^{-5} μSv/h and 10^{-7} μSv/h respectively. At the shielding walls and in the adjacent rooms, the residual dose decreased to 10^{-8} μSv/h after 3 months and is essentially zero after 1 year.

All these results prove that for a 70 MeV proton beam, the residual dose is low after irradiation. Therefore, members of public and the staff working in the research room will not be exposed to high radiation.

At 150 MeV, the residual dose equivalent in air immediately after irradiation is shown in figure 5.18. The results show that at the isocentre the residual dose is around 10 μSv/h and it decreases gradually with distance. In the maze corridor the dose is 0.5 μSv/h and approximately 10^{-2} μSv/h in the facility room. The radiation passes the shielding walls and is attenuated by the concrete walls. The residual dose in the adjacent treatment room is 10^{-2} μSv/h near the shielding walls and 10^{-3} μSv/h further down. The residual dose has the same value in the corridor.

After 1 hour from irradiation, the residual dose equivalent around the isocentre decreases to 0.1 μSv/h and to 10^{-3} μSv/h in the maze corridor as shown in figure 5.19. Outside the

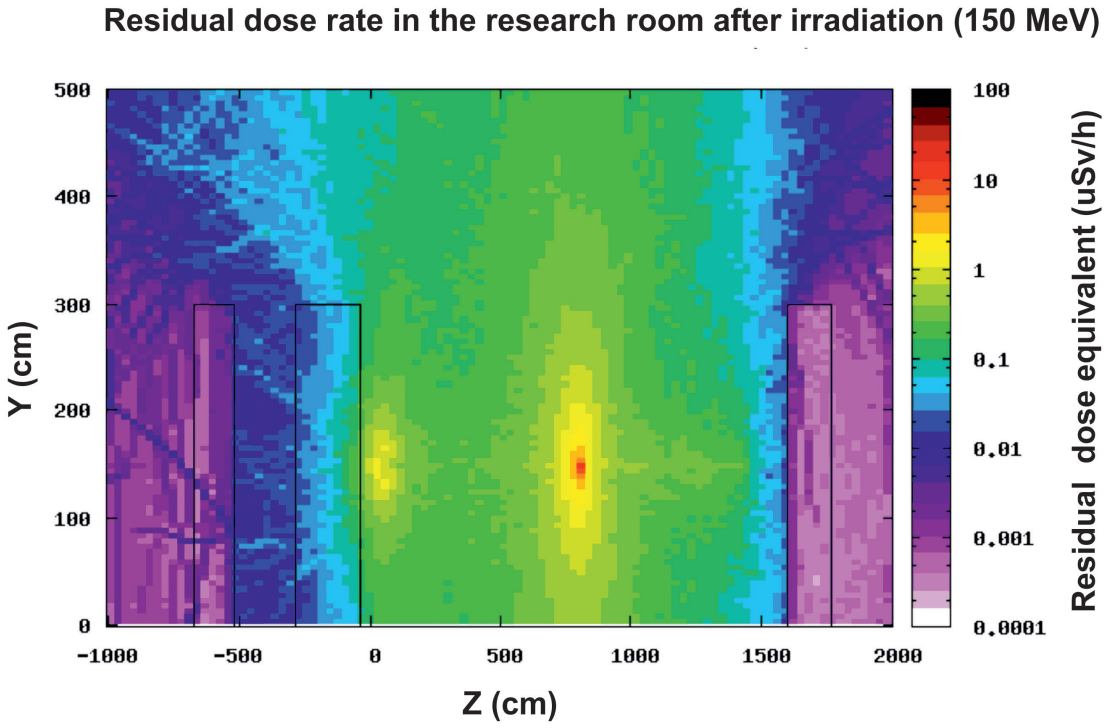

FIGURE 5.18: Residual dose equivalent in beam pipe, graphite phantom, concrete and air after irradiation for a 150 MeV proton beam.

shielding walls, in the treatment room, the residual dose is 10^{-4} μSv/h near the shielding walls and decreases to 10^{-5} μSv/h at a distance of a few metres. In the corridor, the residual dose is 10^{-4} μSv/h.

After 1 day, the residual dose at the isocentre and along the beam line decreases to 10^{-2} μSv/h. In the remaining space of the research room, the residual dose is 10^{-3} μ Sv/h. In the maze and at the exterior of the shielding walls, the residual dose is 10^{-3} μSv/h. In the corridor, the residual dose decreases to 10^{-6} μSv/h as shown in figure 5.20.

After 1 month from irradiation, the results show that the dose is significantly lower than after 1 day. This is understandable as the isotopes produced due to the beam line activation have a $T_{1/2}$ shorter than 1 month. In the research room, the residual dose is 10^{-3} μSv/h and outside the shielding walls and at the points of interest, the dose is 10^{-7} μSv/h as shown in figure 5.21.

The residual dose after 3 months of cooling is significantly low, even around the beam line the dose is 10^{-4} μSv/h and outside the shielding walls the dose decreases down to 10^{-8} μSv/h. After 1 year, the residual dose was found to have approximately the same value as after 3 months of cooling.

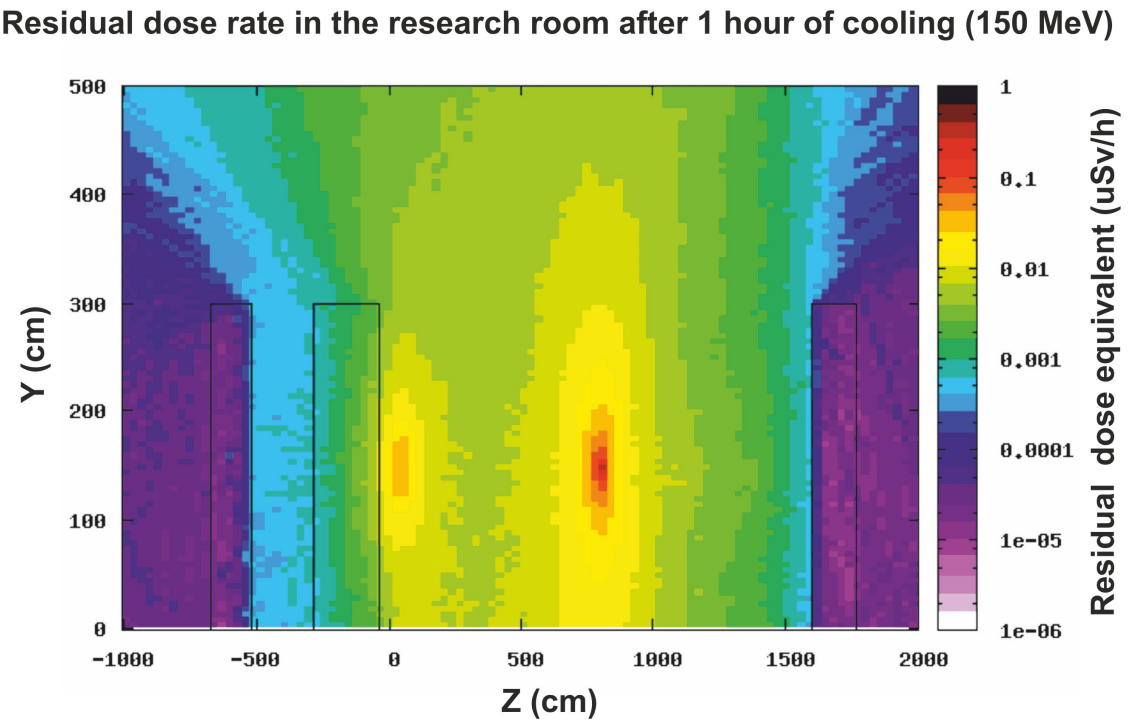

FIGURE 5.19: Residual dose equivalent in beam pipe, graphite phantom, concrete and air after 1 hour of cooling for a 150 MeV proton beam.

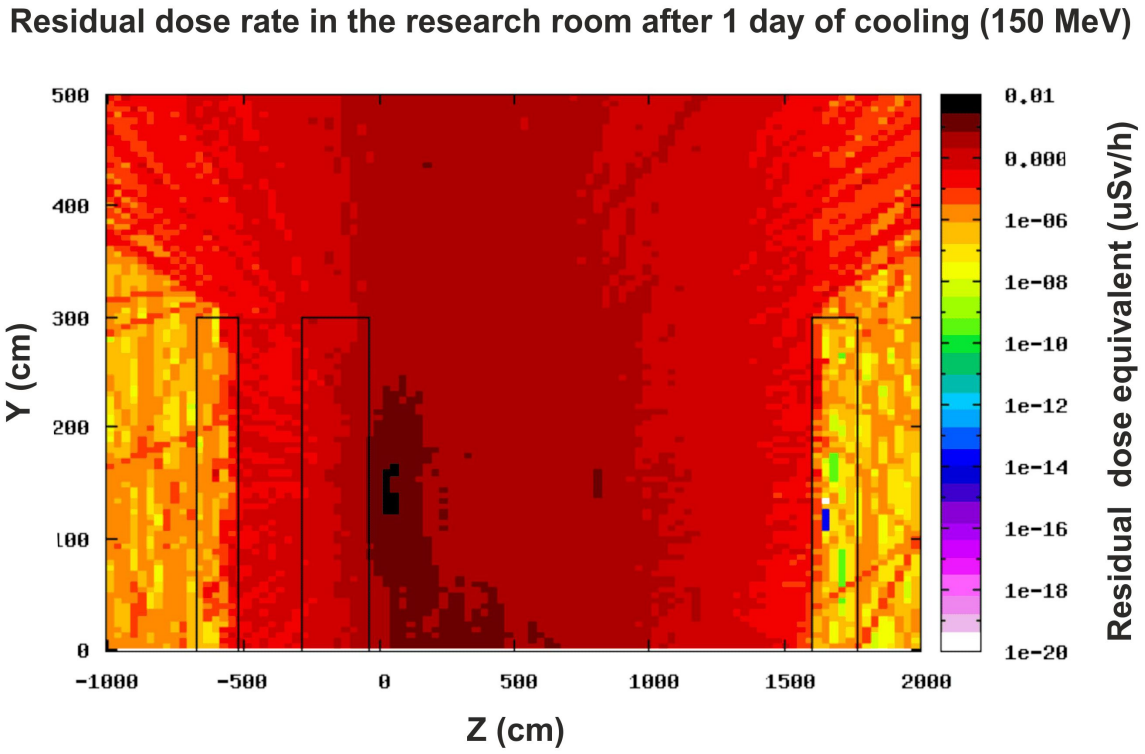

FIGURE 5.20: Ambient dose equivalent in beam pipe, graphite phantom, concrete and air after 1 day of cooling for a 150 MeV proton beam.

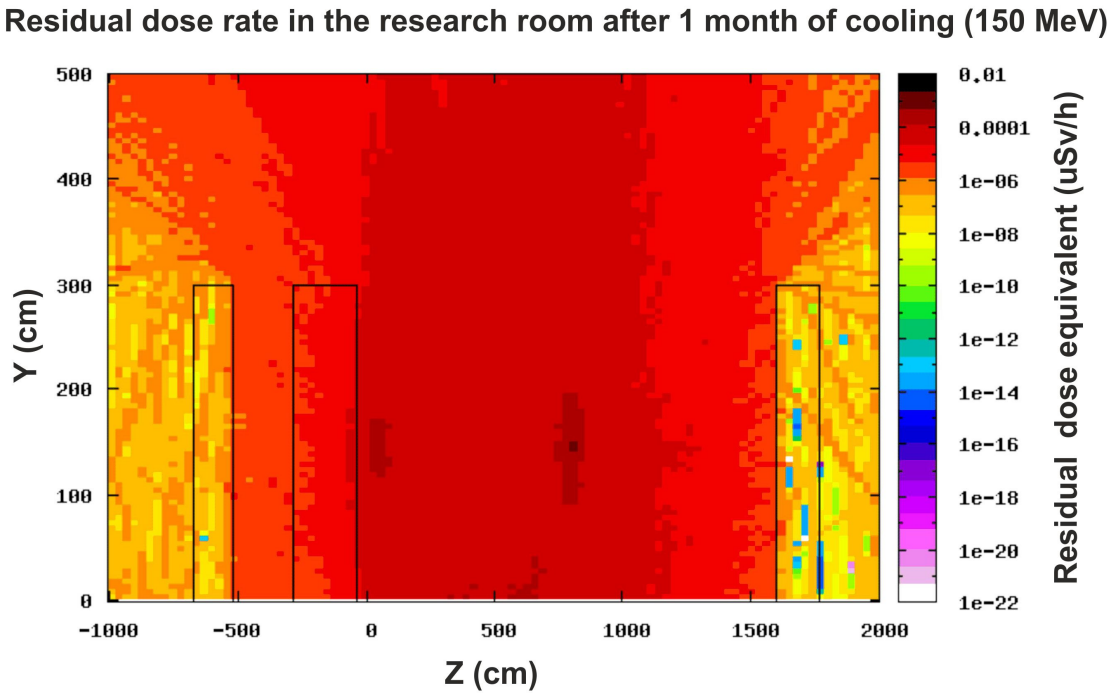

FIGURE 5.21: Residual dose equivalent in beam pipe, graphite phantom, concrete and air after 1 month of cooling for a 150 MeV proton beam.

In conclusion, for a 150 MeV proton beam, the residual dose in the research room due to the beam line activation after irradiation is relatively high, but outside the shielding walls the residual dose is low, 10^{-2} μSv/h. After 1 hour the residual dose decreases to 0.1 μSv/h in the research room and 10^{-4} μSv/h outside the research room. Therefore, the access of the staff in the research room, immediately after irradiation, it is permitted as well the access of public in the corridor or to the facility room.

The residual dose was calculated also for a 250 MeV proton beam. After the irradiation, the results showed that the residual dose at the isocentre is high and reaches 50 μSv/h and 5 μSv/h at the shielding wall behind the isocentre. In the maze, the residual dose has a value of 0.1 μSv/h. Outside the shielding walls, in the corridor the residual dose is 10^{-2} μSv/h as shown in figure 5.22. These results suggest that the access of the employees and members of public should not be limited as the dose values are below the limits suggested by the UK regulations [40].

After 1 hour, the residual dose at the isocentre decreases to 0.5 μSv/h and 10^{-2} μSv/h in the vicinity. At the point of interest, the residual dose is 10^{-3} μSv/h at the maze and 10^{-4} on the corridor μSv/h as shown in figure 5.23.

After 1 day, the residual dose in the research room is 0.05 μSv/h and outside the shielding walls, the residual dose decreases to 10^{-3} μSv/h in the maze and to 10^{-5} μSv/h on the corridor as shown in figure 5.24. After one month of cooling, the residual dose decreases

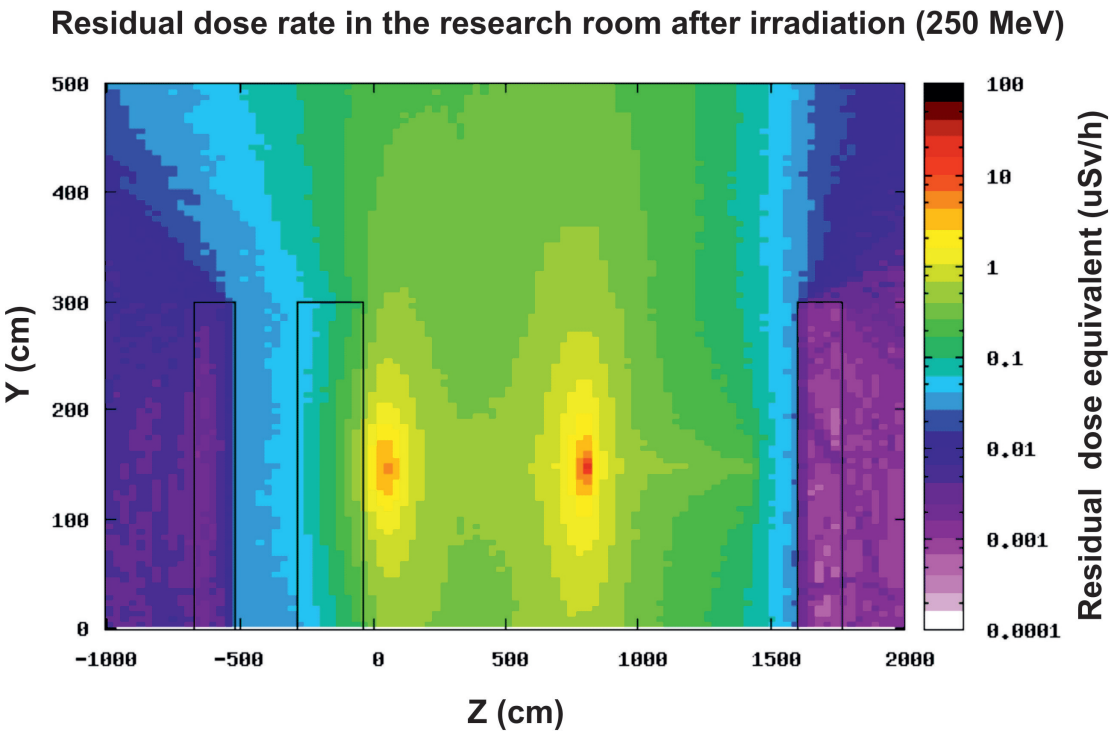

FIGURE 5.22: Residual dose equivalent in beam pipe, graphite phantom, concrete and air after irradiation with a 250 MeV proton beam.

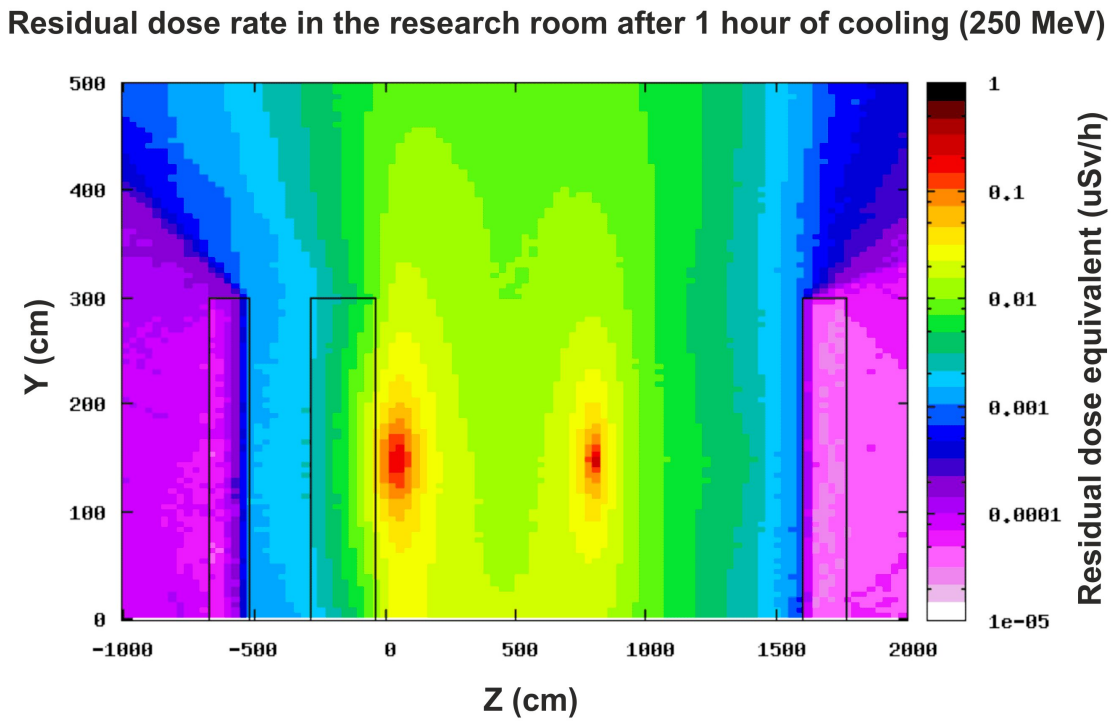

FIGURE 5.23: Residual dose equivalent in beam pipe, graphite phantom, concrete and air after 1 hour of cooling for a 250 MeV proton beam.

considerably to 10^{-3} μSv/h at the isocentre, 10^{-5} μSv/h in the maze and 10^{-6} μSv/h on the corridor as shown in figure 5.25.

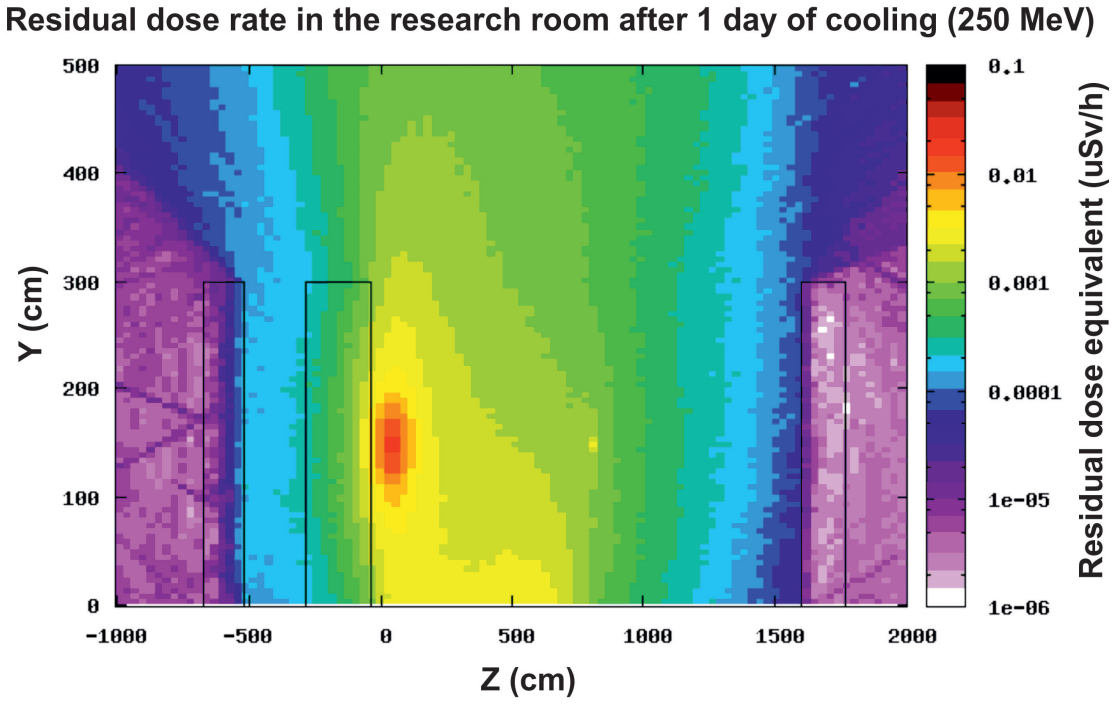

FIGURE 5.24: Residual dose equivalent in beam pipe, graphite phantom, concrete and air after 1 day of cooling for a 250 MeV proton beam.

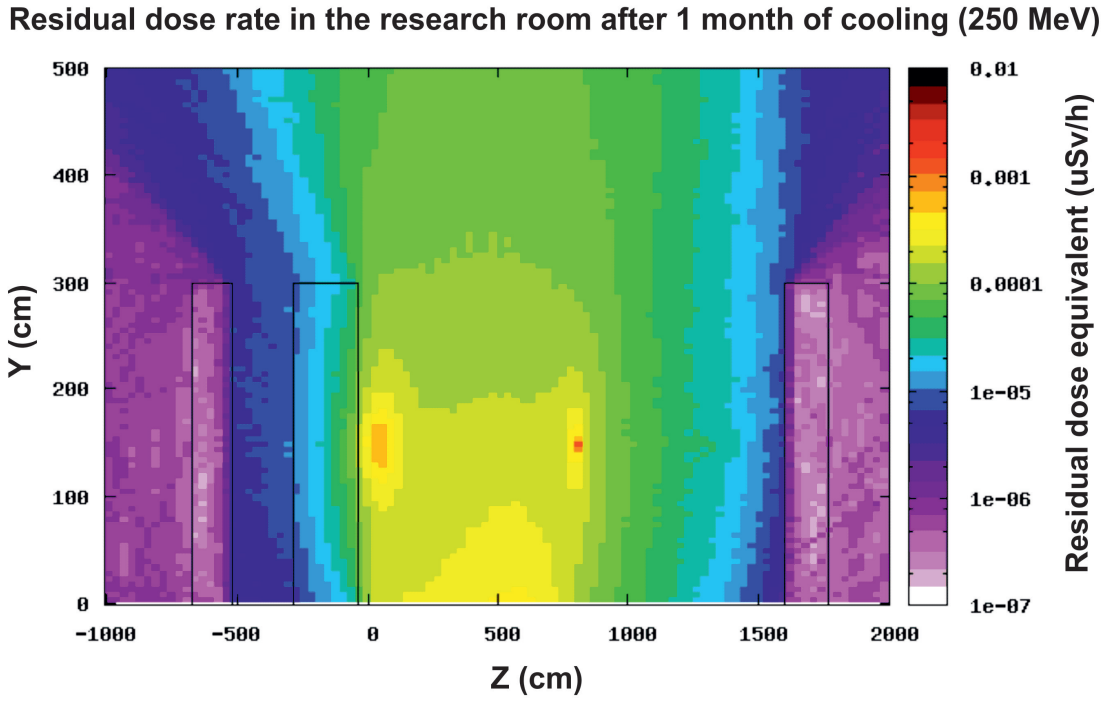

FIGURE 5.25: Residual dose equivalent in beam pipe, graphite phantom, concrete and air after 1 month of cooling for a 250 MeV proton beam.

After 3 months the residual dose in the research room is 10^{-4} μSv/h and outside the shielding walls is 10^{-7} μSv/h. In one year's time, the dose decreases to 10^{-5} μSv/h around the beam line and 10^{-6} μSv/h in the vicinity. Outside the shielding walls the residual dose was found to be 10^{-8} μSv/h.

The results obtained for the residual dose rate in the research room suggest that if the proton beam runs at the maximum energy of 250 MeV, immediately after irradiation, the dose is found to be approximately 50 μSv/h at the isocentre and 10^{-2} μSv/h outside the shielding walls. These values are low enough not to request additional mitigation methods as the limits suggested by the UK regulations are fulfilled [40].

The next task was to calculate the radioactivity induced in the floor. The same irradiation profile as above was used. The floor is 2.5 cm thick and is made of stainless steel. In FLUKA, the typical stainless steel has a composition of 18% ^{24}Cr, 74% ^{26}Fe and 8% ^{28}Ni. The floor does not include the maze. The results are presented in table 5.6 and include only the isotopes with high activity and medium and long half-lives.

a) Immediately (after irradiation)

The results suggest that, immediately after irradiation, the highest activity will be be given by ^{58}Co, ^{57}Ni, ^{56}Mn, ^{55}Co, ^{51}Cr, ^{51}Mn and ^{49}Cr but at 70 MeV and 150 MeV, the activity of these radioisotopes will not reach the limits suggested by the UK regulations [40]. At 250 MeV, only the activity of ^{56}Mn exceeds the limit. Therefore, at maximum energy, the radioactivity induced in the stainless steel floor is below the limits suggested in IRR99 [40], hence the stainless steel floor do not represent a hazard.

b) Cooling time 1 hour (after irradiation)

After 1 hour of cooling, the activity of the radionucliedes mentioned before is decreasing and even at maximum energy, the activity will not exceed the limits as shown in table 5.7.

c) Cooling time 1 month (after irradiation)

After 1 month, the activity of several radioisotopes will decrease significantly down to 3.929017×10^{-17} Bq for ^{55}Co. Therefore, the results for the activity after one month and one year cooling time are not presented as the levels are insignificant.

This study showed that the activation of the stainless steel floor does not represent a factor of exposure for personnel, as the activity is low when compared with the air present in a normal 100 sq meter European home which has up to 30,000 Bq [114].

Isotope	$T_{1/2}$	**A (Bq)**	**A (Bq)**	**A (Bq)**	**Limit from IRR99 (Bq) [40]**
		70 MeV	**150 MeV**	**250 MeV**	
^{65}Ni	2.5172 h	-	5.9×10^{2}	2.1×10^{3}	10^{6}
^{61}Co	1.650 h	4.0×10^{2}	1.2×10^{3}	5.8×10^{3}	10^{6}
^{60}Cu	23.7 m	-	-	2.8×10^{3}	10^{5}
^{58}Co	70.86 d	1.1×10^{3}	4×10^{3}	6.8×10^{3}	10^{6}
^{57}Co	271.74 d	2.1×10^{2}	9.6×10^{2}	2.2×10^{3}	10^{6}
^{57}Ni	35.60 h	2.3×10^{3}	10^{4}	3×10^{4}	10^{6}
^{56}Mn	2.5789 h	6.1×10^{4}	2.7×10^{5}	5.8×10^{5}	10^{5}
^{56}Co	77.233 d	3.8×10^{2}	2×10^{3}	5.2×10^{3}	10^{5}
^{56}Ni	6.075 d	-	5.7×10^{2}	1.7×10^{3}	10^{6}
^{55}Fe	2.737 y	3.6×10^{2}	1.7×10^{3}	3.9×10^{3}	10^{6}
^{55}Co	17.53 h	2.1×10^{3}	1.3×10^{4}	3.2×10^{4}	10^{6}
^{54}Mn	312.03 d	4.1×10^{2}	2.6×10^{3}	6.5×10^{3}	10^{6}
^{52}Mn	5.591 d	9.8×10^{2}	1.3×10^{4}	4.6×10^{4}	10^{5}
^{52}Fe	8.275 h	2.6×10^{2}	1.9×10^{3}	6.2×10^{3}	10^{6}
^{51}Cr	27.7025 d	5.0×10^{3}	2.6×10^{4}	7.3×10^{4}	10^{7}
^{51}Mn	46.2 m	1.8×10^{3}	2.2×10^{4}	8.9×10^{4}	10^{5}
^{49}Cr	42.3 m	2.2×10^{3}	3.2×10^{4}	1.1×10^{5}	10^{6}
^{49}V	329 d	-	8×10^{2}	2.7×10^{3}	10^{7}
^{48}V	15.9735 d	1.6×10^{2}	4.8×10^{3}	2.1×10^{4}	10^{5}
^{48}Cr	21.56 h	-	1.4×10^{3}	5.3×10^{3}	10^{6}
^{47}V	32.6 m	-	5.8×10^{3}	3×10^{4}	10^{5}
^{45}Ti	184.8 m	-	5.5×10^{3}	3.3×10^{4}	10^{6}
^{44}Sc	3.97 h	-	3.5×10^{3}	9.2×10^{3}	10^{5}
^{43}Sc	3.891 h	-	9.8×10^{3}	9.2×10^{4}	10^{6}
^{42}K	12.360 h	-	-	2.4×10^{3}	10^{6}
^{24}Na	14.9590 h	-	-	1.1×10^{3}	10^{5}

TABLE 5.6: The most abundant radionuclides in the floor after irradiation for 70 MeV, 150 MeV and 250 MeV proton beams with the limits allowed by IRR99 [40].

Isotope	$T_{1/2}$	**A (Bq)**	**A (Bq)**	**A (Bq)**	**Limit from IRR99 (Bq) [40]**
		70 MeV	**150 MeV**	**250 MeV**	
^{65}Ni	2.5172 h	-	4.5×10^{2}	1.6×10^{3}	10^{6}
^{61}Co	1.650 h	1.5×10^{2}	7.8×10^{2}	3.8×10^{3}	10^{6}
^{58}Co	70.86 d	1.1×10^{3}	4×10^{3}	6.8×10^{3}	10^{6}
^{60}Cu	23.7 m	-	-	24.8×10^{2}	10^{5}
^{57}Co	271.74 d	2.1×10^{2}	9.6×10^{2}	2.2×10^{3}	10^{6}
^{57}Ni	35.60 h	2.3×10^{3}	10^{4}	3×10^{4}	10^{6}
^{56}Mn	2.5789 h	4.6×10^{4}	2×10^{5}	4.4×10^{5}	10^{5}
^{56}Co	77.233 d	3.8×10^{2}	2×10^{3}	5.2×10^{3}	10^{5}
^{56}Ni	6.075 d	-	5.6×10^{2}	1.7×10^{3}	10^{7}
^{55}Fe	2.737 y	3.6×10^{2}	1.2×10^{3}	3.9×10^{3}	10^{6}
^{55}Co	17.53 h	2×10^{3}	1.7×10^{3}	3.1×10^{4}	10^{6}
^{54}Mn	312.03 d	4.1×10^{2}	2.6×10^{3}	6.5×10^{3}	10^{6}
^{52}Mn	5.591 d	9.7×10^{2}	1.3×10^{4}	4.6×10^{4}	10^{5}
^{52}Fe	8.275 h	2.4×10^{2}	1.7×10^{3}	5.7×10^{3}	10^{6}
^{51}Cr	27.7025 d	5×10^{3}	2.6×10^{4}	7.3×10^{4}	10^{7}
^{51}Mn	46.2 m	7.3×10^{2}	9.2×10^{3}	3.6×10^{4}	10^{5}
^{49}V	329 d	-	8×10^{2}	2.7×10^{3}	10^{7}
^{49}Cr	42.3 m	8.2×10^{2}	1.2×10^{4}	4.3×10^{4}	10^{6}
^{48}V	15.9735 d	1.6×10^{2}	4.8×10^{3}	2.1×10^{4}	10^{5}
^{48}Cr	21.56 h	-	1.4×10^{3}	5.2×10^{3}	10^{6}
^{47}V	32.6 m	-	1.6×10^{3}	8.5×10^{3}	10^{5}
^{45}Ti	184.8 m	-	4.4×10^{3}	2.6×10^{4}	10^{6}
^{43}Sc	3.891 h	-	8.26×0^{2}	7.7×10^{3}	10^{6}
^{42}K	12.360 h	-	-	2.3×10^{3}	10^{6}
^{24}Na	14.9590 h	-	-	1×10^{3}	10^{5}

TABLE 5.7: The most abundant radionuclides in the floor after 1 hour for 70 MeV, 150 MeV and 250 MeV proton beams with the limits allowed by IRR99 [40].

5.4 Conclusion

The prompt ambient dose equivalent for neutrons and photons was calculated for different points of interest like the phantom (isocentre), the maze, the corridor and the treatment room for different energies 70 MeV, 100 MeV, 150 MeV, 200 MeV and 250 MeV. The results showed that the secondary dose increases with energy, especially in the direction of the beam line. At the minimum energy of 70 MeV, the neutron dose equivalent at the isocentre was found to be around 50 μSv/h and it decreases with distance. At the maze level the neutron dose was found to be 1 μSv/h and is even lower on the corridor and the adjacent treatment room. The photon dose was found to be approximately 10 μSv/h around isocentre and 0.1 μSv/h outside the shielding walls, at the facility room (point 4), while in the corridor it was found to be 0.05 μSv/h. Hence, for a 70 MeV proton beam, the neutron and the photon dose equivalent can be regarded as safe for employees or members of public.

If the full proton beam were to be lost in the graphite phantom at the maximum energy 250 MeV, the neutron dose equivalent would be 6 mSv/h at the isocentre, 80 μSv/h in the maze and 8 μSv/h in the accessible areas around the research room, while the photon dose would be 80 mSv/h at the isocentre, 50 μSv/h in the maze and 10 μSv/h in the areas around the research room.

As no person will stay 10 hours per week in the research room or in the maze when the beam is on, these values can be regarded as sufficiently low for employees over 18 years old. For the members of public, working in the accessible areas around the research room, the access should be limited when the beam is on to comply with the legal limits [40].

For the second set of simulations, the radioactivity induced in air, the beam pipe, concrete and other materials of the research room together with the residual dose rate was studied. The irradiation profile was set for 10 hours of activity per week at full intensity (2.75×10^9 protons/s). The results showed that, immediately after irradiation, the residual dose equivalent in the research room is of the order of several μSv/h: 1 μSv/h for 70 MeV and > 100 μSv/h for 250 MeV. After 1 hour, the value of the dose decreases significantly down to 50 μSv/h for 250 MeV. After 3 months, the dose decays down to 10^{-3} μSv/h. The results suggest that at 250 MeV the human intervention in the research room should be kept to a minimum possible after irradiation, but after 1 hour of cooling time, it will be safe for employees to access the room.

It should be noted that these results have been studied for the worst-case scenario, where the maximum beam energy (250 MeV) is used for a period of 1 year. In addition, the

irradiation profile was only presumed and the results will differ depending on the irradiation scenario. Therefore, to obtain more realistic results, it is necessary to develop more irradiation scenarios as detailed and complete as possible, but the results presented in this chapter indicate that the radiation produced during the operation of the accelerator will be well below the regulatory limits [40].

Chapter 6

Radiation protection studies for the OpenMed/BioLeir facility

6.1 Introduction

The OpenMed/BioLeir project at CERN was proposed in 2010 and the proposal consists in using the LEIR (the Low Energy Ion Ring) synchrotron, an existing facility at CERN, to provide beams for experiments to support of cancer treatment centres [116]. The Low Energy Ion Ring (LEIR) facility was proposed in 1993 and it accumulates heavy ions, up to Pb^{54+}, in order to achieve the required luminosity for collisions in the Large Hadron Collider (LHC). LEIR was transformed from a previous synchrotron LEAR (Low Energy Anti-proton Ring) used to decelerate and store anti-protons [116]. LEIR was commissioned in 2005 and now the facility is part of the LHC injection, situated between the Linear Accelerator 3 (LINAC3) and Proton Synchrotron (PS), as illustrated in the figure 6.1.

Even though in Europe many clinics offer the possibility to treat cancer with hadron therapy, beam line time for pre-clinical radiation biology, chemistry, physics studies and for radiological experiments is limited so an additional facility is highly desirable. Therefore detailed studies should be done.

The motivation of using LEIR for medical research is that the facility is not used all the time for the LHC, therefore the provided beam could be used for the development of accurate detectors to be used for dosimetry of active or passive beam delivery systems, and for radiobiological experiments for different beam characteristics, ion species, cell lines and tissue. The beam could also be used to study the interaction of ions with

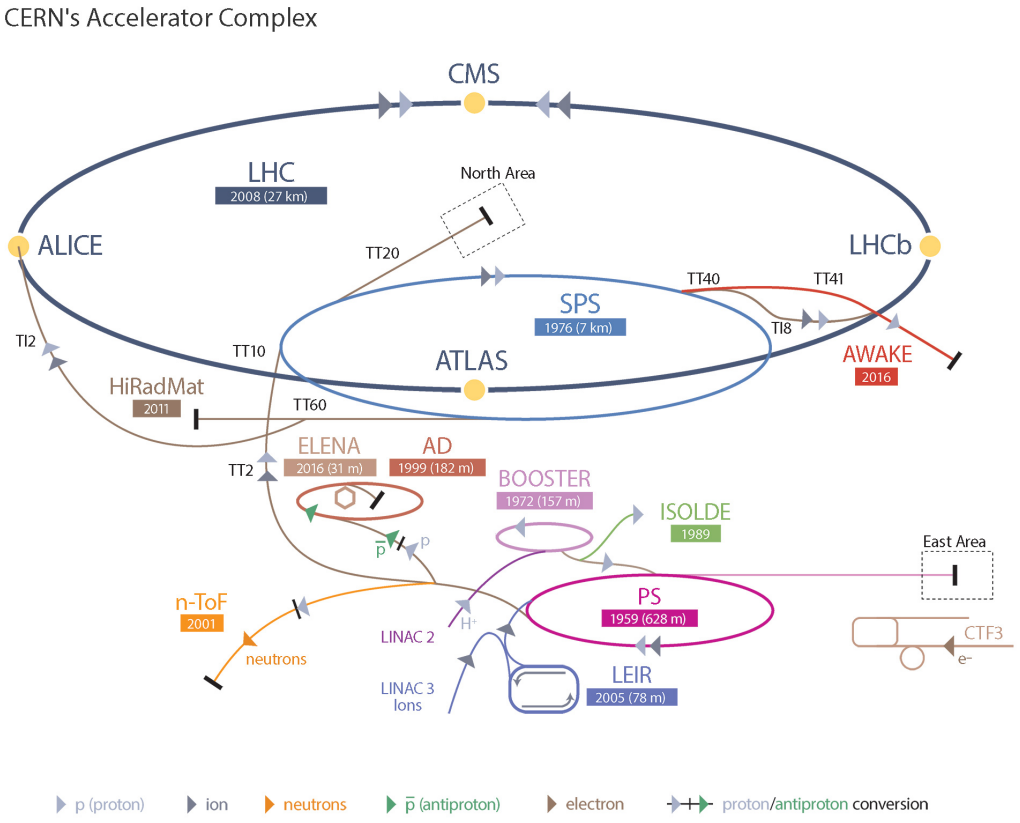

FIGURE 6.1: LHC injection chain [117].

different drugs used for chemotherapy or for developing more precise imaging techniques which could be used to treat moving targets.

LEIR it is specially suitable for a biomedical research facility because it can provide the space needed for experiments, as illustrated in figure 6.2. The LEIR machine occupies only a small part of the hall and almost 1500 m^2 could be used for the installation of experimental systems [116].

Despite all these advantages, there are some limitations of the existing facility regarding the requirements for radio-biological research. With the present main power supply, the energy for ^{12}C and ^{16}O can reach only 240 MeV/n. To reach the maximum energy used in hadron therapy of 400 MeV/n, the facility will need new power supply. The magnets are suitable to reach this energy. This higher energy will increase the radiation protection issues [119].

LEIR is the only accelerator at CERN with possible access for visitors during the machine operation, via a platform installed above the shielding wall, as can be seen in figure 6.3. The first and the only radiation protection calculations were made by Sanja Damjanovic [120]. This work includes only the results for the present situation, where Pb, Xe and

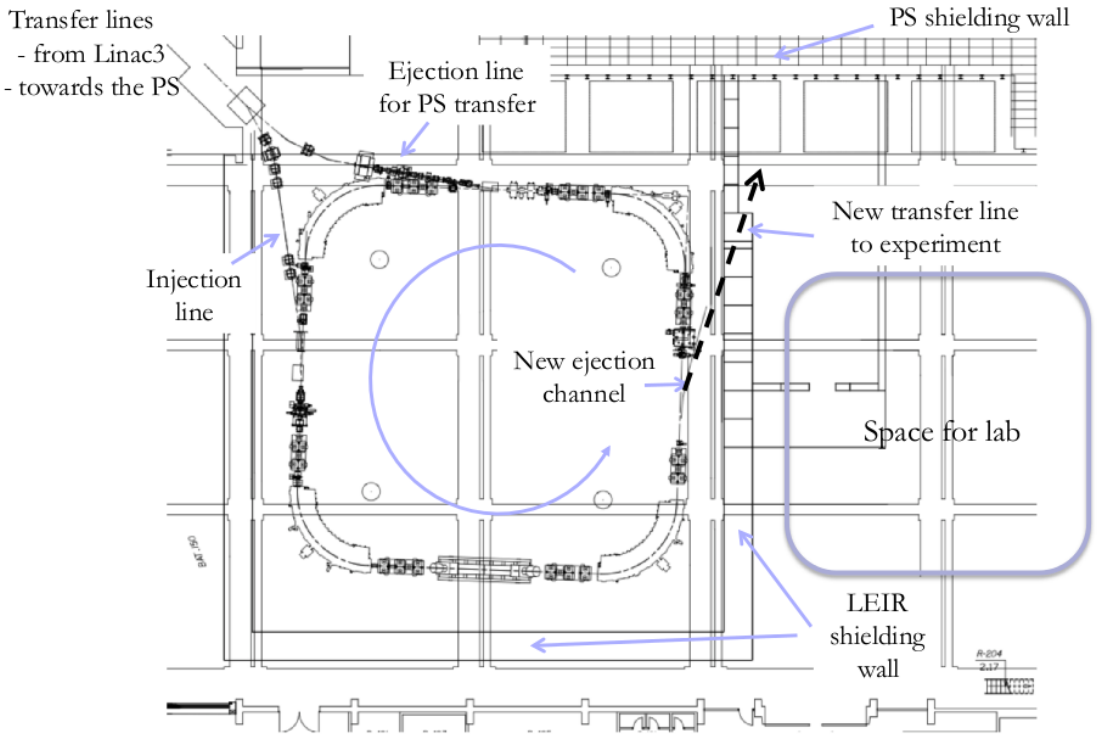

FIGURE 6.2: The LEIR facility layout [118].

Ar ions are accelerated as primary particles. In [120], the dose rates at the visitor platform for different beam losses are presented for Pb, Xe and Ar ion species. The results presented show that the dose at the visitor platform level will be between 0.45-2 μSv/h for these ion species and normal beam losses, while for a continuous full beam loss, the ambient dose equivalent was found to be approximately 4.6 μSv/h. As the visitor platform is classified as a supervised radiation area, the dose at this level should not exceed 10 μSv/h according to the CERN regulations [48]. The results obtain in [120] showed that, for the present situation, the public access to the platform would be permitted. Any changes in operational conditions should be followed by new radiation protection calculations as for Oxygen and Carbon ions with a beam energy of 250 MeV/n, the dose at the visitor platform level is expected to reach 60 μSv/h for 1% beam losses [120].

Using the same geometry as in [120], the aim of this work is to conduct radiation protection studies using the future operational conditions at LEIR, and thus to establish if the existing facility needs an additional roof on top of the machine when using ions from protons up to Oxygen in the range of 1 to 250 MeV/n, and to see if the facility needs extra shielding walls in order to protect the staff working in the adjacent laboratories or the CMS control room.

FIGURE 6.3: The LEIR visitor platform with the LEIR ring behind it [120].

The CERN's radiation safety code [48] is based on international standards and it complies with the IRR99 [40] dose limits:

- 20 mSv whole body annual dose for employees;
- 6 mSv whole body annual dose for trainees;
- 1 mSv whole body annual dose for the members of the public;

The ambient dose equivalent was calculated at three different heights: at the beam line level of 1.7 metres, at 5 metres height where the roof might be placed and 6.5 metres height at the visitor platform level. The dose at 1.7 m height was simulated with the aim of calculating the possible dose received by the personnel working at the beam line level for the maintenance of the machine. The dose at the roof level was calculated to observe the difference of the dose value with roof and without and the dose at the visitor platform level was calculated to establish if the dose exceeds the legal limit [48]. Figure 6.3 shows the visitor platform situated on top of the LEIR synchrotron.

As LEIR is planned to become a biomedical experimental facility, the machine will accelerate protons and carbon ions. There is also a new interest for helium and oxygen ions which are considered good candidates for future clinical use, as helium ions have a

small lateral penumbra when compared with protons, and oxygen ions have a higher RBE compared with carbon which make them a good candidate for radio-resistant tumours [116]. Therefore the simulations were made for ^{1}H, ^{4}He, ^{12}C and ^{16}O ions with an energy of 250 MeV and 250MeV/n respectively. This energy was chosen as this is the maximum energy which can be provided with the current power supply [119].

6.2 The simulations

The essential aim of this project is to determine if the LEIR facility provides appropriate radiation shielding, especially at the visitor platform. The radiation around the LEIR will be mainly formed by neutrons and gamma rays escaping from the radiation sources like beam line components and air. The secondary particles can cause skyshine exposure to members of staff working in the vicinity of the facility. The main goal of the radiation protection calculations is to ensure that the dose equivalent is less than 3 μSv/h outside the shielding walls and less than 10 μSv/h at the visitor platform and that the CERN Radiation Protection rules and regulations complied with: 6 mSv/y in supervised radiation areas and 20 mSv/y in simple controlled radiation areas [48].

The ambient dose equivalent was calculated using the FLUKA Monte Carlo code [79, 86]. The FLUKA code was described in chapter 3. The PRECISIO default was used for all simulation as it is used mainly for precision simulations. This default includes [93]:

- The transport of electrons, positrons and photons is activated;
- The Rayleigh scattering and Compton scattering profiles are activated;
- The neutrons are transported down to thermal energies;
- Fully analogue, the physical reality is simulated without giving any importance to some of the geometry areas, absorption for low-energy neutrons;
- Particle transport threshold set at 100 keV, except for neutrons;
- Multiple scattering threshold at minimum allowed energy, for both primary and secondary charged particles;
- Delta ray production on with threshold 100 keV;
- Heavy particle e^+ e^- pair production activated with full explicit production;
- Heavy fragment transport activated;

The ambient dose equivalent for all particles was calculated using the USRBIN option to score the distribution of the dose in the geometry provided and the AUXSCORE to set the scoring detector and to choose the dose equivalent conversion factor. In this case, the AMB74 option was chosen as it uses the dose equivalent conversion factor implemented by ICRP74 [94] and M. Pellicioni [95]. The simulations were made for ^{12}C, ^{16}O, ^{4}He and ^{1}H and for three for three different beam loss rates: 1% (1.9 $\times 10^{7}$ ions/s) and 20% (3.8 $\times 10^{8}$ ions/s) as these covers the range of losses experienced in normal conditions and 100% (1.9 $\times 10^{9}$ ions/s) which represents full beam loss and is the worst-case scenario.

The ions are assumed to interact with the surface of the stainless steel beam tube with the extraction energy (250 MeV). The impact point is localized in the beam direction (at z=0) and randomly distributed. The stainless steel beam tube outer radius is R_o= 14.8 cm and the inner radius is R_i=14.5 cm. The accelerator structure and room were designed with the FLAIR interface for FLUKA as shown in figures 6.4 and 6.5, using the same model as in [120]. The height of the concrete walls is 4 m and the thickness is 1.6 m [120]. The concrete used at CERN has a density of 2.35 g/cm^3 and a composition of 52.9% ^{16}O, 3.37% ^{28}Si, 1% ^{1}H, 1.6% ^{23}Na, 0.2% ^{24}Mg, 3.4% ^{27}Al, 0.1% ^{12}C, 1.3% ^{39}K, 4.4% ^{40}Ca and 1.4% ^{56}Fe. The concrete composition was provided by Vasilis Vlachoudis from CERN.

FIGURE 6.4: FLUKA plan geometry of the accelerator room.

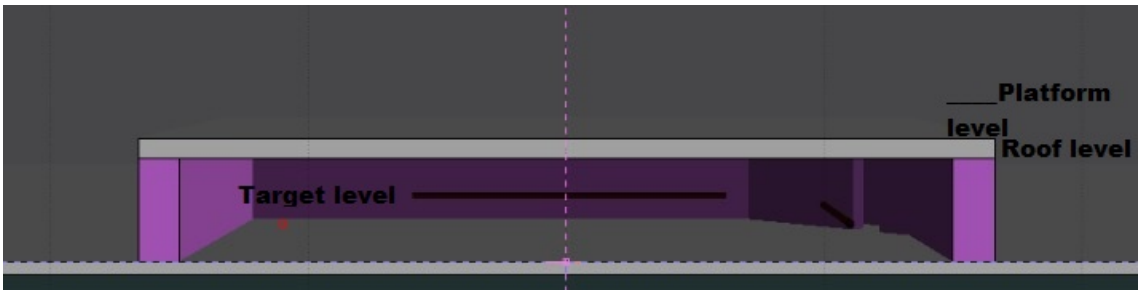

FIGURE 6.5: Elevation view of the accelerator room with the concrete roof.

The materials used in the FLUKA simulations are shown in the table 6.1:

Structure	**Material**	**Density (g/cm^3)**
Walls	Concrete	2.35
Beam tube	Stainless steel	8
Room	Air	1.225×10^{-3}

TABLE 6.1: Materials used in the FLUKA model.

As mentioned before, for radiation protection purposes, the ambient dose equivalent was calculated at three different levels: at the beam line level (1.7 m), at the roof level (5 m) and at the platform level (6.5 m).

6.3 Results

Using the FLUKA Monte Carlo code together with FLAIR interface, the ambient dose equivalent for secondary particles (neutron and gamma radiation) was calculated for ^{12}C, ^{16}O, ^{4}He and ^{1}H ion beams interacting with the stainless steel beam pipe in different sections of the machine: the injection line (SS10), the second section along the shielding wall (SS20), the extraction line (SS30)(see figure 6.6) with the maximum energy of 250 MeV and for three beam losses (1%, 20%, 100%). To reduce the number of scenarios presented it was simulated 1% in SS10, 20% in SS20 and 100% in SS30.

Every simulation was performed with five runs of 10^6 primary particles, giving $5\times$ 10^6 primary particles. The first set of simulations was made with no roof on top of the machine, while for the second set a roof of 80 cm thickness of concrete was added. For both set of simulations, three different simulations were run for all beam losses but I have chosen to include only one image for every beam loss at different heights because the results were very similar.

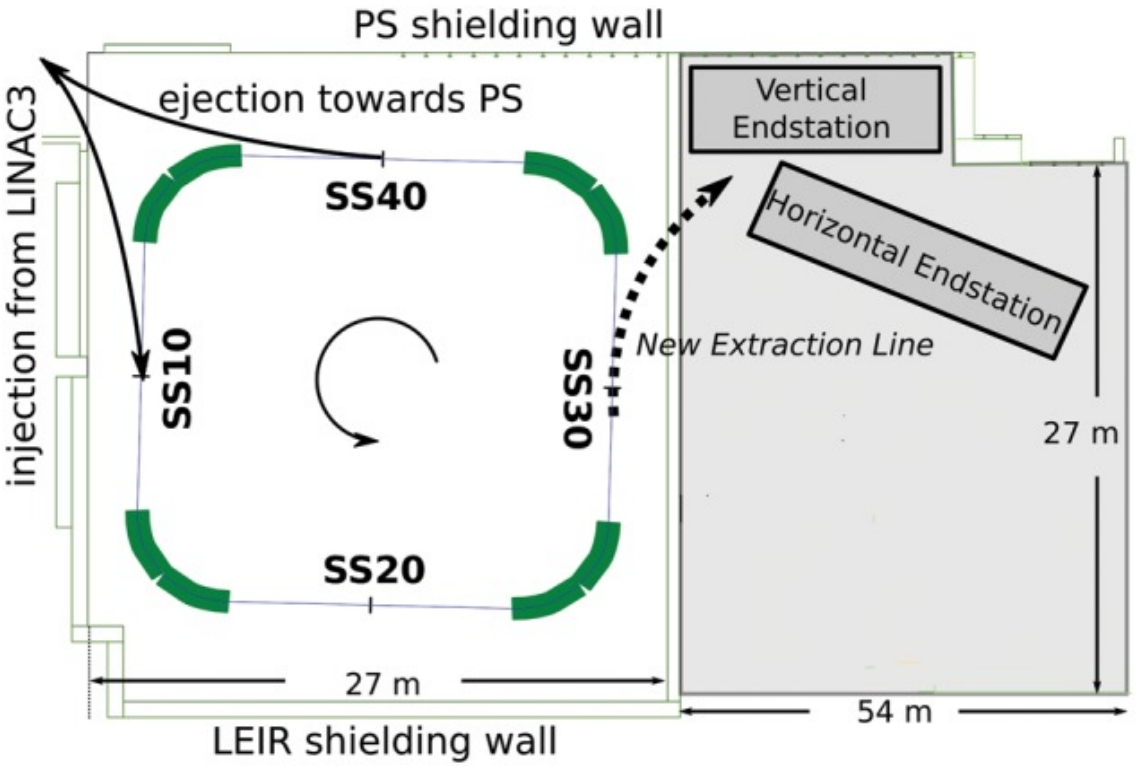

FIGURE 6.6: The LEIR layout [117].

Hydrogen at 1%, 20%, 100% beam loss without roof

For a beam loss of 1% at the beam line level, when the 250 MeV proton beam passes the injection line SS10, it interacts with the beam tube producing a high dose at the interaction point of 10^2 μSv/h. At the chicane, the radiation dose is 1 μSv/h. Behind the shielding walls the ambient dose equivalent is 0.1 μSv/h at the interaction point and 0.01 μSv/h in the laboratories space while at the visitor platform level, the dose is less than 1 μSv/h, as seen in figure 6.7.

As the proton beam goes further, it interacts with SS20, the second section of the beam line along the shielding wall. For a 20% beam loss in SS20, the dose level at the interaction point is 10^4 μSv/h. At the roof level (5 metres above ground) the ambient dose equivalent above the interaction point is 50 μSv/h, while above the chicane it is 1 μSv/h. At the visitor platform, the dose is around 5 μSv/h. Behind the shielding walls, where the interaction occurs, the dose is 5 μSv/h and it decreases down to 0.5 μSv/h in the research laboratory as shown in figure 6.8.

In SS30, for the worst case scenario when the entire beam is lost, the dose at the interaction point is 10^5 μSv/h, while at the platform level (6.5 metres above the beam line), the ambient dose equivalent is 60 μSv/h. Above the chicane the dose is low, 1 μSv/h and outside the shielding walls, where the interaction occurs, the dose equivalent is approximately 5 μSv/h and 1 μSv/h in the laboratory as seen in figure 6.9.

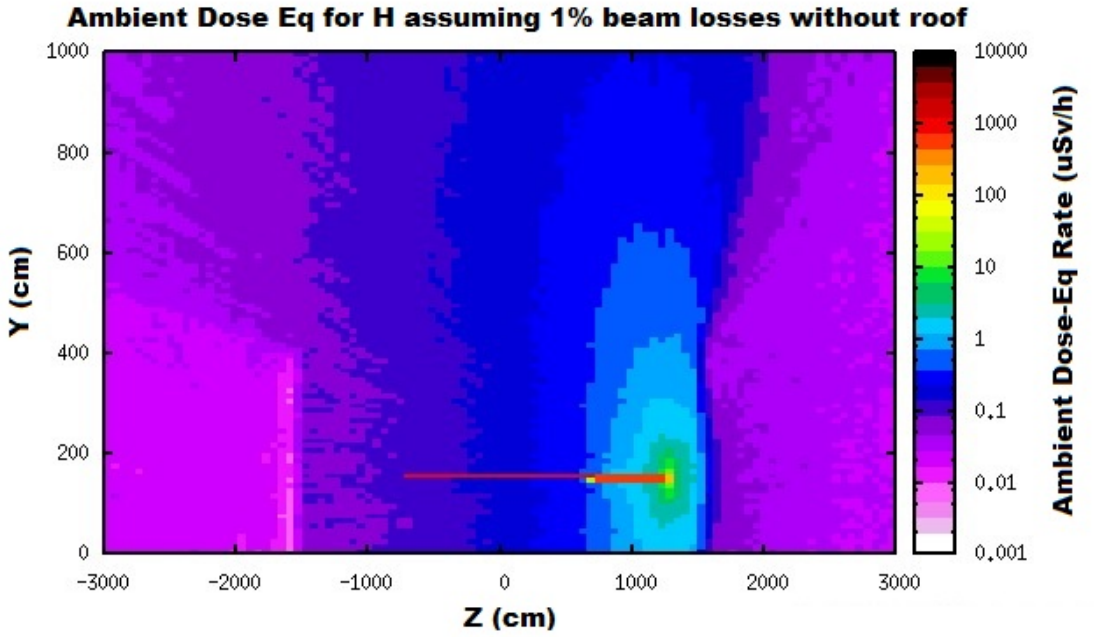

FIGURE 6.7: Ambient dose equivalent in SS10 for H at 1% beam loss.

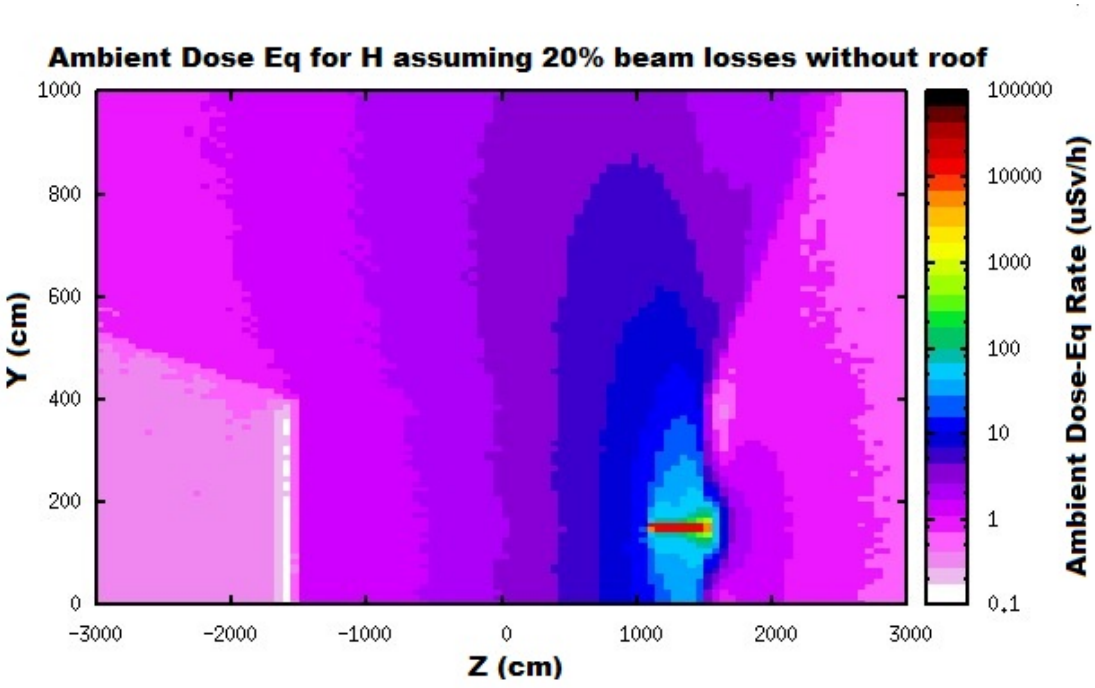

FIGURE 6.8: Ambient dose equivalent in SS20 for H at 20% beam loss.

These results shows that for protons, at 1% and 20% beam losses, the dose at the visitor platform is not higher than 5 μSv/h and in the laboratory the dose is 0.5 μSv/h, therefore the legal limit is not exceeded [48]. In the worst-case scenario, if the entire beam is lost, the dose at the visitor platform is 60 μSv/h, while in the lab it is around 5 μSv/h near the shielding wall and 1 μSv/h in the remaining space. These findings suggest that if the beam losses are higher than 20%, the dose limit allowed at the platform level will be

exceeded, therefore, the area has to be classified as a limited stay radiation area [48] and a roof on top of the machine will be required in order to decrease the dose at this point unless an interlock system is added to stop the beam if the beam loss limit is exceeded.

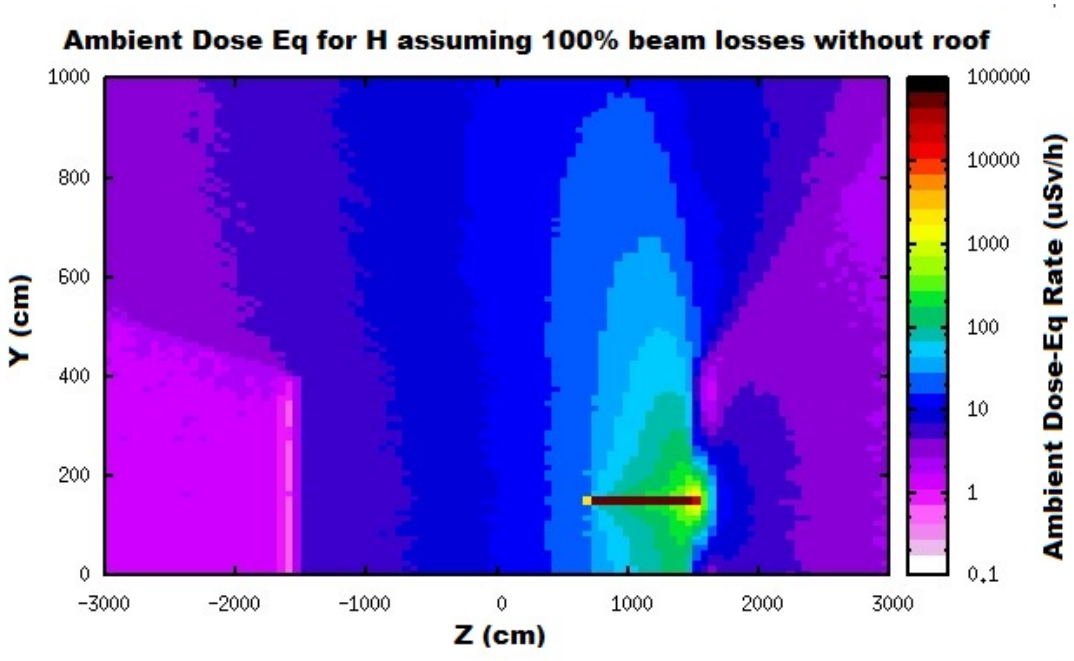

FIGURE 6.9: Ambient dose equivalent in SS30 for H at 100% beam loss.

Helium at 1%, 20%, 100% beam loss without roof

When a 250 MeV helium ion beam interacts with the SS10 injection line, at the beam line level the dose at the interaction point is 50 μSv/h for 1% beam loss. At the chicane, the ambient dose equivalent is 1 μSv/h. Behind the shielding wall including the laboratory, the ambient dose equivalent is 10^{-2} μSv/h as presented in figure 6.10. At the roof level, the dose is 1 μSv/h, while at the platform level it is approximately 0.5 μSv/h.

If the beam losses are increased to 20% in SS20, the dose at the interaction point is 10^2 μSv/h. At the roof level (5 metres above the ground), the ambient dose equivalent is 10 μSv/h above the interaction point. Behind the shielding walls, in the direction of the interaction point, the dose is less than 1 μSv/h and 0.5 μSv/h in the research laboratory. At the platform level, the dose is 5 μSv/h as shown in figure 6.11.

When the entire beam is lost in SS30, the dose at the interaction point is 500 μSv/h and at the visitor platform it is 50 μSv/h. Behind the shielding wall, near the point where interaction occurs, the ambient dose equivalent is 1 μSv/h and decreases to 0.5 μSv/h as we move further away from the interaction point, as shown in figure 6.12.

These calculations suggest that, for 20% beam losses, the dose at the visitor platform is safe and no additional protection should be added as well the dose in the research

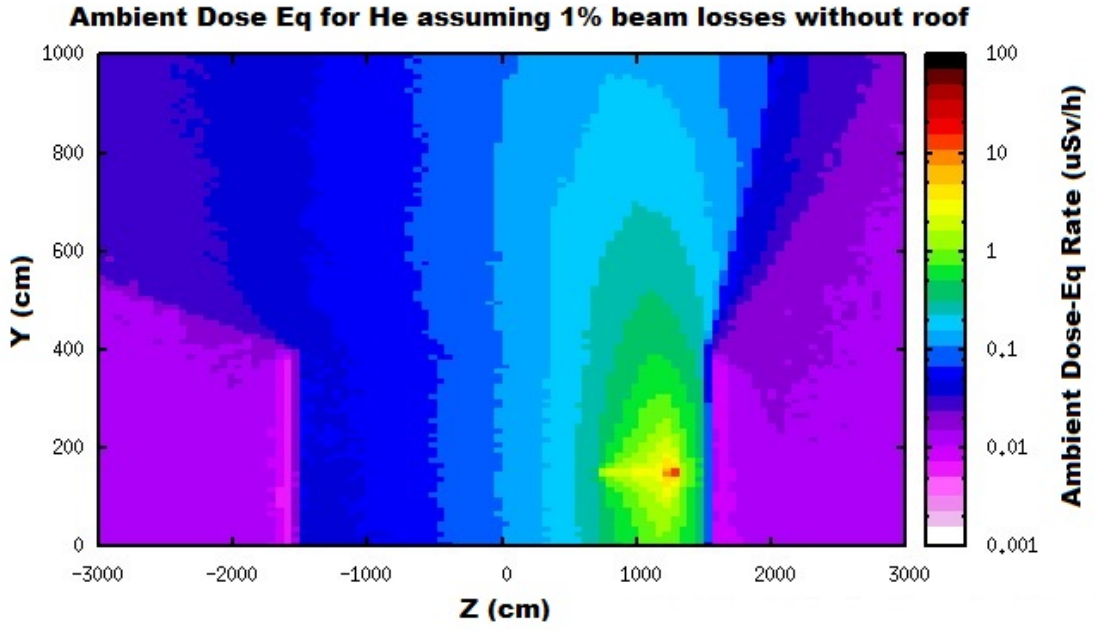

FIGURE 6.10: Ambient dose equivalent in SS10 for He at 1% beam loss.

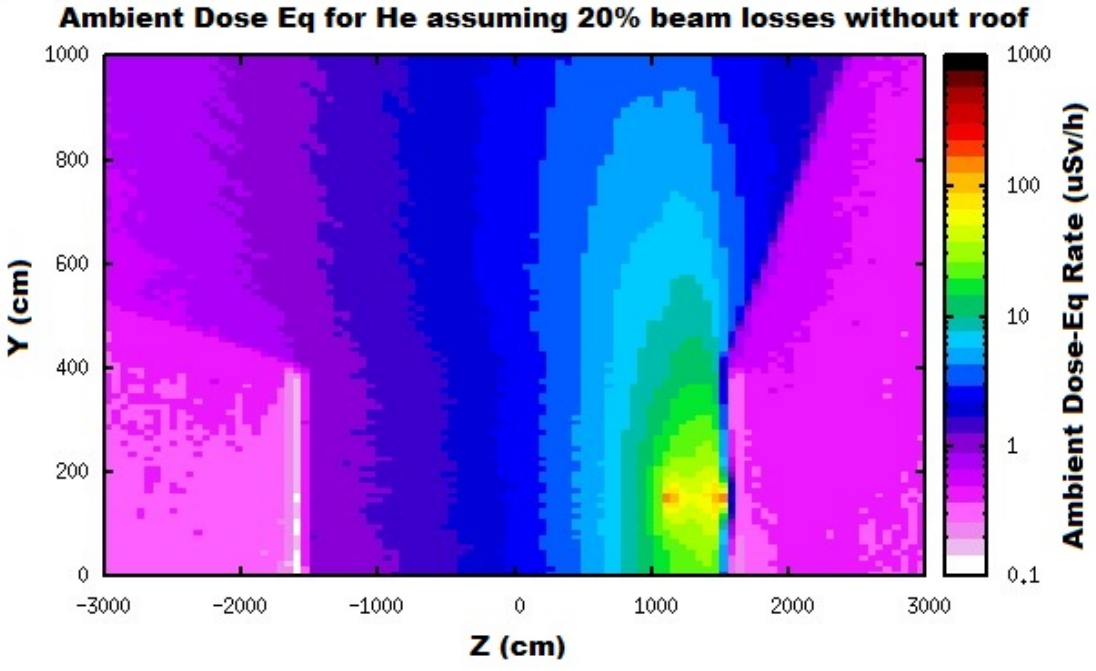

FIGURE 6.11: Ambient dose equivalent in SS20 for He at 20% beam loss.

laboratory, while at 100% beam losses, the dose at this level is 50 μSv/h, and 0.5 μSv/h in the laboratory, therefore a roof should be placed on top of the machine to protect the visitor against an eventual total beam loss.

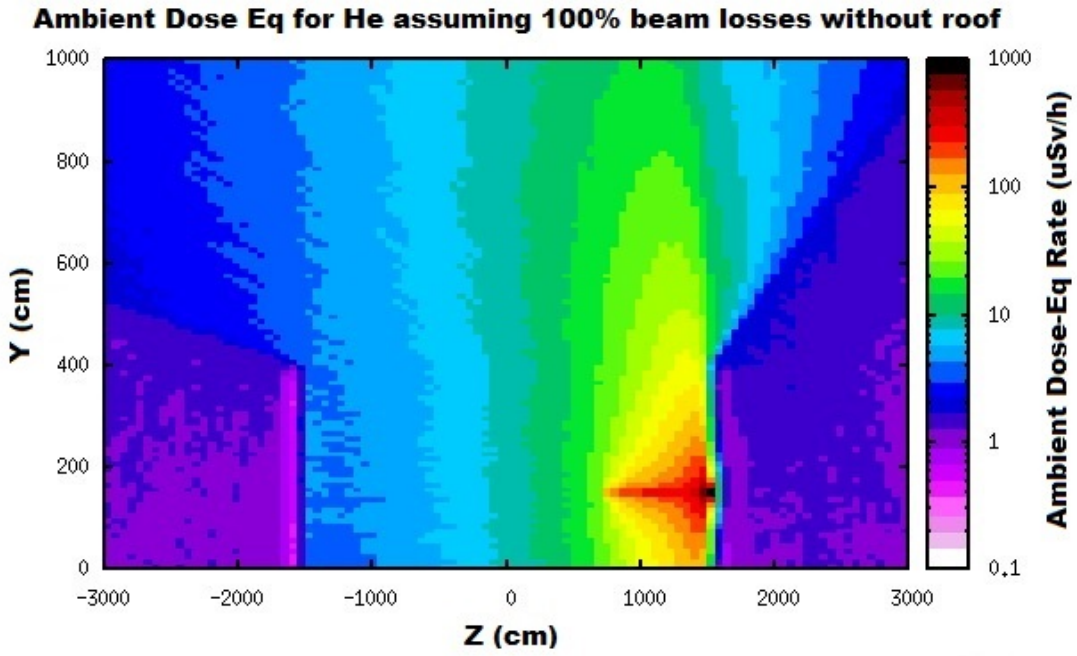

FIGURE 6.12: Ambient dose equivalent in SS30 for He at 100% beam loss.

Carbon at 1%, 20%, 100% beam loss without roof

The ambient dose equivalent was also calculated for a 250 MeV/n carbon beam, interacting with the beam pipe. For 1% beam loss in SS10, the dose at the interaction point is 500 μSv/h. Behind the shielding wall at the interaction point, the dose is 5 μ Sv/h and 0.5 μSv/h in the remaining space, including the laboratory space as shown in figure 6.13. The dose at the roof level is approximately 10 μSv/h and less at the visitor platform level.

If 20% of the carbon beam is lost in SS20, the ambient dose equivalent at the interaction point is 10^3 μSv/h and outside the shielding wall is 10 μSv/h. At the visitor platform the dose is 50 μSv/h, and it is 70 μSv/h at the roof level. In the laboratory area, the ambient dose equivalent is less than 10 μSv/h near the shielding walls and it decreases with distance to 1 μSv/h as shown in figure 6.14.

In the worst case scenario, when the entire beam is lost in SS30, the dose at the interaction point is 10^4 μSv/h. At the visitor platform the dose is high, 500 μSv/h, while at the roof level it is 10^3 μSv/h. In the same direction, but behind the shielding wall, the dose is 10^2 μSv/h and in the laboratory the dose is 10 μSv/h as shown in figure 6.15.

The results indicate that, when 20% of the carbon ion beam is lost, the dose at the visitor platform will not exceed 50 μSv/h. If 100% of the beam is lost in SS30, then the dose at the visitor platform will be 500 μSv/h and in the research laboratory it will be 10 μSv/h. As this dose has a high value and exceeds the legal limits at the visitor

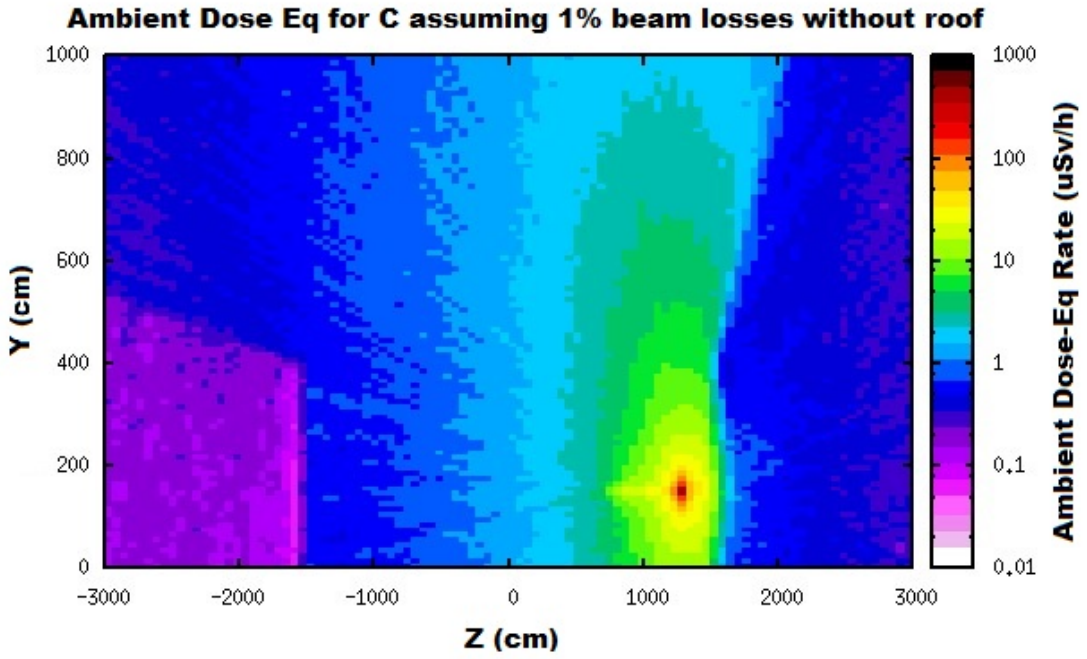

FIGURE 6.13: Ambient dose equivalent in SS10 for ^{12}C at 1% beam loss.

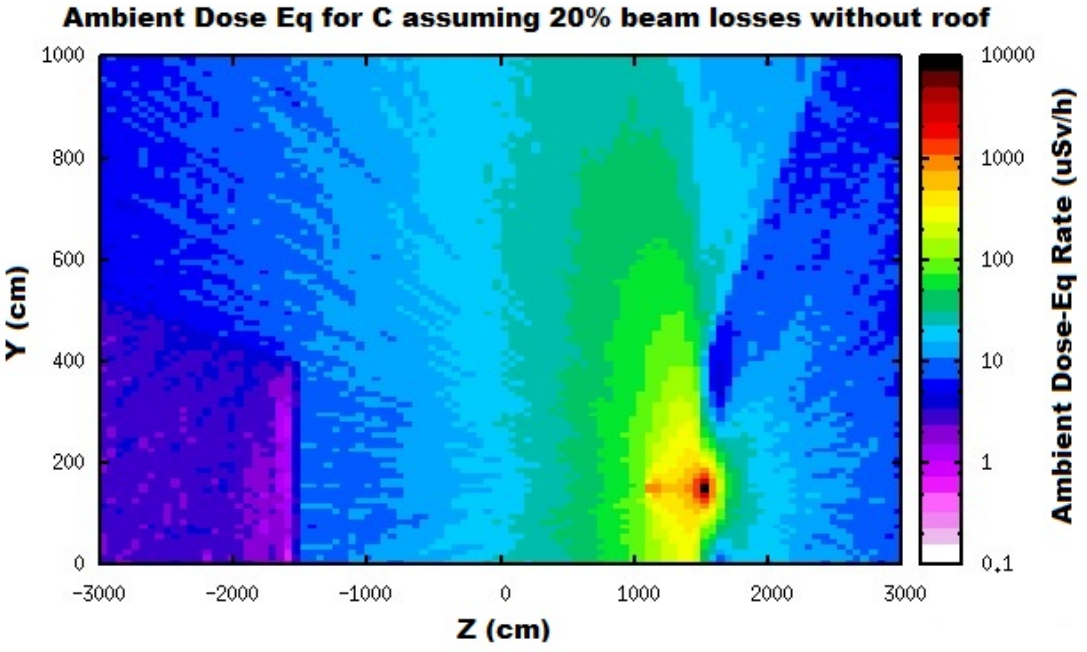

FIGURE 6.14: Ambient dose equivalent in SS20 for ^{12}C at 20% beam loss.

platform, a roof should be added on top of the machine in order to comply with the CERN Safety Code [48].

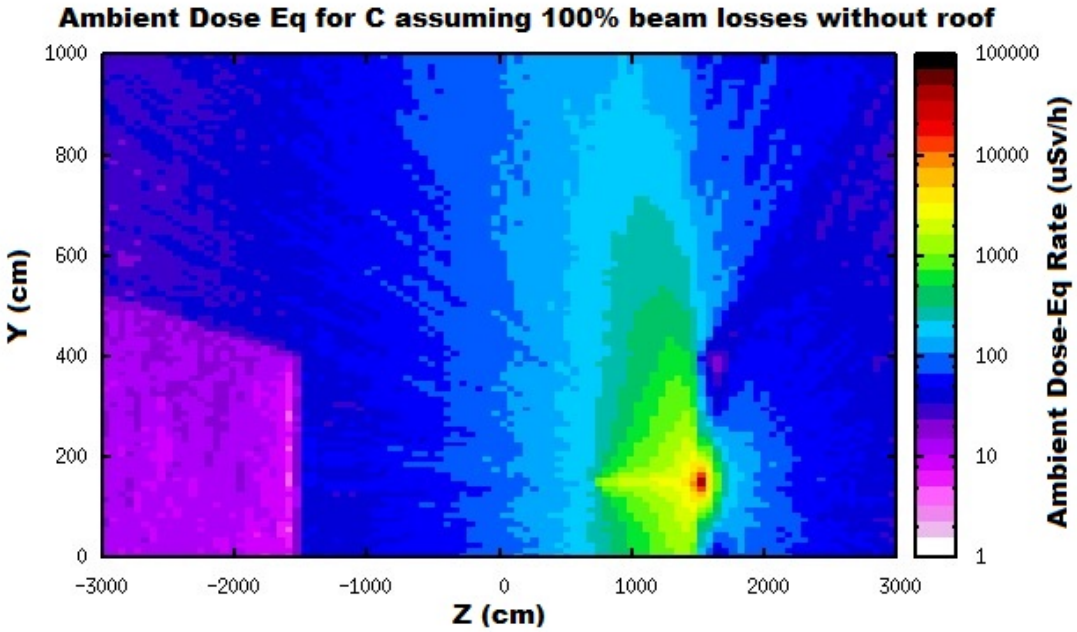

FIGURE 6.15: Ambient dose equivalent in SS30 for ^{12}C at 100% beam loss.

Oxygen at 1%, 20%, 100% beam loss without roof

When a 250 MeV/n oxygen ion beam interacts with the injection line SS10, at the interaction point, the dose will be 500 μSv/h for 1% beam loss. Outside the shielding wall, near the interaction point, the ambient dose equivalent is 3 μSv/h. As suggested by figure 6.16, at the target level, the secondary radiation will be attenuated by the shielding walls, therefore the ambient dose equivalent outside the shielding walls is less than 1 μSv/h. At the roof level, the dose is approximately 10 μSv/h and less at the platform level.

When 20% of the oxygen beam is lost in SS20, the dose produced at the interaction of the beam with the SS20 line is 10^3 μSv/h. Behind the shielding wall, near the interaction point, the dose is 10^2 μSv/h and around 1 μSv/h in the laboratory. At the visitor platform the dose is found to be 50 μSv/h as shown in figure 6.17.

If the entire beam is lost in SS30, the ambient dose equivalent at the interaction point is 10^3 μSv/h and at the platform level (6.5 metres above the beam line) it is 500 μSv/h above the interaction point and 700 μSv/h at the platform level. Behind the shielding wall, the dose is 10^2 μSv/h near the shielding wall and it decreases with distance to 10 μSv/h as shown in figure 6.18.

The results obtained for oxygen showed that for 20% beam losses, the dose at the platform level does not exceed 50 μSv/h, while in the laboratory space, the dose is 1 μSv/h. For 100% beam losses the dose is 500 μSv/h at the platform levels and higher

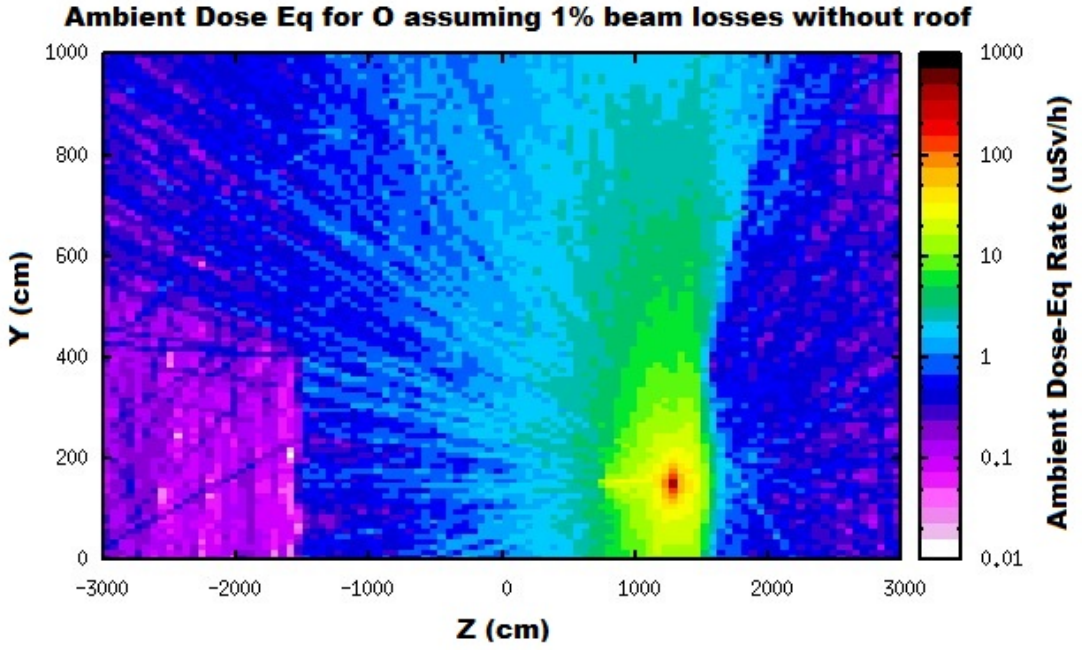

FIGURE 6.16: Ambient dose equivalent in SS10 for ^{16}O at 1% beam loss.

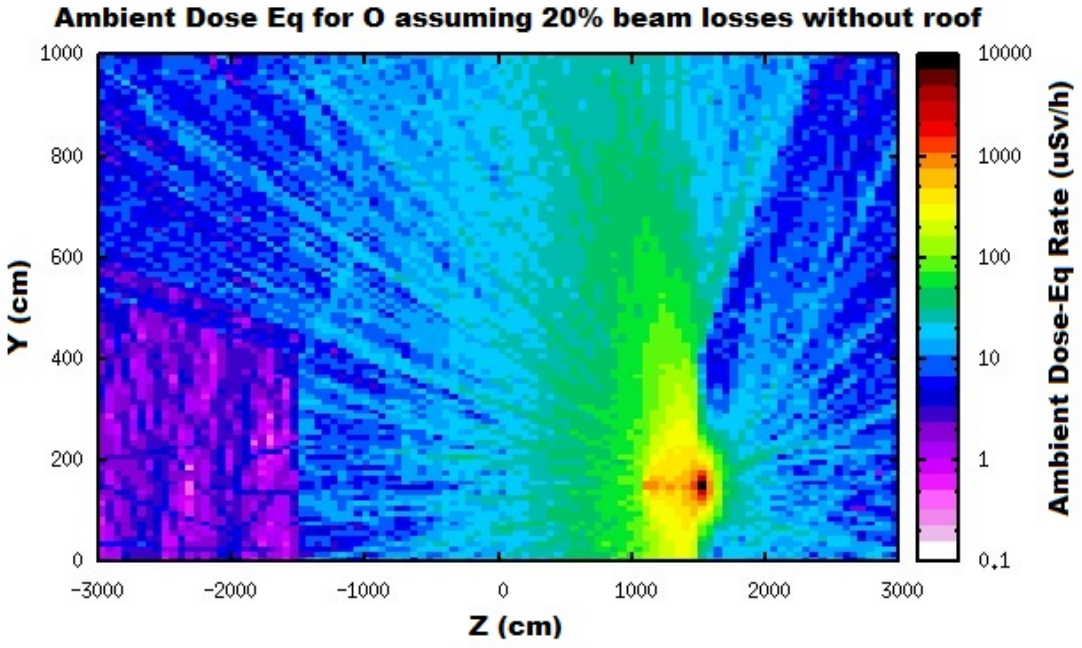

FIGURE 6.17: Ambient dose equivalent in SS20 for ^{16}O at 20% beam loss.

than 1 μSv/h in the lab space. These findings suggest that for beam losses higher than 20%, a roof should be added on top of the machine to protect the personnel and the visitors, according to the safety regulations [48].

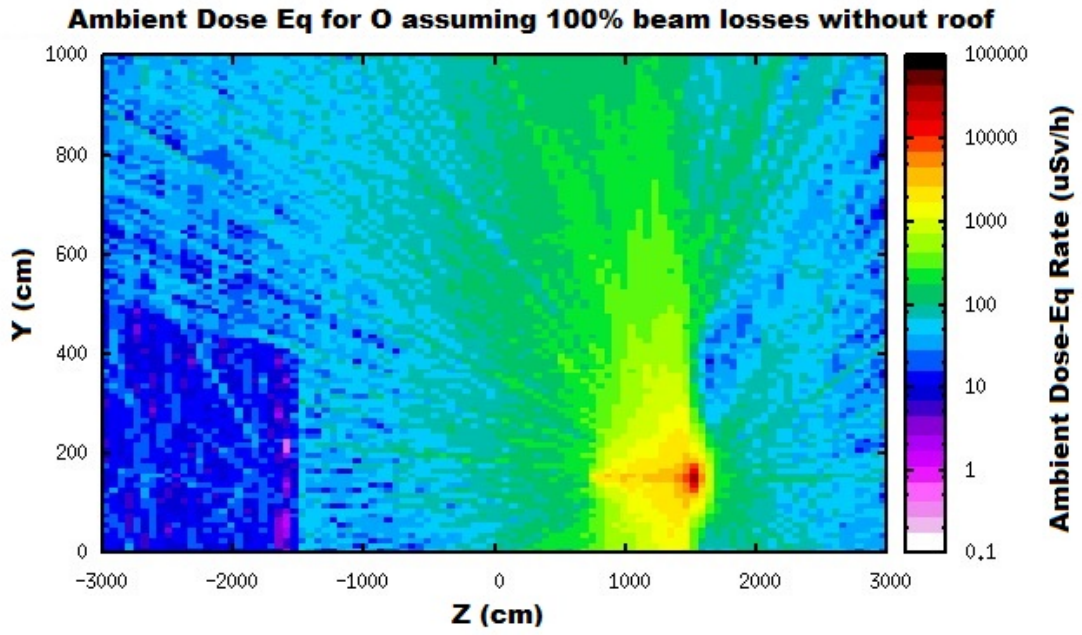

FIGURE 6.18: Ambient dose equivalent in SS30 for ^{16}O at 100% beam loss.

The second set of simulations was made with a concrete roof on top of the machine, at 5 metres above the ground, in order to calculate the ambient dose equivalent at the platform level for the worst case scenario to establish if the roof reduces the dose down to the legal limits [48]. For simulations, the same parameters and the same geometry were used. The thickness of the concrete roof is 80 cm. This is the thickness established by the civil engineering department taking into account the existing walls of the accelerator hall, but the final thickness of the shielding wall has to be decided when the beam loss pattern in the LEIR machine can be estimated more precisely.

Hydrogen at 1%, 20%, 100% beam loss with roof

As shown in figure 6.19, with the roof on top of the machine, the dose inside the accelerator room is 1 μSv/h and at the interaction point is 10^2 μSv/h at the target level for 1% beam loss in SS10. Behind the shielding wall, in the direction of the beam line, the dose equivalent is 10^{-2} μSv/h and it decreases with distance to 10^{-5} μSv/h. Because of the roof, the radiation dose at the platform level is lower than 10^{-2} μSv/h.

As shown in figure 6.20, for 20% beam loss in SS20, the dose at the interaction point is 10^3 μSv/h and it decreases in the accelerator room to 1 μSv/h. At the visitor platform the dose is found to be approximately 0.1 μSv/h. Behind the shielding wall, near the interaction point, the dose is 1 μSv/h. In the laboratory, the roof reduces the dose to 10^{-4} μSv/h.

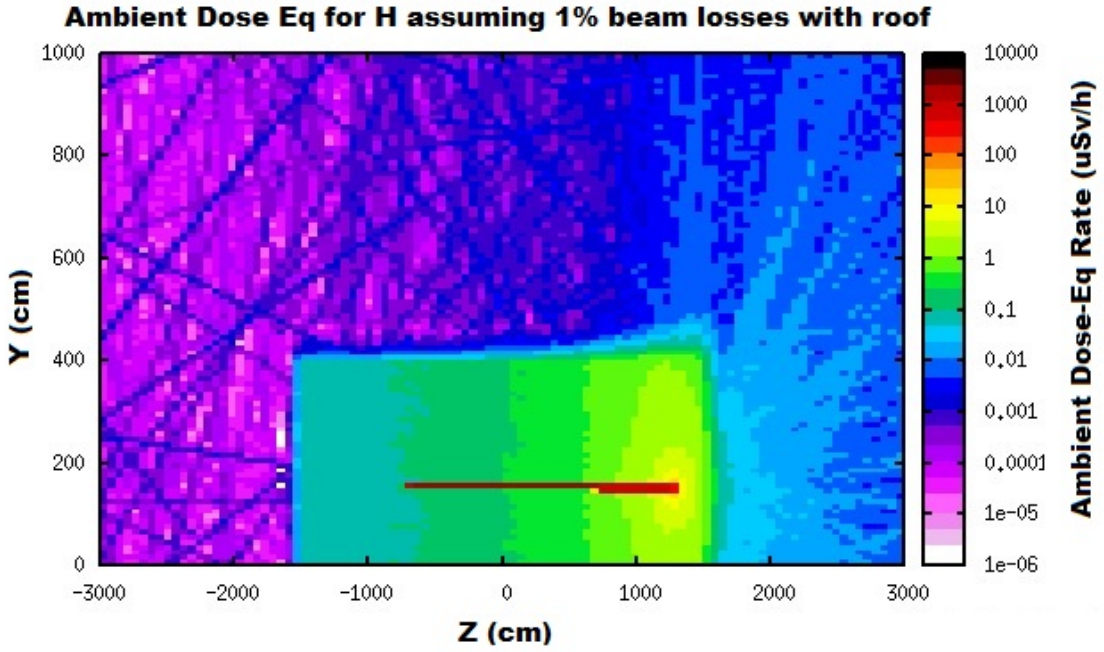

FIGURE 6.19: Ambient dose equivalent in SS10 for H at 1% beam loss with roof.

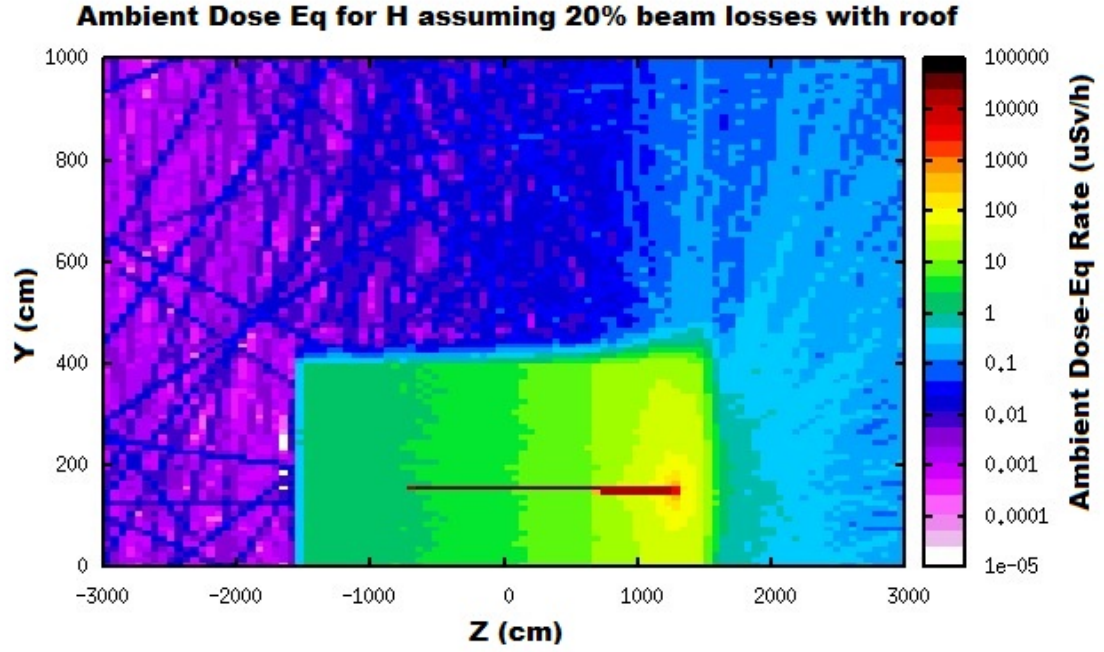

FIGURE 6.20: Ambient dose equivalent in SS20 for H at 20% beam loss with roof.

At the interaction point, for 100% beam losses in SS30, the dose is 10^4 μSv/h. At the visitor platform, the ambient dose equivalent is 1 μSv/h. In the accelerator room the dose was found to be approximately 10 μSv/h. Outside the facility room, in the direction of the interaction point, the ambient dose equivalent is 5 μSv/h and in the remaining space goes down to 10^{-3} μSv/h as shown in figure 6.21.

With a roof on top of the machine, the ambient dose equivalent at the platform level is 0.1 μSv/h at 20% beam losses, while the dose outside the shielding wall is 10^{-4} μSv/h. At 100% beam losses, the ambient dose at the platform level is 1 μ Sv/h and 10^{-3} μSv/h in the laboratory. These values indicate that the concrete roof will attenuate the radiation and the dose at the visitor platform will not exceed the CERN regulations [48], therefore, the public can access the platform during the machine operation. The dose inside the enclosed area is not increased considerable.

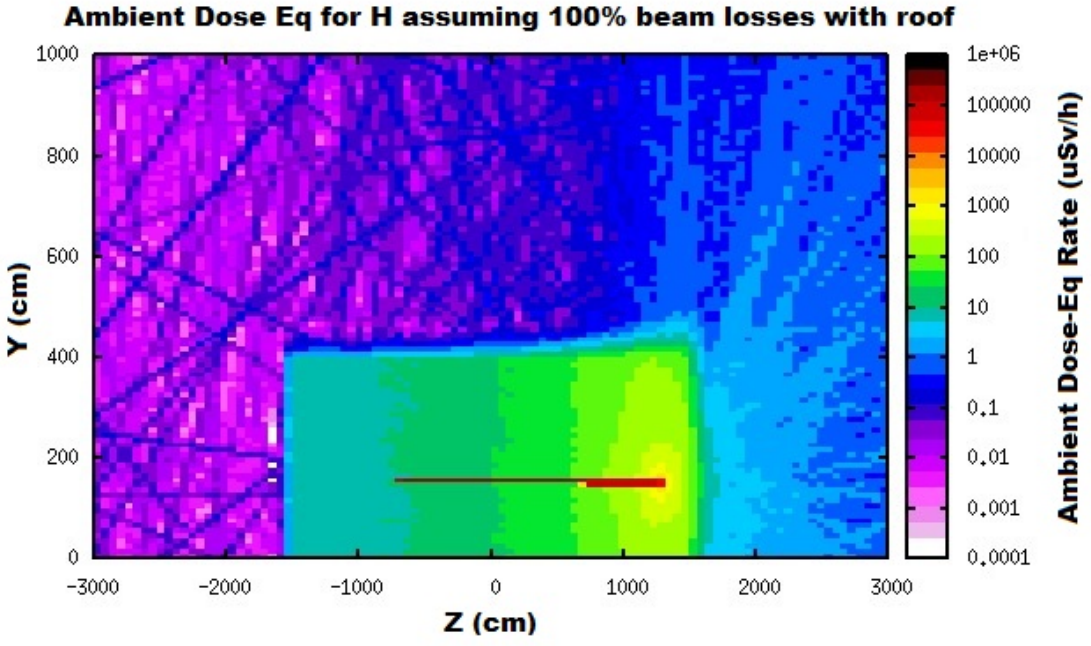

FIGURE 6.21: Ambient dose equivalent in SS30 for H at 100% beam loss with roof.

Helium at 1%, 20%, 100% beam loss with roof

For helium with 1% beam losses in SS10, the ambient dose equivalent at the target level is 10 μSv/h at the interaction point and it decreases to 0.1 μSv/h in the remaining space. At the visitor platform, the dose is only 10^{-2} μSv/h, as shown in figure 6.22, thanks to the roof, compared with the value of 1 μSv/h without it. Outside the shielding walls, near the interaction point, the dose is 10^{-3} μSv/h and 10^{-6} μSv/h in the remaining space, including the laboratory space, as the roof was placed on top of the machine.

When 20% of the beam is lost in SS20, the ambient dose equivalent at the interaction point is 10^{2} μSv/h and it decreases gradually with distance to 1 μSv/h in the accelerator room, while at the visitor platform the dose is 0.5 μSv/h. Behind the shielding wall, in the direction of the interaction point, the ambient dose equivalent is 0.1 μSv/h and it decreases to 10^{-5} μSv/h as shown in figure 6.23.

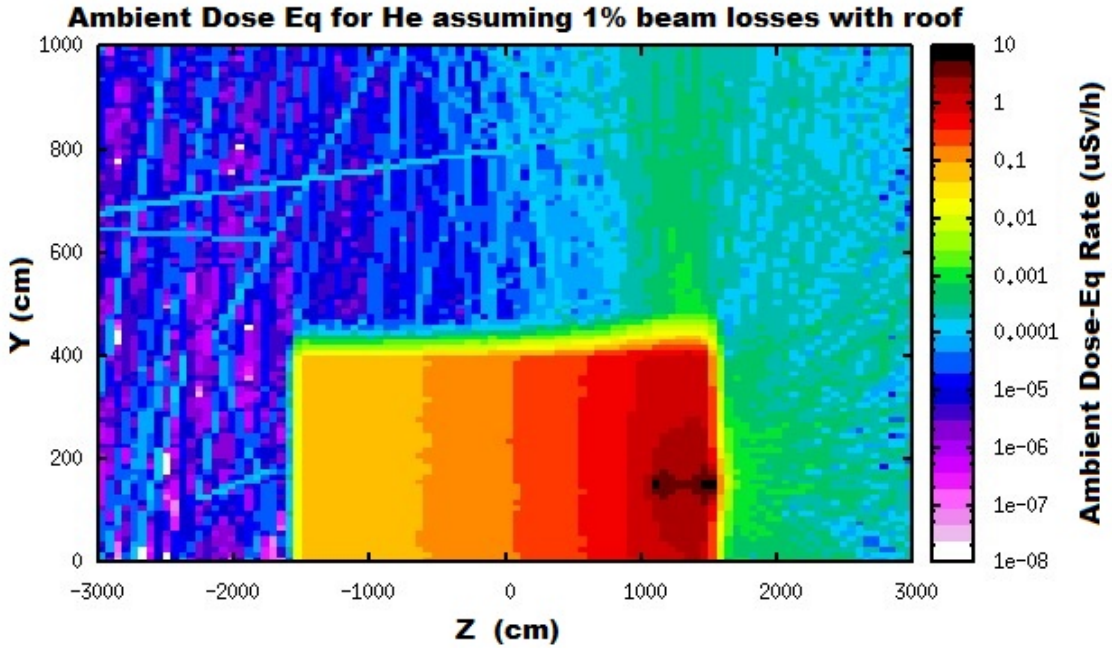

FIGURE 6.22: Ambient dose equivalent in SS10 for He at 1% beam loss with roof.

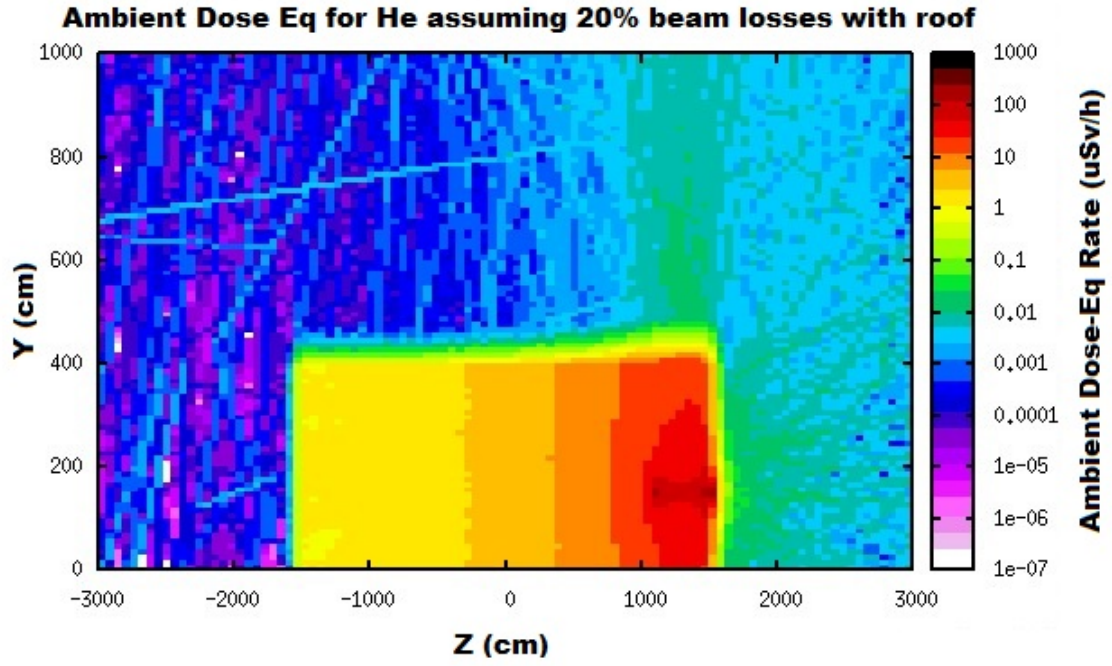

FIGURE 6.23: Ambient dose equivalent in SS20 for He at 20% beam loss with roof.

In the improbable case of 100% beam losses in SS30, the ambient dose equivalent is 500 μSv/h at the interaction point and 10 μSv/h in the remainder space. At the visitor platform, the dose is 0.8 μSv/h. Behind the shielding wall, where the interaction occurs it is 0.1 μSv/h and it decreases with distance down to 10^{-4} μSv/h as shown in figure 6.24.

When the roof is added, the results for a helium ion beam show that the dose at the visitor platform and outside the shielding walls is low and no additional shielding is required.

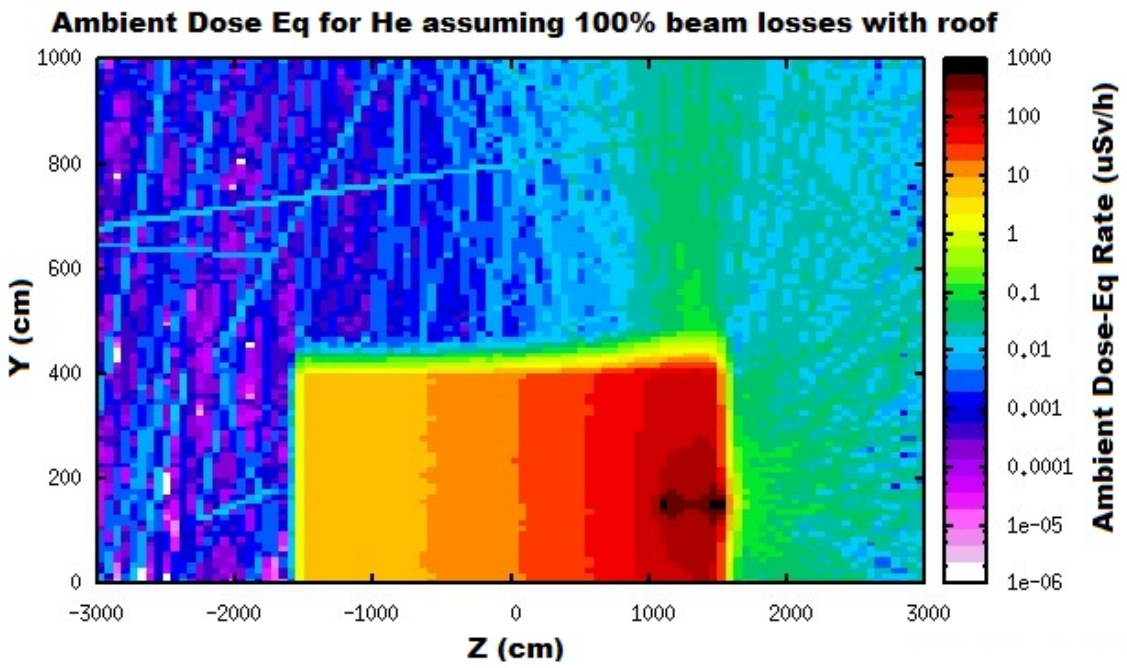

FIGURE 6.24: Ambient dose equivalent in SS30 for He at 100% beam loss with roof.

Carbon at 1%, 20%, 100% beam loss with roof

When a 250 MeV/n carbon beam hits SS10, the dose at the interaction point is 10^2 μSv/h for 1% beam loss and it decreases down to 1 μSv/h in the remaining space of the accelerator room. Behind the shielding wall, the highest dose is found to be in the direction of the beam line and it is 1 μSv/h. At a distance of a few metres, the ambient dose equivalent is 0.01 as shown is figure 6.25. At the visitor platform, the dose goes down to 0.1 μSv/h.

If 20% of the beam is lost in SS20, the dose at the interaction point is 10^3 μSv/h and 10 μSv/h in the remaining space. At the visitor platform it will be around 5 μSv/h. Outside the shielding walls, the dose is 10 μSv/h in the proximity of the interaction point and it decreases to 0.1 μSv/h further from that point as shown in figure 6.26.

Even for 100% beam loss IN SS30, the dose at the interaction point is 10^4 μSv/h and it decreases to 10^2 μSv/h in the accelerator room. At the visitor platform, the dose will be 10 μSv/h. After the shielding wall, the ambient dose equivalent is still high at 10^2 μSv/h and it decreases to 1 μSv/h as shown in figure 6.27.

After the roof was added on top of the machine, the dose at the visitor platform was reduced, even for 100% beam losses, from 100 μSv/h to a safe value of 10 μSv/h.

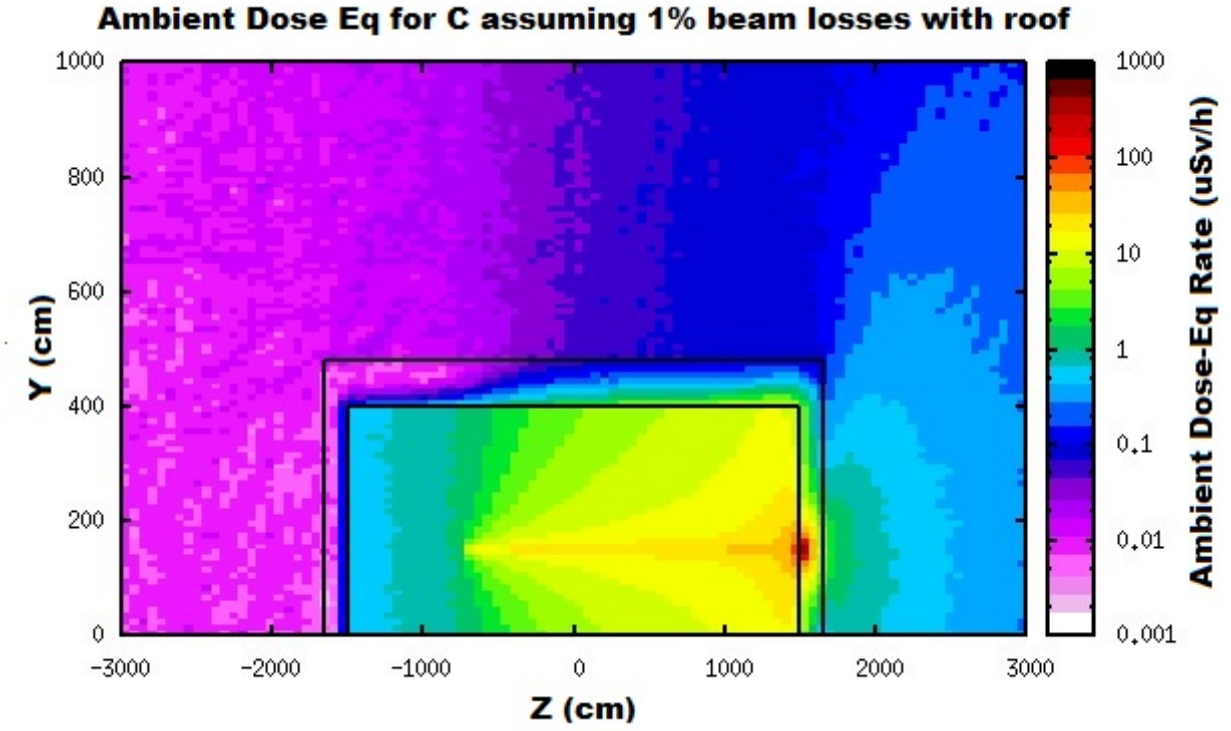

FIGURE 6.25: Ambient dose equivalent in SS10 for ^{12}C at 1% beam loss with roof.

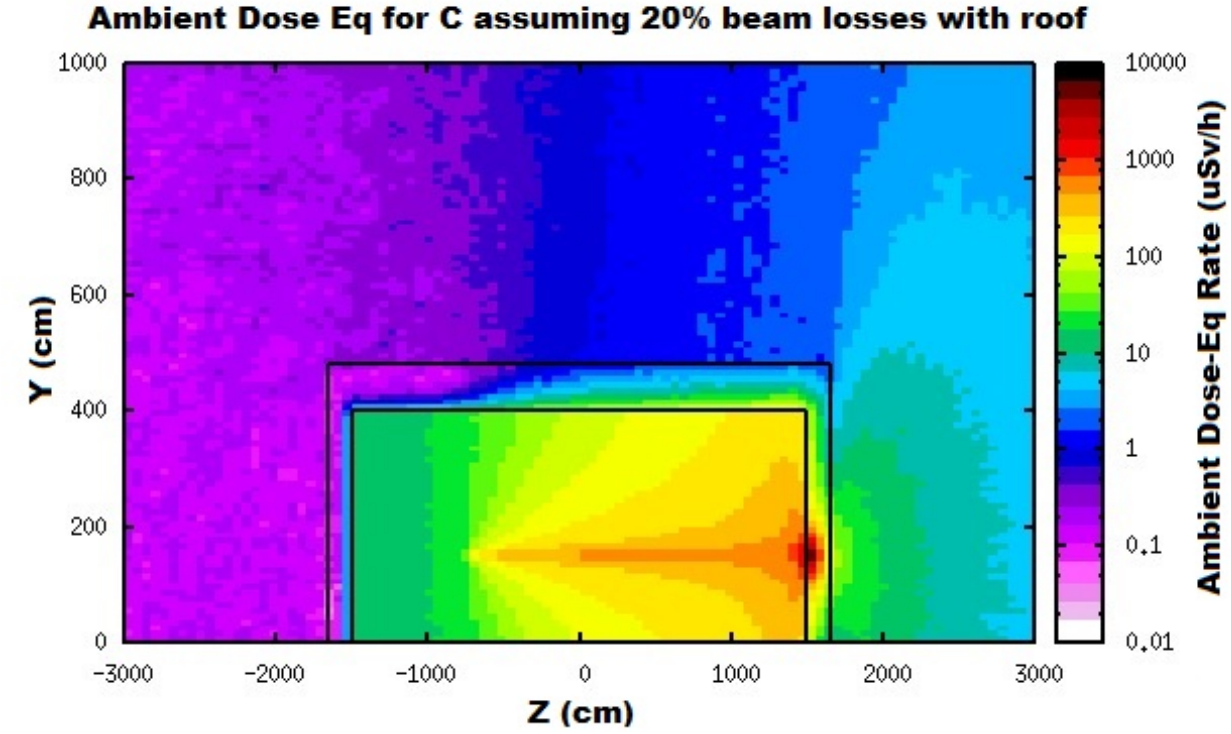

FIGURE 6.26: Ambient dose equivalent in SS20 for ^{12}C at 20% beam loss with roof.

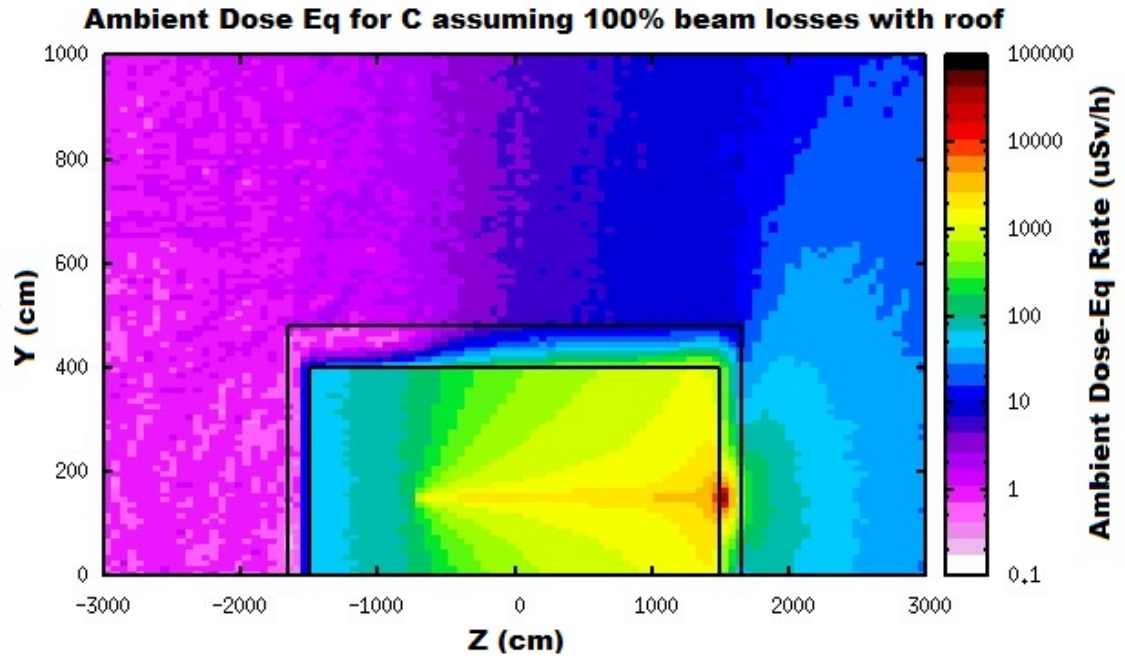

FIGURE 6.27: Ambient dose equivalent in SS30 for ^{12}C at 100% beam loss with roof.

Oxygen at 1%, 20%, 100% beam loss with roof

For a 250 MeV/n oxygen beam, the ambient dose equivalent at the interaction point is 10^2 μSv/h for 1% beam losses in SS10. The dose in the accelerator room will decrease from 10^2 μSv/h to 1 μSv/h at the farthest point, while at the visitor platform, the dose was found to be 5 μSv/h. Outside the shielding wall, near the incident point, the dose is 0.1 μSv/h and near the research lab it decreases to 0.001 μSv/h as shown in figure 6.28.

When the beam losses goes up to 20% in SS20, the ambient dose at the interaction point is 10^3 μSv/h and 10 μSv/h in the remaining space. At the visitor platform the dose will increase to 7 μSv/h. Outside the shielding wall is 5 μSv/h near the interaction point and it decreases with distance to 0.1 μSv/h as shown in figure 6.29.

In the worst case scenario, when the entire beam is lost in SS30, the dose at the interaction point is high, 10^4 μSv/h, and inside the room it is 10^2 μSv/h. At the visitor platform it was found to be approximately 50 μSv/h. In the laboratory, the dose is 10 μSv/h near the incident point but at the farthest point, the dose is 0.5 μSv/h as shown in figure 6.30.

If the roof is placed on the top of th machine, the dose will be reduced to safe levels at the visitor platform and in the research laboratory even at 100% beam losses. Therefore, no additional mitigation methods need to be applied in this case as the concrete roof provides a good shielding.

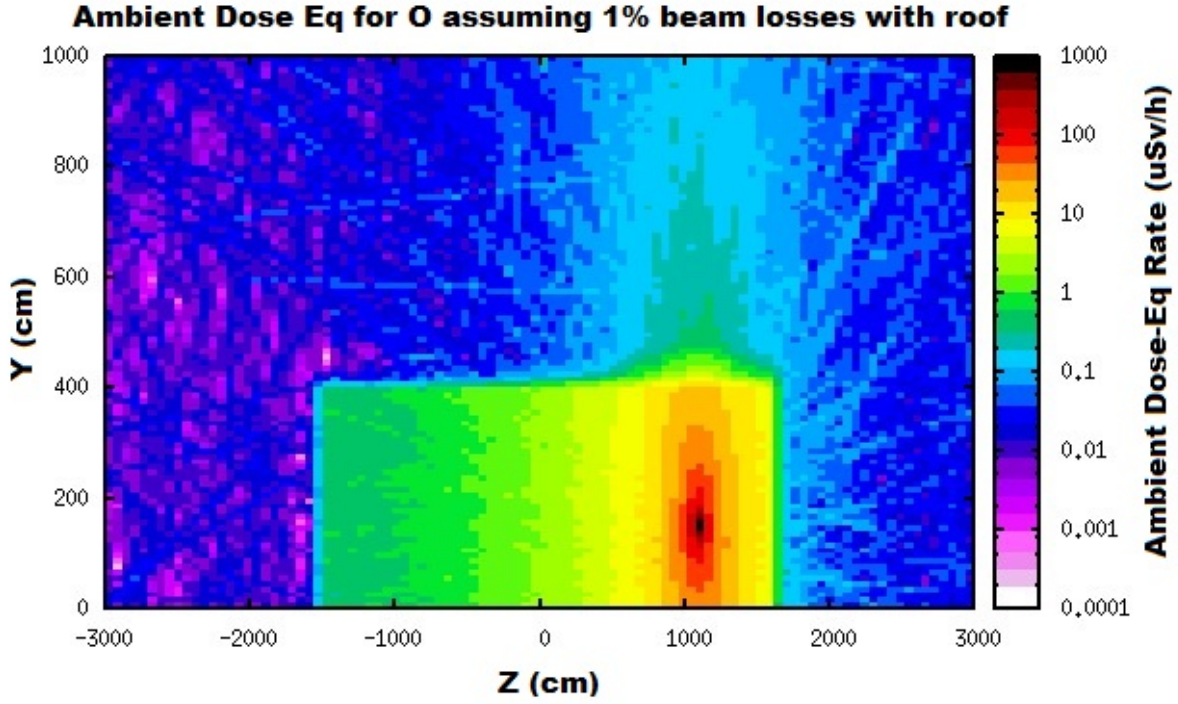

FIGURE 6.28: Ambient dose equivalent in SS10 for ^{16}O at 1% beam loss with roof.

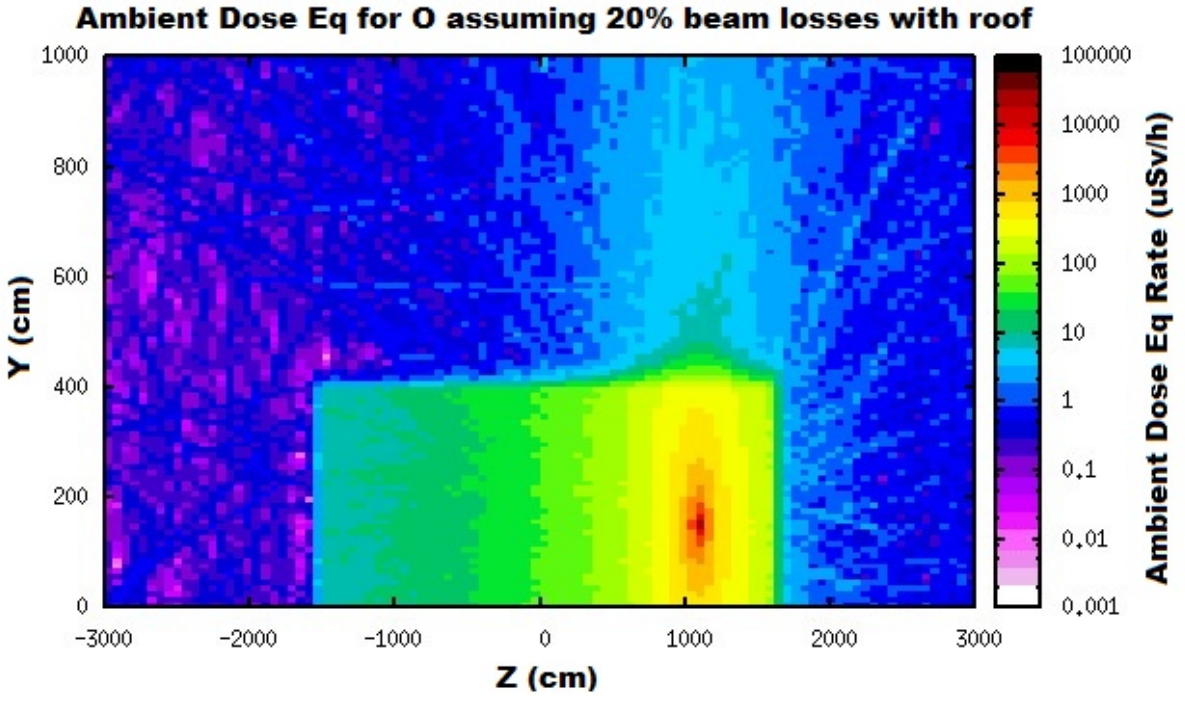

FIGURE 6.29: Ambient dose equivalent in SS20 for ^{16}O at 20% beam loss with roof.

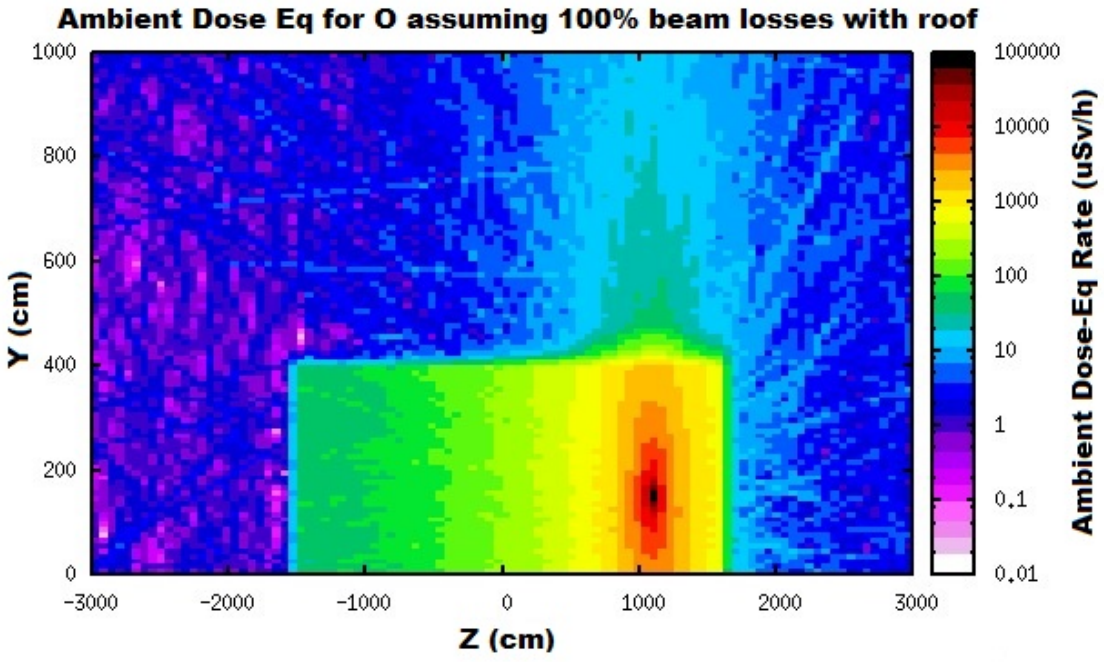

FIGURE 6.30: Ambient dose equivalent in SS30 for ^{16}O at 100% beam loss with roof.

6.4 Conclusion

The aim of this study was to evaluate the ambient dose equivalent rate for the new operation conditions of the LEIR synchrotron. The OpenMed/BioLeir project was proposed as a use of the existing facility at CERN to provide beams for experiments in support of research for hadron therapy centres. The first radiation protection calculations were done only for Pb, Xe and Ar ions [120]. The purpose of this study was to evaluate the ambient dose equivalent for hydrogen, helium, carbon and oxygen ions, as these types of ions are of interest for treating cancer. The calculations were made for these different ion beams for three scenarios, one representing the worst-case scenario (100% beam loss) and the two additional ones corresponding to normal condition (1%, 20%) in different locations and presented for tree different heights (1.7 m, 5 m, 6.5 m). LEIR is the only accelerator at CERN provided with a visitor platform, hence, this study was done in order to establish if the dose at the visitor platform and in the adjacent laboratory space complies with the legal limits stipulated in the CERN Safety Code [48]. The first set of simulations was done with the existing geometry of the facility, while the second set of simulations was done with a concrete roof on top of the machine.

For the first set of simulations, the results showed that the dose at the interaction point is quite significant. At the point on interest, at the platform level (6.5 m) the dose is lower than at the roof level: less than 1 μSv/h for 1% beam loss in SS10, 5 μSv/h for 20% beam losses in SS20 and 60 μSv/h for 100% beam losses in SS30 for protons and

helium ions, while for carbon and oxygen ions the dose is less than 10 μSv/h for 1% beam losses, 50 μSv/h for 20% beam loss and 500 μSv/h for 100% beam loss.

Behind the shielding walls, the dose for carbon and oxygen is 0.5 μSv/h at 1% beam loss, 1 μSv/h at 20% beam loss and 10 μSv/h at 100% beam loss. For hydrogen and helium it is 0.01 μSv/h at 1% beam loss, 0.5 μSv/h at 20% beam loss and higher than 1 μSv/h at 100% beam loss as shown in figure 6.31.

These results suggest that for normal conditions when only 1% up to 20% of the beam will be lost, the ambient dose equivalent at the visitor platform and in the research laboratory is below the CERN limits [48] which are based on the IRR99 [40] limits. In case of an accident, when the entire beam will be lost, the dose at the visitor platform will exceed the legal limit and a concrete roof on top of the synchrotron will help in reducing the dose at this level and also in the research laboratory.

As a consequence, if no roof will be placed on top of the machine, the human intervention (staff and visitors) in the vicinity of the machine has to be kept at minimum as the dose exceeds the limits [48] and the facility room has to be classified as limited stay radiation area [48]. Before access is provided to the irradiation room, the ventilation system has to be flushed and after the flushing has to be verified by the access system. Only after this verification, can access to the irradiation room be granted.

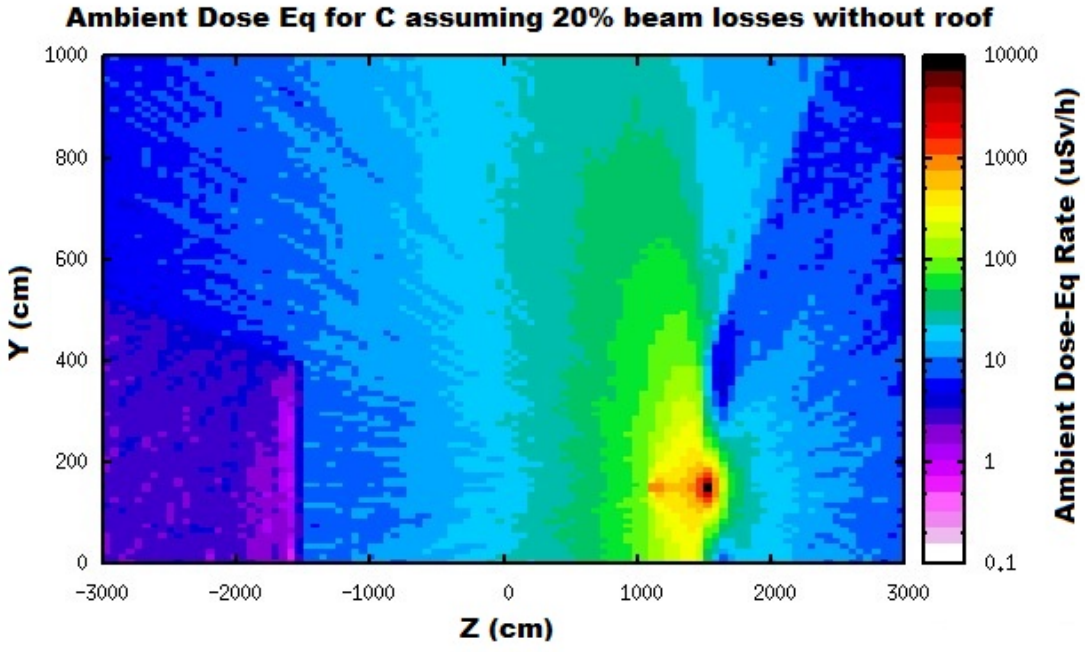

FIGURE 6.31: Ambient dose equivalent at the platform level for ^{12}C at 20% beam loss without roof.

For the second set of simulations, a concrete roof of 80 cm thickness was added at 5 metres height.

The results showed that at the interaction point and in the accelerator room, the ambient dose equivalent has the same value as the dose calculated in the first set of simulations.

However, behind the shielding walls, the ambient dose equivalent is really low for all ions, even 10^{-5} μSv/h a few metres away from the shielding walls, except for the wall side where the interaction occurs.

At the visitor platform level, on top of the roof, the radiation level for protons and helium is 10^{-2} μSv/h for 1% beam losses, 0.1 μSv/h at 20% beam losses and 1 μSv/h for 100% beam losses, while for carbon and oxygen it is 0.1 μSv/h for 1% beam losses, 5 μSv/h for 20% beam losses and below 10 μSv/h for 100% beam losses. These results indicate that, even for 100% beam losses, the roof will attenuate the dose at the visitor platform and the dose will not reach the legal limit of 10 μSv/h [48] as seen in figure 6.32.

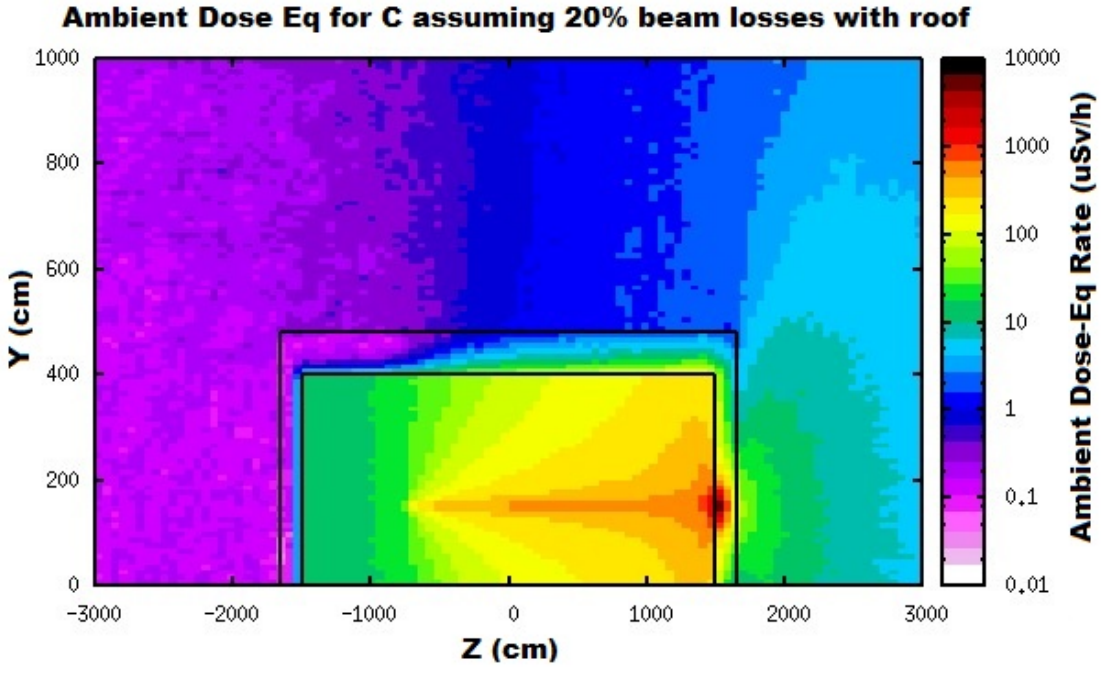

FIGURE 6.32: Ambient dose equivalent at the platform level for ^{12}C at 20% beam loss with roof.

All these results indicate that for an energy of 250 MeV/n, in the present conditions without the concrete roof on top of the machine, the dose at the platform level will not exceed the CERN regulations [48] for normal beam losses (1%, 20%).

Particle	**1%**	**20%**	**100%**
	without/with roof	**without/with roof**	**without/with roof**
Hydrogen	1 μSv/h / 10^{-2} μSv/h	5 μSv/h / 0.1 μSv/h	60 μSv/h / 1 μSv/h
Helium	1 μSv/h / 10^{-2} μSv/h	5 μSv/h / 0.1 μSv/h	60 μSv/h / 1 μSv/h
Carbon	10 μSv/h / 0.1 μSv/h	50 μSv/h / 5 μSv/h	500 μSv/h / 10 μSv/h
Oxygen	10 μSv/h / 0.1 μSv/h	50 μSv/h / 5 μSv/h	500 μSv/h / 10 μSv/h

TABLE 6.2: Ambient dose equivalent at the visitor platform level.

If the beam losses will be higher than 20%, an additional roof should be placed on top of the machine as the dose limit is exceed and the room has to be classified as limited stay radiation area [48] The same argument may be used in case of the ambient dose equivalent found in the research laboratory. In normal condition, the 3 μSv/h will not be exceeded, but in case that the beam losses will reach 100%, the dose limit will be exceeded. All the results are summarized in table 6.2. As the future plans is to upgrade the machine to be able to deliver ion beams with an energy of 430 MeV/n, from the radiation protection point of view, a concrete roof should be placed on top of the machine to minimize the secondary radiation and, therefore, the radiation exposure of visitors and personnel.

Unfortunately, the BIOLEIR project is not going further but if the programme is revived these calculations will be used as primary information for the conceptual design phase.

Chapter 7

Conclusion and future work

Hadron therapy is a complicated technique and the effectiveness of the treatment depends on several factors arising from physical and biological properties of the processes involved and practical constraints of the treatment itself.

An important aspect in hadron therapy is the secondary radiation produced during the treatment. The secondary particles, like neutrons, can have an impact on the total dose received by the patient in the healthy tissues. The main concern is that a small dose of this secondary radiation can induce a secondary cancer as neutrons have a high RBE.

For this work, FLUKA Monte Carlo simulations were performed, using beam line parameters of the Clatterbridge Cancer Centre, the Christie Proton Therapy Centre and the OpenMed facility, to establish if the radiation protection regulations are fulfilled.

7.1 The Clatterbridge Cancer Centre

The aim of this project was to calculate the proton depth-dose distribution, the proton and neutron fluence and dose along the beam line, the neutron dose equivalent in a water phantom and the radioactivity induced in a patient-specific collimator and in the treatment room.

The FLUKA Monte Carlo simulations were used to calculate the Bragg peak for a 60 MeV proton beam. The results showed that the highest dose is delivered at 3 cm depth. This value agrees with the experimental value obtained in Ref. [98].

The proton fluence and the proton dose were also calculated to verify if the quality of the proton beam is not altered along the path. The FLUKA simulations showed that most of the secondary particles are produced in the modulating devices and in the brass

collimator but the fluence and the dose are low, therefore, the components will not alter the proton beam.

The next simulations were made to determine the neutron secondary dose. Generally, the contribution of the secondary particles to the total dose received by the healthy tissue is low. The dose also depends on the material and the geometry of the beam line. For a 60 MeV proton beam, the contribution of the neutrons to the total dose received by the patient is insignificant. The neutron dose equivalent ranged between 50 μ Sv/s and 70 μ Sv/s in the target volume and between 1 μ Sv/s and 20 μ Sv/s outside the target volume. These findings indicate that the secondary neutron dose is relatively low and below the UK limitations.[40] Therefore the precise target conformity of proton therapy is not affected. The FLUKA simulations have been verified with the MCNPX code and the results showed a good agreement, but it will be important to validate the simulations with experimental data as these are the first and the only radiation protection calculations made at the Clatterbridge Cancer Centre. As no experimental data was available at the time, the Monte Carlo results were compared with the experimental data conducted at a similar facility at CCB IFJ PAN in Krakow.[103]. The results obtained were 0.8 μ Sv/s at the patient chair which is good agreement with 1 μ Sv/s found by the FLUKA Monte Carlo Code. These values suggest that the secondary dose received by the patient do not exceed the legal limits of IRR99.[40]

The next simulations involved the study of radioactivity induced in the brass collimator and in the treatment room. The calculations were made for five decay times.

For the brass collimator, the results showed that some radioisotopes like ^{60}Ga, ^{64}Cu, ^{63}Zn, ^{61}Cu and ^{58}Co have a high activity even after 1 hour from irradiation, but the values do not exceed the limits recommended in the IRR99 [40]. Nevertheless, even though the results showed that the collimator is not radioactive, the contact with the contaminated collimator should be avoided for at least one hour to minimize the exposure of the personnel to radiations.

The radioactivity was calculated also in the treatment room. The results suggest that the activity found in the air is low, hence the personnel are not significantly exposed to additional radiation.

However, these results can not be applied in every case as they depend on the duration of each irradiation profile and on the air ventilation scheme in the treatment room.

7.2 The Christie Proton Therapy Centre

The Christie Proton Therapy Centre is planned to treat the first patient in 2018. The facility will have three treatment rooms and one research room.

The objective of this research was to undertake radiation protection studies for the research room and the accessible areas around it. The ambient dose equivalent for neutrons and high energy photons was calculated for proton beams with different energies: 70 MeV, 100 MeV, 150 MeV, 200 MeV and 250 MeV. The production of radioactive isotopes was also investigated.

The results suggest that the secondary dose increases linearly with energy, especially in the direction of the beam line. For 70 MeV, the neutron and the photon dose in the accessible areas was found to be 1 μ Sv/h and 0.1 μ Sv/h respectively. Therefore, for a 70 MeV proton beam, the dose can be regarded as safe for employees and members of public.[40]. In the worst-case scenario when the entire beam is lost at maximum energy, the ambient dose equivalent will not exceed 10 μ Sv/h in the areas adjacent to the research room, while in the research room, the dose will be high, around the beam line the neutron ambient dose equivalent was found to be 6 mSv/h. These values can be regarded safe if we refer to employees over 18 years, but not for members of public or pregnant employees as the limit imposed by the IRR99[40] is 1 mSv in a calendar year. Therefore, the access of the members of public, in the adjacent areas, should be limited when the beam is on to comply with the legal requirements.[40] The results of the dose rate obtained with FLUKA were compared with the MCNPX results presented in Ref.[113]. The comparison showed that the values are quite similar. In the maze, the dose equivalent calculated with FLUKA is with 1 mSv higher than the dose equivalent calculated with MCNPX, while on the corridor, the dose equivalent has approximately the same value for both codes. The dose in the treatment room was found to be 100 times higher with FLUKA. These difference could appear due to the detectors position or due to the different physics properties enabled in the input files used for MCNPX and FLUKA codes. To resolve these discrepancies, an additional set of simulations should be done with a more detailed geometry.

For the second set of simulations, the radioactivity induced in the room together with the residual dose rate was studied. The irradiation profile was set for 1.4 hours per day of activity at full intensity (10^9 protons/s). Immediately after irradiation at 70 MeV the most abundant isotopes are ^{15}O, ^{13}N and ^{11}C, while at 150 MeV it was found that the activity of ^{41}Ar increased, simultaneously with the activity of ^{15}O, ^{13}N and ^{11}C. At 250 MeV, the activity of ^{11}C increases considerably up to the IRR99 limit.[40]. For ^{15}O, ^{13}N and ^{11}C, the activity induced in the research room air is below the limits given in

IRR99.[40] If the accelerator is operated at maximum energy, only ^{11}C will exceed the limit. These results demonstrate that the research room has a low risk of contamination and the personnel will not be exposed, as the activity of the most important radioisotopes is below the limits given in the IRR99.[40]. It should be noted that these results have been studied for the worst-case scenario, where the accelerator is operated at maximum beam energy (250 MeV) for a period of 1 year. In addition, the irradiation profile was only presumed and the results will differ depending on the scenario. To obtain more realistic results, it will be necessary to develop more irradiation scenarios, as detailed and complete as possible.

The residual dose induced in the research room was also calculated. The results showed that, immediately after irradiation, the residual dose equivalent in the research room is of the order of several $\mu Sv/h$: 1 $\mu Sv/h$ for 70 MeV and $>$ 100 $\mu Sv/h$ for 250 MeV. After 1 hour, the value of the dose decreases significantly down to 50 $\mu Sv/h$ for 250 MeV. After 3 months, the dose decays down to 10^{-3} $\mu Sv/h$. The results suggest that at 250 MeV the human intervention in the research room should be kept as minimum possible after irradiation, but after 1 hour of cooling time, it can be seen as safe.

7.3 The OpenMed facility

The OpenMed project involved radiation protection calculations for the new planned facility at CERN. The plans are to use an existing facility for radiological studies. The first radiation protection simulations were made for the present conditions: Pb, Xe and Ar ions. After the machine is upgraded, it will accelerate different ion beam used in pre-clinical radiation biology: hydrogen, helium, carbon and oxygen.

The main interest of this project was to decide if under the new conditions, the existing shielding will protect the workers and visitor, as the LEIR synchrotron is the only accelerator at CERN provided with a visitor platform. Therefore, the ambient dose equivalent was calculated for four different types of ion beams at different room heights in order to see if a roof needs to be placed on top of the synchrotron and to ensure that the shielding provided is safe enough for workers and visitors and that the ambient dose equivalent is within the legal limits applied at CERN.[48]

For the first set of simulations, with no roof on top of the machine, the results showed that the dose at the point of interest, at the platform level (6.5 m), is less than 1 $\mu Sv/h$ for 1% beam loss, 5 $\mu Sv/h$ for 20% beam losses and 60 $\mu Sv/h$ for 100% beam losses for protons and helium ions, while for carbon and oxygen ions the dose is less than 10

$\mu Sv/h$ for 1% beam losses, 50 $\mu Sv/h$ for 20% beam loss and 500 $\mu Sv/h$ for 100% beam loss.

Outside the shielding walls, the dose for carbon and oxygen is 0.5 $\mu Sv/h$ at 1% beam loss, 1 $\mu Sv/h$ at 20% beam loss and 10 $\mu Sv/h$ at 100% beam loss. For hydrogen and helium is 0.01 $\mu Sv/h$ at 1% beam loss, 0.5 $\mu Sv/h$ at 20% beam loss and higher than 1 $\mu Sv/h$ at 100% beam loss.

These results suggest that for normal conditions when 1% up to 20% of the beam will be lost, the ambient dose equivalent at the visitor platform and in the research laboratory is below the CERN limits [48] which are compatible with the IRR99[40] limits. If the entire beam is lost, the dose at the visitor platform will exceed the legal limit and a concrete roof on top of the synchrotron will help in reducing the dose at this level and also in the research laboratory.

As a consequence, if no roof will be placed on top of the machine, the human intervention (staff and visitors) in the vicinity of the machine has to be kept at minimum.

If a 80 cm thickness concrete roof will be placed on top of the machine, the dose at the platform level will be reduced by a factor of 100, even in case of 100% beam losses. This is a strong argument that the roof should be placed on top of the machine, especially if the machine is planned to be upgraded to deliver ion beams with an energy of 430 MeV/n/

Overall, in this work, Monte Carlo simulations, of practical cases from operational hadron therapy centres, have been presented in order to improve the quality and the precision of hadron therapy treatment procedures from radiation protection point of view.

Even though some of the results obtained in this thesis with FLUKA Monte Carlo code were verified with a different Monte Carlo code like MCNPX, the results can not represent a standard. There are limitations, like to recreate an exact irradiation profile, due to missing details. Therefore, all these results should be compared with experimental data.

Some of the simulations represent the first calculation of the secondary ambient dose equivalent at these facilities. Therefore, I strongly believe that this work is extremely useful as it will be used to improve the irradiation conditions, hence to protect the patients and the personnel from possible radiation exposure.

Appendix

This is the FLUKA input file used for radiation protection studies for the Christie Proton Therapy Centre (simulation with a beam energy of 250 MeV). File for the other simulations are similar apart form the geometry.

```
* Set the defaults for precision simulations

DEFAULTS

PRECISIO

* Define the beam characteristics

BEAM -0.25 1.0 1.0 PROTON

* Define the beam position

BEAMPOS 150.0 550.0 1570.

NEGATIVE

PHYSICS 3. EVAPORAT

PHYSICS 3. COALESCE

PHYSICS 2. EM-DISSO

IONTRANS HEAVYION

EMFCUT -0.0001 1E-4 VACUUM @LASTMAT

PROD-CUT

GEOBEGIN

COMBNAME

0 0

* Black body

SPH blkbody 0.0 0.0 0.0 100000.0

* Void sphere

SPH void 0.0 0.0 0.0 10000.0

RPP body1 0.0 300.0 1000.0 1300.0 -321.01 1557.18
```

RPP body2 0.0 300.0 -200.0 0.0 -156.29 1357.18

RPP body3 0.0 300.0 1000.0 1150.0 -663.54 -321.01

RPP body4 0.0 300.0 1000.0 1060.0 -666.15 -663.54

RPP body5 0.0 300.0 516.0 1000.0 -663.54 -513.54

RPP body6 0.0 300.0 456.0 516.0 -666.29 -513.54

RPP body7 0.0 300.0 0.0 746.5 -156.29 -31.29

RPP body8 0.0 300.0 -200.0 -50.0 -663.54 -156.29

RPP body9 0.0 300.0 -110.0 -50.0 -666.29 -663.54

RPP body10 0.0 300.0 -50.0 746.5 -281.09 -156.29

RPP body11 0.0 300.0 250.0 300.0 -666.29 -281.09

RPP body12 0.0 300.0 746.5 807.5 -281.09 29.91

RPP body13 0.0 300.0 -685.0 -200.0 -663.54 -513.54

RPP body14 0.0 300.0 250.0 900.0 1600.0 1765.0

SPH body16 0.0 746.5 -156.29 5108.8159097779

XYP Zmin 600.0

BOX body17 0.0 390.0 1690.0 0.0 -510. -470. 0.0 -105.4224251945 114.39454648764 1000.0 0.0 0.0

BOX body15 0.0 1000.0 1400.0 0.0 -230. 360. 0.0 94.216306066234 60.19375109788 1000.0 0.0 0.0

XZP CutY -200.0

XYP CutZ 1765.0

ZCC BTOut 150.0 550.0 5.0

ZCC BTIn 150.0 550.0 4.8

XYP Zmax 1550.0

RPP Phantom 145.0 155.0 545.0 555.0 565.0 605.0

RPP floor -2.0 0.0 0.0 1000.0 0.0 1550.0

END

* Black hole

BLKBODY 5 +blkbody -void

* Void around

VOID 5 +void +void -body1 -body2 -body3 -body4 -body5 -body6 -body7 -body8 -body9 -body10 -body11 -body12 -body13 -body14 -body16

Wall1 5 +body1 -body15

Wall2 5 +body2 -body17-CutY

Wall3 5 +body3

Wall4 5 +body4

Wall5 5 +body5

Wall6 5 +body6

Wall7 5 +body7

Wall8 5 +body8

Wall9 5 +body9

Wall10 5 +body10

Wall11 5 +body11

Wall12 5 +body12

Wall13 5 +body13

Wall14 5 +body14 -body15 -(body17+CutZ)

Air 5 +body16 -body1 -body2 -body10 -body11 -body12 -body13 -body14 -body3 -body4 -body5 -body6 -body7 -body8 -body9 -(body15 +CutZ) -(body17 -CutY +CutZ) -Phantom -(+BTOut -BTIn +Zmax -Zmin)-floor

BLOCK1 5 +body17 -CutY +CutZ

BLOCK2 5 +body15 +CutZ

BeamTube 5 +BTOut -BTIn +Zmax -Zmin

BeamVac 5 +BTIn +Zmax -Zmin

PHANTOM 5 +Phantom

FLOOR 5 +floor

END

GEOEND

* Concrete * Concrete has a wide variation in density and composition. The above * description is for poured structural concrete with 10% moisture * content. Concrete block will have a density of about 2.05 g/cm3. * Ranges of concrete composition are : C (8-25%), O (38-60%), Si (8-18%). * Concrete composition can be analysed cheaply by commercial laboratories.

MATERIAL 2.34

Concrete

COMPOUND 23.0 CARBON 40.0 OXYGEN 12.0

SILICON Concrete

COMPOUND 12.0 CALCIUM 10.0 HYDROGEN 2.0 MAGNESIU Concrete

LOW-MAT Graphite 6. -3. 296. CARBON

MATERIAL 6. 2.26

Graphite

MATERIAL 24. 7.18

CHROMIUM

MATERIAL 25. 7.21

MANGANES

MATERIAL 15. 1.82 PHOSPHO

MATERIAL 16. 2.07 SULFUR

* Steel316LN

* Stainless steel AISI316LN

MATERIAL 7.8 SS316LN

COMPOUND -.67145 IRON -0.185 CHROMIUM -0.1125 NICKELSS316LN

COMPOUND -0.02 MANGANES -0.01 SILICON -4.5E-4 PHOSPHOSS316LN

COMPOUND -3.E-4 SULFUR -3.E-4 CARBON SS316LN * ..+....1....+....2....+....3....+....4....+....5....+

ASSIGNMA BLCKHOLE BLKBODY

ASSIGNMA VACUUM VOID

ASSIGNMA Concrete Wall1

ASSIGNMA Concrete Wall2

ASSIGNMA Concrete Wall3

ASSIGNMA Concrete Wall4

ASSIGNMA Concrete Wall5

ASSIGNMA Concrete Wall6

ASSIGNMA Concrete Wall7

ASSIGNMA Concrete Wall8

ASSIGNMA Concrete Wall9

ASSIGNMA Concrete Wall10

ASSIGNMA Concrete Wall11

ASSIGNMA Concrete Wall12

ASSIGNMA Concrete Wall13

ASSIGNMA Concrete Wall14

ASSIGNMA AIR air

ASSIGNMA Concrete BLOCK1

ASSIGNMA Concrete BLOCK2

ASSIGNMA ALUMINUM BeamTube

ASSIGNMA VACUUM BeamVac

ASSIGNMA WATER PHANTOM

ASSIGNMA SS316LN FLOOR

* irradiation profile

* ——— RADDECAY 1. 3.0 99999

* 1.4h irradiation

IRRPROFI 5040.0 1.E9 82800. 0.0 5040.0 1.E9

IRRPROFI 82800. 0.0 5040.0 1E9 82800.0 1E9

* 1.4h irradiation

IRRPROFI 5040.0 1.E9 82800. 0.0 5040.0 1.E9

IRRPROFI 82800. 0.0 5040.0 1E9 82800.0 1E9

* cooling times: 0min 1 hour 1 day 1 month 3 months 1 year

DCYTIMES 0.0 3600.0 86400.0 2592000.0 7776000.0 31104000.

* Floor activation

DCYSCORE 1. FlAct-0s

RESNUCLE

RESNUCLE 3. -21. FLOOR

FlAct-0s

DCYSCORE 2. FlAct-1h

RESNUCLE

RESNUCLE 3. -22. FLOOR

FlAct-1h

DCYSCORE 3. FlAct-1d

RESNUCLE

RESNUCLE 3. -23. FLOOR

FlAct-1d

DCYSCORE 4. FlAct-1m

RESNUCLE

RESNUCLE 3. -24. FLOOR

FlAct-1m

DCYSCORE 5. FlAct-3m

RESNUCLE

RESNUCLE 3. -25.

FlAct-3m

DCYSCORE 6. FlAct-1y

RESNUCLE

RESNUCLE 3. -26.

FlAct-1y

* Air activation

DCYSCORE 1. Air-0s

RESNUCLE

RESNUCLE 3. -27. air Air-0s

DCYSCORE 2. Air-1h

RESNUCLE

RESNUCLE 3. -28. air Air-1h

DCYSCORE 3. Air-1d

RESNUCLE

RESNUCLE 3. -29. air Air-1d

DCYSCORE 4. Air-1m

RESNUCLE

RESNUCLE 3. -30. air Air-1m

DCYSCORE 5. Air-3m

RESNUCLE

RESNUCLE 3. -31. air Air-3m

DCYSCORE 6. Air-1y

RESNUCLE

RESNUCLE 3. -32. air Air-1y

* Neutron prompt dose eq

USRBIN 10. DOSE-EQ -33. 500.0 2000.0 2000.0 DoseeqN

USRBIN -2.0 -1000.0 -1000.0 100.0 100.0 100.0

AUXSCORE USRBIN NEUTRON DoseeqN AMB74

* Photon prompt dose eq

USRBIN 10. DOSE-EQ -34. 500.0 2000.0

2000.0DoseeqPh

USRBIN -2.0 -1000.0 -1000.0 100.0 100.0 100.0

AUXSCORE USRBIN PHOTON DoseeqPh AMB74

* Residual Dose equivalent rate

*

DCYSCORE 1. Doseeq0s USRBIN

AUXSCORE USRBIN Doseeq0s AMB74

USRBIN 10. DOSE-EQ -35. 500.0 2000.0 2000.0Doseeq0s

USRBIN -2.0 -1000.0 -1000.0 100.0 100.0 100.0

DCYSCORE 2. Doseeq1h USRBIN

AUXSCORE USRBIN Doseeq1h AMB74

USRBIN 10. DOSE-EQ -36. 500.0 2000.0 2000.0Doseeq1h

USRBIN -2.0 -1000.0 -1000.0 100.0 100.0 100.0

DCYSCORE 3. DoseEq1d USRBIN

AUXSCORE USRBIN DoseEq1d AMB74

USRBIN 10. DOSE-EQ -37. 500.0 2000.0 2000.0DoseEq1d

USRBIN -2.0 -1000.0 -1000.0 100.0 100.0 100.0

DCYSCORE 4. Doseeq1m USRBIN

AUXSCORE USRBIN Doseeq1m AMB74

USRBIN 10. DOSE-EQ -38. 500.0 2000.0 2000.0Doseeq1m

USRBIN -2.0 -1000.0 -1000.0 100.0 100.0 100.0

DCYSCORE 5. Doseeq3m USRBIN

AUXSCORE USRBIN Doseeq3m AMB74

USRBIN 10. DOSE-EQ -39. 500.0 2000.0 2000.0Doseeq3m

USRBIN -2.0 -1000.0 -1000.0 100.0 100.0 100.0

DCYSCORE 6. Doseeq1y USRBIN

AUXSCORE USRBIN Doseeq1y AMB74

USRBIN 10. DOSE-EQ -40. 500.0 2000.0 2000.0Doseeq1y

USRBIN -2.0 -1000.0 -1000.0 100.0 100.0 100.0

* Set the random number seed

RANDOMIZ 1.0

* Set the number of primary histories to be simulated in the run

START 1000000.0

STOP

Bibliography

[1] Bert, C., Durante, M. (2011). Motion in radiotherapy: particle therapy. *Phys Med Biol,56*(16). doi:10.1088/0031-9155/56/16/R01

[2] Particle Therapy Cancer Research Institute. (2014). Retrieved from url = http://www.ptcri.ox.ac.uk/.

[3] Podgorsak, E.B. (2010). *Radiation Physics for Medical Physics* (2nd ed.). London: Springer.

[4] Lennox, A.J. (2001). Accelerators for cancer therapy, *Radiation Physics and Chemistry*, *61* (3-6), 223-226, doi:10.1016/S0969-806X(01)00244-4

[5] Scholz, M. (2006). Chapter 1-Dose Response of Biological Systems to Low and High-LET Radiation, *Theory and Applications to Dosimetry*, 1-73, doi: 10.1016/B978-044451643-5/50013-7

[6] Amaldi, U., Kraft, G. (2006). Particle accelerators take up the fight for cancer. *CERN Courier*, Retrieved from url = http://cerncourier.com/cws/article/cern/29777/.

[7] World Health Organization WHO (2016). Ionizing radiation, health effects and protective measures, Retrieved from url = http://www.who.int/mediacentre/factsheets/fs371/en/

[8] Kacperek, A. (2009). Protontherapy of eye tumours in the UK: A review of treatment at Clatterbridge. In *Applied Radiation and Isotopes*, *67* (3) 378-386. doi:10.1016.2008.06.012

[9] Owen, H. (2015). The Christie Proton Beam Therapy Centre and Accelerator Research. Retrieved from url = https://www.stfc.ac.uk/stfc/cache/file/F7EF2F1D-CEC2-4CD5-90DF95819903AF99.pdf

[10] Ghithan, S., Roy, G., Schuh, S. (2017). Feasibility Study for BioLeir, *CERN Yellow Reports: Monographs*, CERN-2017-001-M, doi:10.23731.2017.001

[11] Chen, W.Z, Xiao, Y., Li, J. (2014). Impact of dose calculation algorithm on radiation therapy, *World J Radiol.*, textit6(11), 874-880. Retrieved from url = https://www.ncbi.nlm.nih.gov/pmc/articles/PMC4241494/

[12] Battistoni, G., et al. (2007). The FLUKA code: description and benchmarking, *AIP Conference Proceedings*, textit896 (31), doi:10.1063.1.2720455

[13] Giap, H., Giap, B. (2012), Historical perspective and evolution of charged particle beam therapy, *Translational Cancer Research*, textit1 (3), doi: 10.3978/j.issn.2218-676X.2012.10.09

[14] Slater, J.M. (2011), *From X-Rays to Ion Beams: A Short History of Radiation Therapy*. London: Springer, pp 3-16.

[15] Particle Therapy Co-Operative Group (2017), textitParticle Therapy Facilities in Operation. Retrieved from https://www.ptcog.ch/index.php/facilities-in-operation

[16] Paganetti, H. (2012). *Proton Therapy Physics*. New York: CRC Press.

[17] Gagnebin, S.E. (2010). *Experimental determination of absorbed dose to water in a scanned proton beam using a water calorimeter and an ionization chamber* (Degree dissertation). Retreived from url = http://e-collection.library.ethz.ch/eserv/eth:1841/eth-1841-02.pdf

[18] Vana, N. et al. (2014) , Applicability of Ambient dose equivalent H*(d) in mixed radiation field-a critical discussion. Retrieved from url =http://irpa11.irpa.net/pdfs/2i11.pdf

[19] Nucleonica. (2014). *Ambient dose equivalent*. Retrieved from url = http://www.nucleonica.net/wiki/
index.php?title-Ambient-dose-equivalent-281029

[20] National Physical Laboratory. (2014). *Measurement of dose rate*. Retrieved from url = http://www.npl.co.uk/publications/good-practice-online-modules/radiation/practical-radiation-monitoring-units/measurement-of-dose-rate/

[21] Sanchez Parcerisa, D. (2012). *Experimental and computational investigations on the water-to-air stopping power ratio for ion chamber dosimetry in carbon ion radiotherapy* (Doctoral Thesis). Retreived from url = http://archiv.ub.uni-heidelberg.de/volltextserver/13619/

[22] Highland, V.L. (1975). Some practical remarks on multiple scattering. *Nuclear Instruments and Methods*, *129*(42), 497-499. doi:10.1016/0029-554X(75)90743-0

[23] Soukup, M., et al. (2003). The importance of nuclear interactions for dose calculations in proton therapy. *Radiotherapy and Oncology, 68*. Retrieved from https://www.medizin.uni-tuebingen.de/medphys

[24] Paganetti, H., Bortfeld, T. (2005). Proton Beam Radiotherapy - The State of the Art. *Medical Physics*, textit32(6). doi:10.1118/1.1999671

[25] Marc, M. (2010) Proton therapy: scattering versus scanning. *Medical Physics Web*. Retrieved from url = http://medicalphysicsweb.org/cws/article/opinion/42793

[26] Wilson, R. (1946). Radiological Use of Fast Protons. Retrieved from url = http://users.physics.harvard.edu/ wilson/cyclotron.html

[27] CURA Medical Technologies (2014), Retrieved from url = http://www.curamedtech.com/

[28] ProCure Treatment Centers(2014). Retrieved from url = http://www.procure.com/OurLocations.aspx.

[29] International Commission on Radiation Units and Measurements (1993). *ICRU-50 Prescribing, Recording, and Reporting Photon Beam Therapy*. Retrieved from url = http://www.icru.org/home/reports/prescribing-recording-and-reporting-photon-beam-therapy-report-50

[30] Wedenberg, M. (2013). *From Cell Survival to Dose Response –Modeling Biological Effects in Radiation Therapy* (Degree Dissertation). Retrieved from url = http://www.raysearchlabs.com/globalassets/about-overview/media-center/wp-re-ev-n-pdfs/publications/thesis-minna.pdf

[31] Kraft, G. (2000). Tumor therapy with heavy charged particles. *Progress in Particle and Nuclear Physics*, *45*(2), S473-S544. doi: 10.1016/S0146-6410(00)00112-5

[32] Paganetti, H., et al. (2002), Relative biological effectiveness (RBE) values for proton beam therapy, *Int. J. Radiat. Oncol. Biol. Phys.*, [53], 407-421. doi:10.1016/S0360-3016(02)02754-2

[33] Takatsuji, T., et al. (1999). Generalized Concept of the LET-RBE Relationship of Radiation Induced Chromosome Aberration and Cell Death. *J. Radiat. Res.*, *40*(1), 59-69. doi:10.1269/jrr.40.59.

[34] Vandana, S. (2011). *LET, RBE and OER*. Retrieved from url = https://fr.slideshare.net/vandanart

[35] Song, H. et al. (2012). OER, Alpha Particle Emitter Radiolabeled Antibody for Metastatic Cancer: What Can We Learn from Heavy Ion Beam Radiobiology?. *Antibodies*, *1*(2), 124-148, doi:10.3390/antib1020124

[36] NEA (1994),Radiation protection overview:international aspects and perspective. *NEA Issue Brief: An analysis of principal nuclear issues*, 10. Retrieved from url = https://www.oecd-nea.org/brief/brief-10.html

[37] ICRP (2006). The Optimisation of Radiological Protection - Broadening the Process. *ICRP Publication 101b. Ann.* ICRP *36*(3). Retrieved from url = http://www.icrp.org/publication.asp?id=ICRP

[38] ICRP (1990), Recommendations of the International Commission on Radiological Protection, *ICRP Publication 60*. Pergamon, Oxford. Retrieved from url = https://www.ncbi.nlm.nih.gov/pubmed/2053748

[39] Whaites, Drage (2013). Summary of Current UK Legislation and Guidelines, Essentials of Dental Radiography and Radiobiology 5e , *Elsevier*. ISBN 978-0702045998

[40] The Ionising Radiation Regulations (1999). textit3232. Retrieved from url = http://www.legislation.gov.uk/uksi/1999/3232/contents/made

[41] The Ionising Radiation (Medical Exposure) Regulations (2000). Retrieved from url = http://www.legislation.gov.uk/uksi/2000/1059/regulation/1/made

[42] Newhauser, W.D., Titt, U. (2002). An overview of shielding considerations in constructing a proton-radiation cancer-therapy facility. *Sixth Meeting of the Task Force on Shielding Aspects of Accelerators, Targets and Irradiation Facilities, SLAC, USA*. Retrieved from url = https://www.researchgate.net/publication/258096468An-Overview-of-Shielding-Considerations-in-Constructing-a-Proton-Radiation-Cancer-Therapy-Facility

[43] Tit, U., et al. (2000). Neutron Shielding Calculations for a 230-MeV Proton Therapy Facility, *Adv. Monte Carlo for Radiat. Phys., Part. Transp. Simul. Appl. Proc.. Monte Carlo Conf., Portugal*

[44] Newhauser W., et al. (2002). Neutron Shielding Verification and Simulations for a 235-MeV Proton Therapy Centre, *Nucl. Instr. Meth.*, A 476, 80-84

[45] XU, J. et al. (2013). Radiation Calculations for Advanced Proton Therapy Facility, *Proceeding of IPAC, Shanghai, China* ISBN 978-3-95450-122-9, pp 3201-3203

[46] Pelliccioni, M. (2011). Radiation Protection at Hadron Therapy Facilities. *Radiation Protection Dosimetry, 146*(4), pp. 407-413. doi:10.1093/rpd/ncr242

[47] Forkel-Wirth, D. et al.(2013), Radiation Protection at CERN. doi: 10.5170/CERN-2013-001.415

[48] CERN (2006), Safety Code F, EDMS 335729. Retrieved from https://espace.cern.ch/Safety-Rules-Regulations/en/rules/byType/OldClassification/Pages/sc.aspx

[49] Vollaire, J. (2015). Radiation Protection and Radiation Safety for Particle Accelerators Facilities, *Compact Accelerators for Isotope Production, Cockcroft Institute, UK*.

[50] Andreo, P. (1991). Monte Carlo techniques in medical radiation physics. *Phys. Med. Biol.*, *36*, pp. 861-920. Retrieved from url = http://iopscience.iop.org/article/10.1088/0031-9155/36/7/001/pdf

[51] Archambault, L. et al. (2003). Overview of Geant4 Applications in Medical Physics, *IEEE Xplore*. doi:10.1109/NSSMIC.2003.1352215,

[52] Mairani, A. et al. (2016). Recent Improvements and Applications of the FLUKA Monte Carlo code in Hadrontherapy, *Radiotherapy and Oncology*. doi:10.1016/S0167-8140(16)30140-2

[53] Los Alamos National Laboratory, *Practical MCNP® for the Health Physicist, Medical Physicist, and Radiological Engineer*. Retrieved from url = http://www.lanl.gov/orgs/rp/mcnp.shtml

[54] Larsson, S., *Radiation transport calculations for narrow scanned photon beams using Geant4* (Unpublished Master Dissertation), University of Technology, Sweden

[55] Guatelli, S. (2002). *Interstitial brachytherapy with I-125: experimental measurements and Monte Carlo simulation* (Unpublished Master Dissertation), University of Gebia, Italy

[56] Foppiano, F. et al. (2003). From DICOM to GRID: a dosimetric system for brachytherapy born from HEP, *IEEE Xplore*, *3*. doi: 10.1109/NSSMIC.2003.1352216

[57] Cirrone, G. et al. (2003). Implementation of a New Monte Carlo Simulation Tool for the Development of a Proton Therapy Beam Line and Verification of the Related Dose Distribution. *Proceedings NSS*.

[58] Aguer, P. et al. (2003). Simulation of cellular irradiation with the CENBG microbeam line using Geant4, *Proceedings NSS*

[59] Strul, D. et al. (2002). GATE(Geant4 Application for Tomographic Emission): a PET/SPECT general purpose simulation platform (Innovative Particle and Radiation Detectors. *Proceedings, Siena, Italy*

[60] Briesmeister, F. (1997). MCNP-A general Monte Carlo N-Particle Transport Code (version 4B), *Los Alamos National Laboratory Manual*

[61] Kieger, W. et al. (2005). Performance Enhancements of MCNP4B, MCNP5 and MCNPX for Monte Carlo Radiotherapy Planning Calculations in Lattice Geometries, *11th International Symposium on Neutron Capture Therapy, Boston, USA*

[62] Juste, B. et al. (2005). Considerations of MNCNP Monte Carlo code to be used as a radiotherapy treatment planning tool, *Annual International Conference of the IEEE Engineering in Medicine and Biology Society. IEEE Engineering in Medicine and Biology Society. Conference.* doi:10.1109/IEMBS.2005.1617062

[63] Sullivan, A. H. (1992), *A guide to radiation and radioactivity levels near high energy particle accelerators.* Ashford, Kent: Nuclear Technology Publishing

[64] Cossairt, J. D. (2008), Induced radioactivity at accelerators, Professional Development School: Topics in Accelerator Health Physics. In *Proceedings of the Health Physics Society 2008 Professional Development School - Topics in Accelerator Health Physics, Oakland CA, California.* Retrieved from url =http://lss.fnal.gov/archive/2007/pub/fermilab-pub-07-201-esh.pdf

[65] NCRP Report.(2005), *Radiation protection for particle accelerator facilities: recommendations of the National Council on Radiation Protection and Measurements, 144.* Retrieved from url =http://ncrponline.org/wp-content/themes/ncrp/PDFs/ExecSumm-NCRP-Report-No-144.pdf

[66] Barbier, M.(1969). *Induced Radioactivity.* Amsterdam: North-Holland Pub.Co

[67] Bevelacqua, J.(2008). *Health Physics in the 21st Century. Health Physics in the Twenty-First Century.* Wiley: Weinheim

[68] La Torre, F. (2014), *Study of induced radioactivity in proton accelerator facilities*(Doctorate Thesis). Retrieved from url = https://cds.cern.ch/record/1666527/files/CERN-THESIS-2014-009.pdf

[69] Bungau, C. et al. (2014). Induced activation in accelerator components, *Physical Review Special Topics- Accelerators and Beams, 17.* doi:10.1103/PhysRevSTAB.17.084701

[70] Tommasino, F. et al. (2016). New Ions for Therapy, *International Journal of Particle Therapy, 2*(3), 428-438. doi:10.14338/IJPT-15-00027.1

[71] Weber, U, Kraft, G.(2009). Comparison of Carbon Ions versus Protons, texitThe Cancer Journal, *15*(4),325-332. doi:10.1097/PPO.0b013e3181b01935

[72] Dunn W., & Shultis, J (2012). *Exploring Monte Carlo methods.* Burlington: Academic Press, Elsevier

[73] Metropolis, N.(1987). The beginning of the Monte Carlo method. *Los Alamos Science, Special Issue.* Retrieved from url = https://dasher.wustl.edu/chem430/reading/lascience-14-125-87.pdf

[74] Kajaria, A., et al. (2013), Review of Monte Carlo Simulation in Radio Therapy Treatment Planning System for Moddeling of Radiation Transport & Dose Calculation. Retrieved from url = https://www.researchgate.net/publication/289952636-Review-of-Monte-Carlo-Simulation-in-Radio-Therapy-Treatment-Planning-System-for-Modelling-of-Radiation-Transport-Dose-Calculation

[75] Seco, J., Verhaegen, F. (2013). *Monte Carlo Techniques in Radiation Therapy.* Florida: CRC Press

[76] Rogers, D. W. O. & Bielajew, A. F. (1990). *The Dosimetry of Ionizing Radiation.* NewYork: Academic, *3*, 427 – 539

[77] Andreo, P. (2014), The Monte Carlo Method in Medical Radiation Physics. In *International Conference on Radiation Medicine (ICRM), Riyadh, Saudi Arabia.* doi: 10.13140/RG.2.2.11061.68328

[78] Rogers, D. W., et al. (1995), BEAM: A Monte Carlo code to simulate radiotherapy treatment units. *Medical Physics*, *22*(5), 503-524. doi: 10.1118/1.597552

[79] Fasso, A., Ferrari, A., Ranft, J., and Sala, P. (2005). FLUKA: a multi-particle transport code. SLAC-R-773. Retrieved from url =http://slac.stanford.edu/pubs/slacreports/reports16/slac-r-773.pdf

[80] Battistoni, G., et al. (2006). The FLUKA code: Description and benchmarking, In *Proceedings of the Hadronic Shower Simulation Workshop 2006, Albrow.* Retrieved from url =http://www.fluka.org/content/publications/2007-fermilab.pdf

[81] Kafi, A., et al. (2005). The use of MCNP code for radiation transport and dosimetry calculations in training medical physics students. *Int.J.Sci.Res*, *15.* Retrieved from url = http://faculty.kfupm.edu.sa/phys/aanaqvi/naqresum-files/papa-papers/papa-2006-2007-papersfolder/mcnp-code-abdallah-kafi.pdf

[82] Yang, Z., et al. (2017), Inter-comparison of Dose Distributions Calculated by FLUKA, GEANT4, MCNP, and PHITS for Proton Therapy. *EPJ Web of Conferences*, *153.* doi:10.1051/epjconf/20171530411

[83] Agostinelli, S., et al.(2003). GEANT4-a simulation toolkit. *Nuclear Instruments and Methods in Physics Research Section A: Accelerators, Spectrometers, Detectors and Associated Equipment*, *506*(3), 250 - 303. doi:10.1016/S0168-9002(03)01368-8

[84] Foppiano, F., et al.(2003). Overview of Geant4 applications in medical physics, *IEEE*. doi: 10.1109/NSSMIC.2003.1352215

[85] Bohlen, T., el al. (2010). Benchmarking nuclear models of FLUKA and GEANT4 for carbon ion therapy. *Phys. Med. Biol.*, *55*, 5833-5847. doi:10.1088/0031-9155/55/19/014

[86] Battistoni G., et al. (2011). The application of the Monte Carlo code FLUKA in radiation protection studies for the Large Hadron Collider. *Progress in Nuclear Science and Technologies*, *2*, 358-364. doi:10.15669/pnst.2.358

[87] Andersen, V., et al. (2004). The FLUKA code for space applications: recent developments.*Advances in Space Research*, 34, (6) 1302-1310. doi: 10.1016/j.asr.2003.03.045

[88] Cerutti, F., et al. (2006). Low energy nucleus-nucleus reactions: the BME approach and its interface with FLUKA. In *11 th Intl. Conf. on Nucl. React. Mech.*, pp. 507-511. Retrieved from url = http://www0.mi.infn.it/ gadioli/Varenna2006/Proceedings/Cerutti-F.pdf

[89] Parodi, K., et al. (2007). Clinical CT-based calculations of dose and positron emitter distributions in proton therapy using the FLUKA Monte Carlo code. In *Phys. Med. Biol.*, *52*(12), 3369-3387. doi:10.1088/0031-9155/52/12/004

[90] Battistoni G et al. (2006). Recent developments in the FLUKA nuclear reaction models. In *11 th Intl. Conf. on Nucl. React. Mech*, 12-16. REtrieved from url = https://www.researchgate.net/publication/267221999-Recent-Developments-in-the-FLUKA-nuclear-reaction-models

[91] Rinaldi, I., et al. (2011). An integral test of FLUKA nuclear models with 160 MeV proton beams in multi-layer Faraday cups. *Phys. Med. Biol*, *56*(13) 4001. doi:10.1088/0031-9155/56/13/016

[92] Parodi, K., et al. (2010). The FLUKA code for application of Monte Carlo methods to promote high precision ion beam therapy. In *12th International Conference on Nuclear Reaction Mechanisms, Villa Monastero, Varenna, Italy*. Retrieved from url = http://cds.cern.ch/record/1238366/files/p509.pdf?version=1

[93] FLUKA. *FLUKA Manual*. Retrieved from url = http://www.fluka.org

[94] ICRP. (1996). Conversion Coefficients for use in Radiological Protection against External Radiation, *ICRP Publication*, *74*. Ann. ICRP 26 (3-4)

[95] Pelliccioni, M. (2000). Overview of Fluence-to-Effective Dose and Fluence-to-Ambient Dose Equivalent Conversion Coefficients for High Energy Radiation Calculated Using the FLUKA Code, *Radiation Protection Dosimetry*, *88*(4), 279-297. doi: 10.1093/oxfordjournals.rpd.a033046

[96] ICRU (2007). *Prescribing, recording, and reporting proton-beam therapy Report*, *78*

[97] Paul, H. (2012). Modern Practices in Radiation Therapy. Croatia: InTech/ doi:10.5772/34974

[98] Kacperek, A. (2009). Protontherapy of eye tumours in the UK: A review of treatment at Clatterbridge. In *Applied Radiation and Isotopes*, 67 (3) 378-386.

[99] Adrian (2012). Proton beam blasted away my eye cancer. Retrieved from url = http://www.express.co.uk/life-style/health/351040/Proton-beam-blasted-away-my-eye-cancer

[100] Paganetti, H., (1999). Monte Carlo method to study the proton fluence for treatment planning. In *Medical Physics*, *25*, 2370-2375. doi:10.1118/1.598447

[101] Newhauser, W., Zhang, R.(2015), The physics of proton therapy, *Phys. Med. Biol.*, *60*(8), 155 –209. doi:10.1088/0031-9155/60/8/R155

[102] Laidler, A. (2015), Neutron Dose Received by the patient from the CCO Proton Beamline, Internal Report Unpublished

[103] Jakubowska, E., et al. (2016). Ambient dose equivalent measurements in secondary radiation fields at proton therapy facility CCB IFJ PAN in Krakow using recombination chambers. *NUKLEONIKA*, *61*(1), 23-28. doi:10.1515/nuka-2016-0006

[104] Fasbender, M. et al. (2007). Experimental studies and nuclear model calculations of the formation of radiactive products in interactions of medium energy protons with copper, zinc and brass: Estimation of Collimator activation in proton therapy facilities. *Appl. Radiat. Isot.*, *48*(9), 1221-1230. doi:10.1016/S0969-8043(97)00102-4

[105] Cesana, A. et al. (2010). Induced radioactivity in a patient-specific collimator used in proton therapy. *Nuclear Instruments and Methods in Physics Research B*, *268*, 2272-2280. doi:10.1016/j.nimb.2010.03.004

[106] Lee, S., et al. (2012). Evaluation of radioactivity induced by patient-specific devices in proton therapy. *Journal of the Korean Physical Society*, *60* (1), 125-128. doi:10.3938/jkps.60.125

[107] Mukherjee, B. (2012). Radiation safety issues relevant to proton therapy and radioisotope production medical cyclotrons. *Radiation Protection and Environment*, *35*(3). doi:10.4103/0972-0464.117668

[108] Charitonidis, N., et al. (2011). *Prompt, Activation and Background radiation studies for the HiRdMat facility of CERN/SPS*. Retrieved from url = https://infoscience.epfl.ch/record/175668/files/TN-RADIATION-STUDIES-FINAL-including-accident-scenarioV2.pdf

[109] Hardy, M. (2015). *Radiation Protection Considerations in Proton Therapy Centre Design*, Presentation given at the Aurora Workshop, New Castle, UK.

[110] The Christie civil engineering plans (2016). Received on 24/05/2016 from Dr. Michael Taylor

[111] Knowles, H. et al. (1993). Shielding and Activation Study for Proton Medical Accelerators. In *Particle Accelerator Conference (PAC)*. doi:10.1109/PAC.1993.309114

[112] DeMarco, J. et al. (2013), Shielding implications for secondary neutrons and photons produced within the patient during IMPT. *Medical Physics*, *40*(7):071701. doi:10.1118/1.4807089

[113] Flynn, A. (2015). *The Christie Proton Therapy Centre* (Unpublished Master Dissertation)

[114] Hallenbeck, W. (1994). *Radiation Protection*. US: Lewis Publishers.

[115] Poggi, C, Sandri, S. et al. (2014), A proton therapy test facility: the radiation protection design. In *Proceedings of IPAC2014*, Germany.

[116] Abler, D., et al. (2013). Feasibility study for a biomedical experimental facility based on LEIR at CERN. In *Journal of Radiation Research*, 54, i162–i167 doi: 10.1093/jrr/rrt056.

[117] Retrieved from url=http://www.stfc.ac.uk/research/particle-physics-and-particle-astrophysics/large-hadron-collider/cern-accelerator-complex/

[118] Carli, C. (2012). *LEIR Facility for Biomedical Studies*, Erice. Retrieved from url=https://indico.cern.ch/event/215087/contributions/342218/477460/CarliErice121023.pdf

[119] Abler, D., Garona, A., Carli, C. (2014). Proposal for a new LEIR Slow Extraction Scheme dedicated to Biomedical Research, ATS Report, CERN-ACC-2014-0095

[120] Damjanovic, S. (2013). *Radiation level at the LEIR visitors platform. Present and future*, CERN. Presentation received from Sanja Damjanovic via email on 30/06/2015.

[121] Weber, U., Kraft, G. (2009). Comparison of Carbon Ions versus Protons. In *The Cancer Journal*, 15(4):325-332

[122] Randeniya, R. D. et al. (2009). Intercomparison of Monte Carlo Radiation Transport Codes MCNPX, GEANT 4, and FLUKA for Simulating Proton Radiotherapy of the Eye. In *Nuclear Technology*, 2-333-202 105

[123] Retrieved from url=http://truenorthreports.com/facts-and-information-about-radiation-exposure

[124] Allisy A., et al. (1993). Report 51.*Journal of the International Commission on Radiation Units and Measurements*, *os26*(2). doi:10.1093/jicru/os26.2.Report51

[125] Chen Y., Ahmad S. (2011). Empirical model estimation of RBE for proton beam therapy. *Radiation Protection Dosimetry*, *149*(2):116-23. doi:10.1093/rpd/ncr218

[126] Patterson H., Thomas R. (1973). *Accelerator Health Physics*, New York and London: Academic Press.